Detecting Recent Snow Accumulation and Meltwater Storage in Firn Aquifers on Ice Sheets Using Remote and Field Observations

by

Lynn Nicole Montgomery

B.S., University of Maryland, College Park, 2016

M.S., University of Colorado, Boulder, 2020

A thesis submitted to the

Faculty of the Graduate School of the

University of Colorado in partial fulfillment

of the requirement for the degree of

Doctor of Philosophy

Department of Atmospheric and Oceanic Sciences

December 2020

Committee Members:

Lora Koenig, National Snow and Ice Data Center

Jan Lenaerts, University of Colorado

Jennifer Kay, University of Colorado

Ted Scambos, Cooperative Institute for Research in Environmental Sciences

Rick Forster, University of Utah

ABSTRACT

Montgomery, Lynn Nicole (Ph.D., Department of Atmospheric and Oceanic Sciences)

Detecting Recent Snow Accumulation and Meltwater Storage in Firn Aquifers on Ice Sheets Using Remote and Field Observations

Thesis directed by Senior Research Scientist Lora Koenig and Assistant Professor Jan Lenaerts.

Mass loss from ice sheets has been identified as a major contributor to sea level rise by the Intergovernmental Panel on Climate Change from detailed observations in the past few decades. In order to understand how sea level rise will be influenced by ice sheets, we must quantify their total mass balance (through surface mass fluxes and ice discharge) over time. This dissertation focuses on the component of surface mass balance, presenting new in-situ and remote observations of accumulation and meltwater storage in firn aquifers.

In Chapter 2, I present the 2018 Surface Mass Balance and Snow on Sea Ice Working Group database, a standardized, formatted, community-based dataset housed at the Arctic Data Center. It consists of sub datasets of density, accumulation, 10 m borehole temperatures, and snow depth on sea ice measurements. I analyze temporal and spatial patterns across the Greenland Ice Sheet and conclude that observations are oversampled in higher elevation, colder regions and undersampled at warmer, lower elevations. In addition, there was a large temporal gap from 2000 into more recent decades, but since then that has been reconciled in the 2019 and 2020 SUMup database releases.

In Chapter 3, I use NASA's Operation IceBridge airborne snow radar to derive annual accumulation over 8 consecutive years (2009-2017) in Southeast Greenland, the highest snowfall region on the ice sheet which largely influences the sign of the mass balance. I compare these derived accumulations with two regional climate models, the Modèle Atmosphérique Régional

version 3.9 (MAR) and the Regional Atmospheric Climate Model version 2.3p2 (RACMO2), to evaluate model biases. Results indicate that MAR agrees with the derived accumulations well, but underestimates interannual variability while RACMO2 underestimates accumulation but is able to capture the interannual variability.

Finally, in Chapter 4, I present hydrological and geophysical observations of meltwater storage and flow in a firn aquifer on the Wilkins Ice Sheet, Antarctica and its impact on ice shelf stability. Results from a borehole dilution test, slugs tests, ground penetrating radar, and groundwater flow modeling show that the aquifer is highly permeable and flowing into a nearby rift. Based on these observations and model output, we conclude that the aquifer is likely not in steady state near our measurement site, could have influenced past ice shelf breakups, and may impact ice shelf stability in the future.

DEDICATION

To my family.

To my mom for endless conversations of love and support and for telling me it was okay to miss Christmas because I was stuck on an ice sheet.

To my dad for my sense of drive and for letting me know that I can always come home.

To my brother for lending an open ear anytime I needed advice or encouragement.

To my cats, Oscar and Lily, for providing emotional support day and night.

To Brennan - thank you for letting me run around the world from pole to pole while you take care of our crazy cats. Thank you for being there to put me back on my feet when I fall into the abyss of self-doubt. Thank you for being there to remind me to celebrate all of my successes, no matter how small.

ACKNOWLEDGMENTS

I want to acknowledge my PhD advisers and committee for the endless time and effort spent teaching me how to be a competent and successful scientist. To Lora Koenig for being the best adviser any student could ever ask for, full of knowledge and guidance, and genuinely caring about me as a person. To Jan Lenaerts for many, many, many long meetings about surface mass balance, and for being an amazing mentor. To Ted Scambos for teaching me how to survive on an Antarctic field campaign and answering email questions even after 7 pm. To Jen Kay for always having an open door and providing an unending amount of support. And finally, to Rick Forster for a great amount of glaciological insight and opening your home every time I came to Utah for research.

I want to thank my undergraduate adviser and first mentors, Timothy Canty, Ross Salawitch, and Russ Dickerson from the University of Maryland for the endless advice, support, and knowledge provided which jump-started my passion for atmospheric science and fieldwork. I also want to thank Nick Schmerr who was an amazingly supportive mentor that I am so grateful to have been able to work with in and out of the field. Also, to the most amazing group of friends that I gained along the way Alexa Maines, Doug Kahn, Mike Natoli, Kelsey Malloy, Keenan Eure, Alex Ortiz, and Meredith Nichols.

I want to thank all of my professors, friends, and classmates from the University of Colorado. To my first year cohort, I do not know how I would have passed my classes without all of the treasured memories of long hours spent studying and doing homework together at SEEC. A very special thank you to my research group for many long meetings and discussions. I could not imagine a better group of people to share, learn, and grow with. In addition, a very

special thank you to Laurie Conway, J. Reeves, and Andy Wang for making the logistics of graduate school and finances as smooth as imaginable, you are all superstars.

Finally, I want to thank my fieldwork tent-mates Olivia Miller, Clement Miege, and Bruce Wallin. Fieldwork is physically and emotionally difficult and it makes it a million times easier when you have such wonderful people to share the experience with. To Olivia Miller for making me pancakes on my 20th birthday when we were still in the field and enjoying many (very chilly) spa nights together. To Bruce Wallin for an endless supply of dumb jokes that always made me laugh and for saving me from falling into a crevasse during rescue training. And to Clement Miege for teaching me the vast majority of what I know about living and working on the ice and in academia with unending patience and the most positive spirit.

TABLE OF CONTENTS

1 Introduction **1**

1.1 Sea Level Rise and Ice Sheet Mass Balance 1

1.2 Surface Mass Balance 3

1.2.1 Accumulation 3

1.2.2 Meltwater Runoff and Storage 5

1.2.2.1 Meltwater Runoff from Supraglacial Streams 8

1.2.2.2 Meltwater Storage through Refreezing 9

1.2.2.3 Meltwater Storage in Supra and Sub-Glacial Lakes 10

1.2.2.4 Meltwater Storage in Firn Aquifers 11

1.3 Summary and Project Overview 12

2 **The SUMup dataset: compiled measurements of surface mass balance components over ice sheets and sea ice with analysis over Greenland** **14**

2.1 Introduction and Background 14

2.2 The SUMup Dataset 16

2.2.1 Overview 16

2.2.2 Sources 18

2.2.3 Contributing to the Dataset 19

2.2.4 Structure and Metadata 19

2.2.4.1 Snow Density 21

2.2.4.2 Snow Accumulation on Land Ice 22

2.2.4.3 Snow Depth on Sea Ice 24
2.3 Spatial and Temporal Data Analysis 26
2.3.1 Snow Density 29
2.3.2 Accumulation 31
2.3.3 Snow Depth on Sea Ice 34
2.3.4 Analysis over the Greenland Ice Sheet 34
2.3.4.1 Greenland Density distributions with Elevation, Latitude and Temperature 36
2.3.4.2 Accumulation distributions with Elevation and Latitude 40
2.3.4.3 Year-round density and accumulation measurements from Summit Station 41
2.4 Data Availability 43
2.5 Discussion and Conclusions 43
2.6 Acknowledgements 45

3 **Accumulation rates (2009–2017) in Southeast Greenland derived from airborne snow radar and comparison with regional climate models** **46**
3.1 Introduction 46
3.2 Observations, Instruments and Models 48
3.2.1 Operation IceBridge Airborne Snow Radar Data 48
3.2.2 In-Situ Density Observations 49
3.2.3 MAR and RACMO2 Simulated SMB 50
3.2.4 Crocus and FDM Modelled Density 50
3.3 Methods 51

3.3.1 Selecting Flight Tracks 52

3.3.2 Density profiles and associated uncertainties 52

3.3.3 Determining layer age and total accumulation uncertainty 55

3.4 Results 56

3.4.1 Radar derived accumulation rates 56

3.4.2 Comparison with RCMs: interannual variability 58

3.4.3 Comparison with RCMs: spatial variability 59

3.5 Discussion 62

3.6 Conclusions 66

3.7 Data availability 67

3.8 Acknowledgements 67

4 **Hydrologic properties of a highly permeable firn aquifer in the Wilkins Ice Shelf, Antarctica** **68**

4.1 Introduction 68

4.2 Study Site 69

4.3 Methods 71

4.3.1 Borehole drilling and firn/ice cores 71

4.3.2 Hydraulic conductivity estimate 72

4.3.3 Borehole dilution test 72

4.3.4 Geophysical surveys and water-table elevation estimate 73

4.3.5 Flow-rate modelling 74

4.4 Results 75

4.4.1 Firn Core Characteristics 75
4.4.2 Hydraulic Conductivity 75
4.4.3 Borehole dilution test 76
4.4.4 GPR Survey of the Rift 78
4.4.5 Groundwater Flow Modelling 79
4.5 Discussions and Conclusions 81
4.6 Acknowledgements, Samples, and Data 84
4.7 Supplemental Material 85
4.7.1 Supplemental Text 85
4.7.2 Supplemental Figures 89
4.7.3 Supplemental Tables 94

5 **Conclusions** **97**
5.1 Synopsis and Chapter Summaries 97
5.1.1 The SUMup Database 97
5.1.2 Radar Derived Accumulation Observations in Southeast Greenland 98
5.1.3 Hydrological Observations from a Firn Aquifer in the Wilkins Ice Shelf, Antarctica 99
5.2 Outlook 99

6 **References** **103**

LIST OF TABLES

Table 2.1: SUMup Snow Density Dataset Vairables and Units 22

Table 2.2: SUMup Snow Accumulation on Land Ice Variables and Units 23

Table 2.3: SUMup Snow Depth on Sea Ice Variables and Units 25

Table 2.4: SUMup statistics for all Arctic measurements 28

Table 2.4: SUMup statistics for all Antarctic measurements 28

Table 4.S1: Model output from regional climate models, RACMO2 and MAR, of snowfall and melt at the closest matched grid point to the field site 94

Table 4.S2: SEEP2D model input and output of variables in Darcy's Law 95

LIST OF FIGURES

Figure 1.1. Sea level rise projections from RCP Scenarios 2

Figure 1.2. Updated SUMup density, accumulation, and 10m temperature subdatasets from Greenland and Antarctica 4

Figure 1.3. Elements of the Greenland ice sheet hydrologic system 6

Figure 1.4. Examples of major components of surface hydrological systems from Antarctica 7

Figure 1.5. Locations of simulated firn aquifers from snowpack models 12

Figure 2.1. Measurement locations for accumulation and snow density SUMup dataset on the Greenland and Antarctic Ice Sheets 17

Figure 2.2 SUMup measurement methods in the density and accumulation subdatasets 27

Figure 2.3. SUMup snow density measurements by date taken 30

Figure 2.4. SUMup snow density measurements by midpoint depth 31

Figure 2.5. SUMup accumulation on land ice measurements by date taken 32

Figure 2.6. SUMup accumulation measurements by year 33

Figure 2.7. SUMup snow depth on sea ice measurements by date taken 34

Figure 2.8. SUMup density measurements by elevation and latitude 36

Figure 2.9. SUMup density measurements by modelled 3m air temperature 37

Figure 2.10. Mean annual 3m temperature compared to density at shallow snow depths 39

Figure 2.11. SUMup accumulation measurements by elevation and latitude 40

Figure 2.12. Monthly mean density and standard deviation at Summit Station, Greenland 42

Figure 2.13. Monthly mean accumulation and standard deviation at Summit Station, Greenland 43

Figure 3.1. Overall and flight line case study region 48

Figure 3.2. Average density comparison in the top meter of snow between regional climate models and observations 54

Figure 3.3. Average density comparison in the top 5 meters of snow between regional climate models and observations 55

Figure 3.4. Annual Accumulation derived from OIB Snow Radar from 2009 to 2017 57

Figure 3.5. Inter-annual variability of derived accumulation rates compared to regional climate models 59

Figure 3.6. Relative difference between derived accumulation and regional climate models 61

Figure 3.7. Average annual snowfall from 2009-2017 from regional climate models 65

Figure 4.1. Field overview of the Wilkins Ice Shelf, Antarctica including water table depth from airborne and ground penetrating radar and local surface mass balance conditions 70

Figure 4.2. Firn characteristics and dilution test results 77

Figure 4.3. GPR profile across the rift and analysis of water flow and drainage of the firn aquifer layer 80

Figure 4.S1. Airborne MCoRDS profile taken on November 16, 2014 89

Figure 4.S2. Firn density and stratigraphy for all three boreholes drilled at the field site 90

Figure 4.S3. Slug test set-up and water level change data 91

Figure 4.S4. Borehole dilution test set-up and homogenization of salt concentration 92

Figure 4.S5. 8-day continuous stationary GPS survey at the drill site 93

1 Introduction

1.1 Sea Level Rise and Ice Sheet Mass Balance

Over 250 million people live in coastal regions that are located less than five meters above sea level, making sea level rise an important global issue (Kulp and Strauss, 2019; Siegart et al., 2017). Rising ocean levels can endanger necessary resources including safe drinking water, farming and food production, infrastructure, as well as human lives. In Florida, seawater is contaminating aquifers where coastal communities pump unsustainable amounts of groundwater, limiting the future availability of safe drinking water (Hurdle, 2020). Farmers in Bangladesh have seen an increase in soil salinity due to frequent flooding from sea water and are expected to lose 21% of their crop revenue per year due to this contamination (Chen and Mueller, 2018). By 2100, coastal flooding influenced by increased global temperatures and sea level rise could cost up to 100 trillion dollars (Hinkel et al., 2014). In order to mitigate the negative impacts of sea level rise, and prepare our natural and human environments, we must understand what factors contribute to rising ocean levels.

Since the early 1970's, thermal expansion of water and mass loss from glaciers have been identified as the most important contributors to global mean sea level rise (GMSLR), with the rest due to changes in land water storage (Church et al., 2013). However, in recent decades with more detailed observations, the Greenland Ice Sheet (GrIS) and Antarctic Ice Sheet (AIS) were also identified as important factors, contributing ~40% of the total GMSLR (3.0 ± 0.38 mm yr^{-1}) from 2006-2015 (Oppenheimer et al., 2019). Future projections from the worst-case Representative Concentration Pathway (RCP) 8.5 scenario show that with continued warming, GMSLR will rise by 0.84 ± 0.25 m by 2100 (Figure 1.1), with 0.12 ± 0.10 m coming from the AIS and 0.12 ± 0.11 m from the GrIS (Oppenheimer et al., 2019). Similar values of GMSLR are

presented in the recent Ice Sheet Model Intercomparison for CMIP6 (ISMIP6) project, with 21st century contributions to sea level rise of 0.09 ± 0.05 m from the GrIS (Goelzer et al., 2020) and 0.11 ± 0.18 m for the AIS (Seroussi et al., 2020) in the highest-emission scenario. Under all RCP scenarios, mass loss from both the GrIS and the AIS will increase as we approach 2100 (Pattyn et al., 2018). Therefore, it is essential to understand how ice sheets are changing, and will change in the future, to better predict future GMSLR

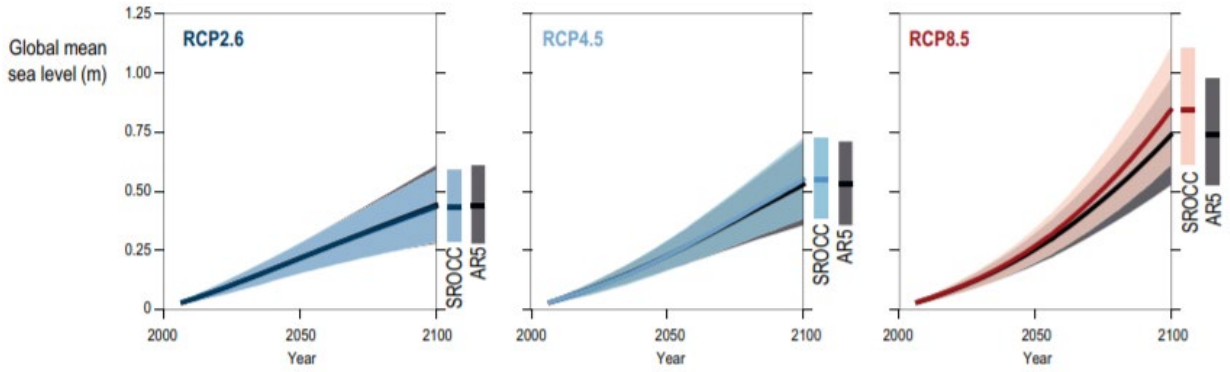

Figure 1.1 - Time series of Global Mean Sea Level for RCP 2.6, RCP4.5, and RCP8.5 Results are based on AR5 results for all components except the Antarctic contribution. Adapted from Chapter 4 of the 2018 IPCC Report.

An ice sheet will grow or shrink based on its mass balance, which will lead to an associated sea level fall or rise, respectively. Ice sheet mass balance is defined as the difference between surface mass fluxes or surface mass balance (SMB) and the flux of ice across the grounding line referred to as ice discharge (Lenaerts et al., 2019). Total ice sheet mass balance can be estimated through three independent methods: (1) ice mass change through gravimetry (Jeon et al., 2018), (2) ice volume change via satellite altimetry based surface elevation change (Schröder et al., 2019), and (3) from the input-output method (The IMBIE Team, 2020 and 2018). The first method uses the Gravity Recovery and Climate experiment (GRACE), which consists of two polar orbiting

satellites that can detect variations in Earth's gravity field and, therefore can estimate mass variations on ice sheets (Ramillien et al., 2004). The second method uses altimetry-based mass balance studies to estimate volume change based on surface height changes (which are often measured from satellites). These methods are novel and useful to estimate mass balance change remotely and on large scales from the ice sheets. However, the only way to understand the individual components of mass balance is by examining the input-output which quantifies mass input through cumulative surface mass balance (SMB) processes and mass output through discharge.

1.2 Surface Mass Balance

In this dissertation, we focus on the SMB component of total ice sheet mass balance. SMB is defined as snow accumulation and wind-driven snow redistribution (through erosion or redeposition), minus runoff, where accumulation is the difference between snowfall and evaporation/sublimation (Equation 1; Lenaerts et al, 2019).

Equation 1: SMB = Precipitation - Runoff - Sublimation/Evaporation - Blowing Snow Erosion

For this research, we ignore snow redistribution because it is small when integrated over large areas and not well constrained by models or observations (Lenaerts et al., 2019). Therefore, in this research, SMB is defined as snow accumulation minus meltwater runoff.

1.2.1 Accumulation

Accumulation is commonly measured directly through ice cores, stake measurements (Takahashi and Kameda, 2007), and ground penetrating radar surveys. Ice cores provide a long temporal record of accumulation at a single point location while stake field measurements provide better spatial resolution but are only feasible at a small scale. Ground penetrating radar surveys allow

for accumulation observations that show both temporal and spatial variability over large areas. However, none of these methods can provide an accurate estimate of ice sheet wide accumulation over space and time. In addition, most field measurements of accumulation are dispersed across multiple data centers with no standardized format which limits scientific applications. To address this issue, the Surface Mass Balance and Snow on Sea Ice Working Group (SUMup) database was created, which includes subdatasets of accumulation, density, 10 meter borehole temperature, and snow depth on sea ice measurements (Chapter 2). SUMup is a standardized, publicly available database that is easily expandable to benefit researchers. Since the first release on the Arctic Data Center in May 2017, the datasets have been used extensively by the cryospheric community and have been downloaded over 7,500 times Currently, the SUMup database includes ~2.5 million measurements at over 600 unique locations on the GrIS and AIS (Figure 1.2). The SUMup database validates that accumulation observations are sparse across space and time for both ice sheets.

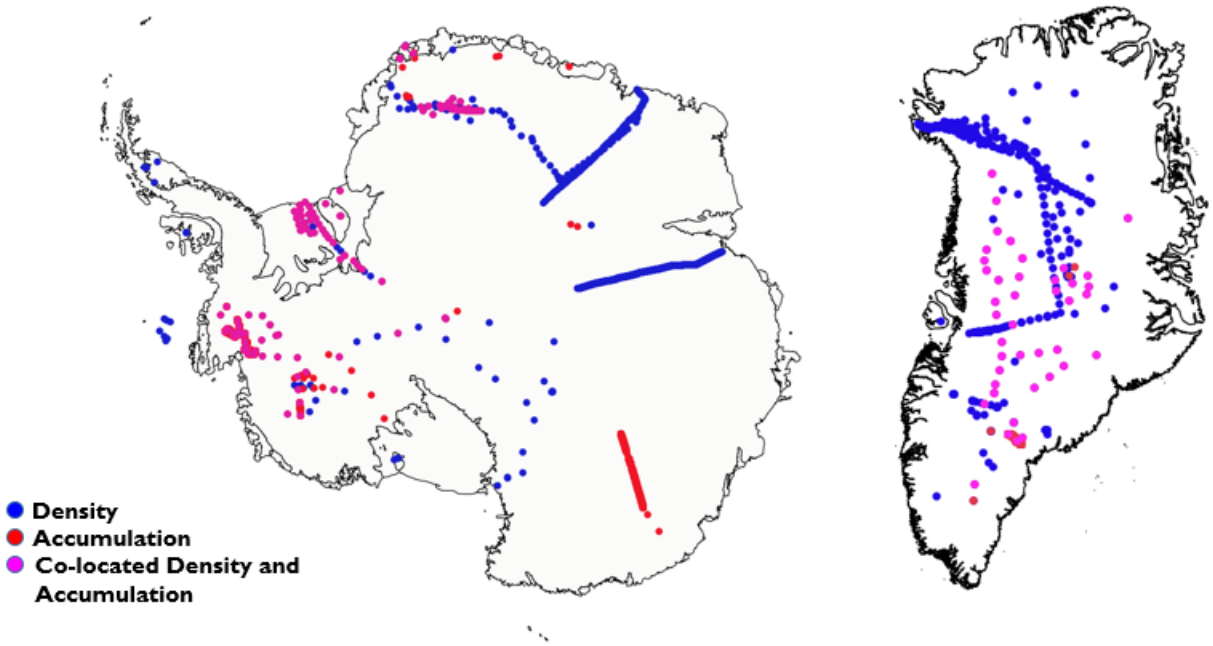

Figure 1.2 - Updated SUMup database locations of density and snow accumulation on the Antarctic and Greenland Ice Sheets from November 2020.

New measurement techniques have been developed over the last few decades to provide more spatial and temporal accumulation coverage. In 2008, NASA's Operation IceBridge (OIB) began a unique campaign to measure snow properties over both ice sheets using radar systems on airborne surveys. Using this method, scientists were able to derive accumulation estimates across much larger areas of the ice sheet taking into account the density of the snow, depth of the snow, and age of the snow layers (Montgomery et al., 2020a, Koenig et al., 2016, Medley et al., 2013). With this new technique we focused on the data-sparse region of Southeast Greenland, which receives the most annual snowfall on the GrIS. In fact, variation in accumulation in this region heavily influences the total SMB of the GrIS and can even determine whether the total mass balance in some years is positive or negative (Burgess et al., 2010). We derived a new 9-year long dataset (2009–17) of accumulation rates that can be used to evaluate regional climate models where few in-situ observations are available (Chapter 3). Current machine learning research is using this dataset to train neural networks to automate (and better quantify the uncertainty) of tracking internal layers of accumulation from the OIB radar (Rahnemoonfar et al., 2020).

1.2.2 Meltwater Runoff and Storage

The other component of surface mass balance includes meltwater processes. Meltwater from ice sheets can either be refrozen into the snowpack, stored in or on the ice sheet or ice shelves, or runoff into the ocean. On the GrIS, the hydrological system is characterized by supraglacial streams and lakes that can drain through moulins, or vertical fractures, providing an influx of meltwater into englacial and subglacial environments (Chu, 2014; Figure 1.3). These meltwater

features provide storage or runoff mechanisms which can increase glacial flow and lead to sea level rise (Figure 1.3). Conversely, on the AIS nearly all meltwater produced on the surface of the ice sheet or ice shelves, extensions of ice sheets past the grounding line and are afloat on the ocean, refreezes (Lenaerts et al., 2019). However, recent studies show Antarctic meltwater in coastal areas and ice shelves stored englacially in lakes (Dunmire et al., 2019) or firn aquifers (Montgomery et al., 2020b; Chapter 4). Understanding meltwater storage in and on ice shelves is especially important because meltwater storage has been shown to be a precursor to hydrofracture and ice shelf disintegration (Bell et al., 2018; Scambos et al., 2004, Scambos et al., 2000). Additionally, meltwater runoff can form supraglacial streams which drain into moulins and crevasses (Bell et al., 2018; Figure 1.4).

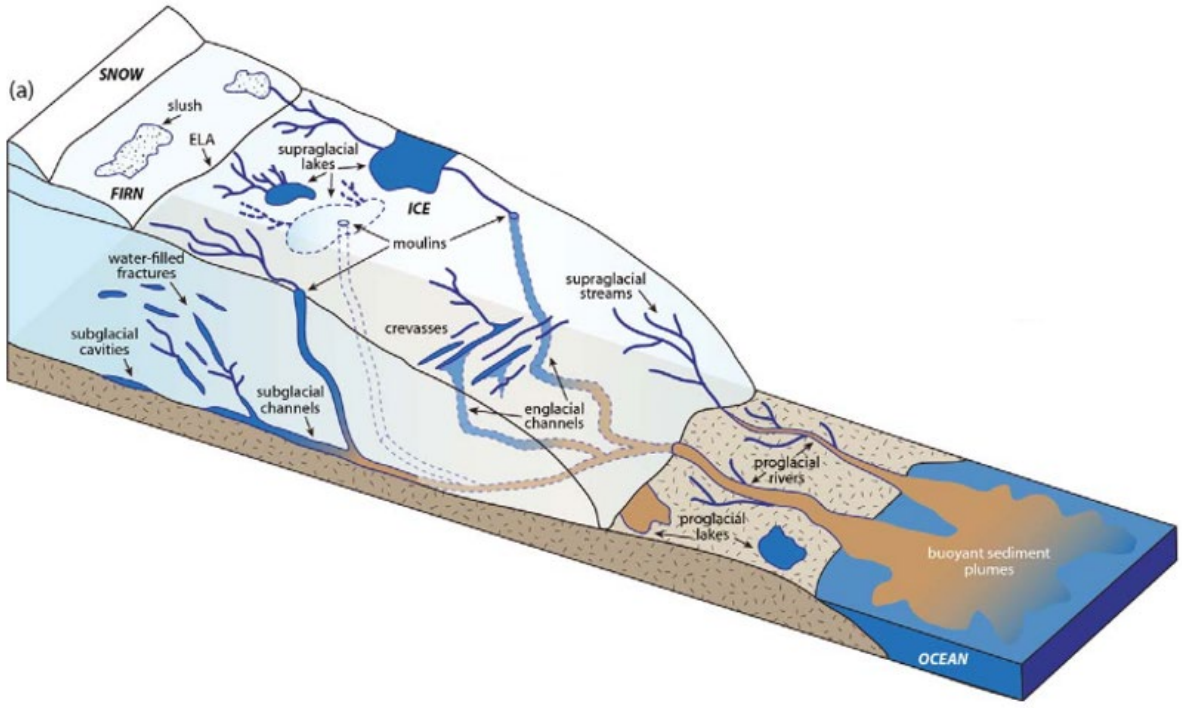

Figure 1.3 - Elements of the Greenland ice sheet hydrologic system. (a) In the accumulation zone above the equilibrium line altitude (ELA), water percolating through the snow/firn can pool

into slush regions and channelize into supraglacial streams. In the ablation zone beneath the ELA, meltwater pools in supraglacial lakes and flows through streams into crevasses and moulins, entering englacial and subglacial conduits emerging into proglacial rivers and lakes. As meltwater moves through the system, erosional debris increases sediment concentration making glacial-melt lakes and rivers sediment-rich (leaving precipitation and snow-melt lakes clear of sediment). Finally, meltwater entering the ocean produces a buoyant sediment plume in the fjord. Modified from Chu et al., (2014) and Cuffey and Paterson (2010).

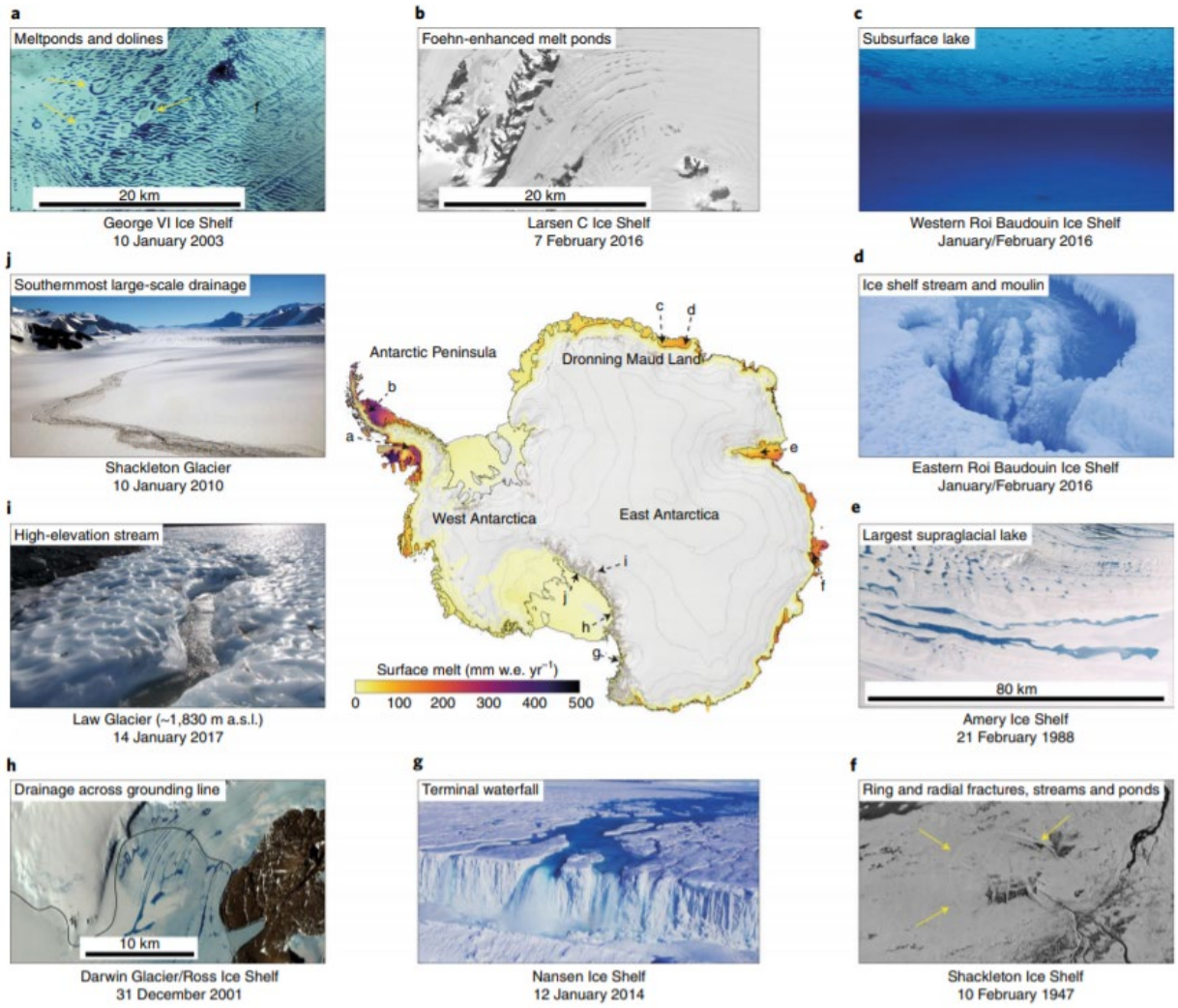

Figure 1.4 - Examples of major components of surface hydrological systems located on a present-day Antarctic surface melt map. The central map shows 2000–2009 Antarctica surface melt from QuikSCAT satellite observation 7; the locations of the images in a–j are indicated. a, Meltwater lakes and dolines (arrows), b, Foehn wind-enhanced meltwater ponding. c, Buried lake. d, Moulin draining surface stream. e, Elongate supraglacial lake. f, Fractures around a drained lake. Scale unknown. g, Persistent waterfall draining water. h, Supraglacial streams transporting water across the grounding line of the Darwin Glacier onto the Ross Ice Shelf. i, High-elevation (1,830 m) meltwater stream. j, Meltwater stream crossing the grounding line. Images reproduced from: US Geological Survey (a,b,e,h); ref. 8, Springer Nature Limited (c); Sanne Bosteels (d); USGS/EROS and the Polar Geospatial Center (f); Won Sang Lee (g); Mike Kaplan (i); John Stone (j). From Bell et al. (2018).

1.2.2.1 Meltwater Runoff from Supraglacial Streams

Supraglacial streams are channels of meltwater that activate during the summer, are a transport mechanism for meltwater, and link to englacial/subglacial systems via moulins, crevasses, and shear fractures (Smith et al., 2014). Formation of these streams occurs when one of the following occurs: 1) meltwater percolates through underlying snow and ice, refreezes, and establishes impermeable superimposed ice lenses allowing for water to flow along this barrier or 2) when surface snow and ice reach saturation and drainage begins to mobilize a slush flow of snow, firn, and meltwater (Pitcher and Smith, 2019). These channels establish predominantly in the direction of the steepest surface slopes and therefore mostly transport water downslope towards the edge of the ice sheet, depositing it into the ocean. This impacts the mass balance of the ice sheet through mass loss of surface snow, firn, and meltwater to the ocean. Supraglacial streams also impact ice sheets by reinforcing impermeable ice layers at the surface that allow downslope

flow into the ocean which can lead to larger, perineally active supraglacial rivers mostly observed in Greenland (Pitcher and Smith, 2019) and on ice shelves in Antarctica (e.g. Amery Ice Shelf) (Bell et al., 2018; Kingslake et al., 2017; Phillips, 1998). Additionally, these streams can terminate in moulins or crevasses which can lead to hydrofracture to the bed of the ice sheet or ice shelf causing local velocity accelerations or ice shelf breakups.

1.2.2.2 Meltwater Storage through Refreezing

Refreezing occurs when there is available liquid meltwater either at the surface or in the snowpack and temperatures drop below 0 degrees Celsius, causing an ice lens or ice layer to form. If the meltwater percolates into the snowpack and reaches an impermeable layer, then it can spread out laterally and freeze, thus increasing the thickness of the ice lens. Refreezing impacts the ice sheet system by creating dense, impermeable ice layers, and decreasing the available air content in the snowpack. This impact is important because the firn (multiyear compressed snow) layer buffers the ice-sheet contribution to sea-level rise by retaining a fraction of summer melt as liquid water and refrozen ice (Vandecrux et al., 2019). On the GrIS, refreezing occurs in both the accumulation and ablation zones. In the accumulation zone, where mass gain from snowfall exceeds the mass losses of melt and evaporation, these ice layers often form below the surface as the water percolates into the snowpack and reaches colder, denser layers below. Conversely, in the ablation zone, where mass loss from melt and evaporation exceed snowfall, meltwater can form ice layers at the surface late in the season. Additionally, bare ice layers at the surface create an impermeable surface, allowing for the formation of supraglacial meltwater streams leading to more surface meltwater runoff into the ocean (Macferrin et al., 2019). In Antarctica, very little meltwater is produced on the grounded ice

sheet (where the ice sheet is in contact with bedrock). Surface meltwater on ice shelves mostly refreezes locally in the firn layer.

1.2.2.3 Meltwater Storage in Supra and Sub-Glacial Lakes

Supraglacial lakes are bodies of meltwater that form in topographic depressions of the ice sheet surface during summer. They store meltwater in these basins and influence ice sheet dynamics on hourly through interannual timescales if they rapidly drain via hydrofracture (which occurs when water pressure activates/initiates fractures in the ice) which can relate the signal of surface melt to local ice motion (Sundal et al., 2009). These drainage events can cause increases in ice velocity by lubricating the ice-bedrock interface. Recent observations in Greenland and Antarctica also show that supraglacial lakes can become buried lakes, where water is retained within the at shallow depths throughout the winter season (Dunmire et al., 2020; Benedek and Willis, 2020; Miles et al., 2017; Koenig et al., 2014). Although they do not store a significant amount of meltwater, they can influence the local hydrology and can drain via hydrofracture by initiating or reactivating pre-existing fractures which is currently a poorly understood process (Dunmire et al., 2020; Benedek and Willis, 2020).

Subglacial lakes are bodies of water that form below ice masses. They can form from meltwater that is transported to the bedrock from the ice sheet surface through crevasses or moulins or also by basal melting due to the weight of the overlying ice. These subglacial lakes are important because they can lead to subglacial ice streams which can cause accelerated mass loss from lubrication. Over 400 subglacial lakes have been found beneath the AIS ranging from lengths of 1 km to 250 km using altimetric measurements from satellites (Siegert et al., 2016). Few subglacial lakes have been discovered below the GrIS until recently when a study

found 54 potential subglacial lakes using airborne echo-soundings and ice sheet elevation changes (Bowling et al., 2019).

1.2.2.4 Meltwater Storage in Firn Aquifers

Firn aquifers are an englacial meltwater storage system where meltwater from the surface is perennially stored within the firn. These aquifers are important because they can contribute to sea level rise if connected to the ocean by slowly draining into crevasses or mitigate sea level rise by storing water (Koenig et al., 2014). Firn aquifers are located where there is enough pore space to store meltwater and often in regions of high accumulation, which provides insulation that permits the saturated subsurface layer to remain at or above freezing (Kuipers Munneke et al., 2014). These conditions occur mainly in the southeast and northwest sectors of the GrIS where accumulation rates ~1-5 meters water equivalent per year and melt rates are >650 mm water equivalent per year (Montgomery et al., 2020; Bell et al., 2018; Noël et al., 2018). On the AIS, regions with similarly high surface melt and snow accumulation rates are scarce, though recent observational and modelling studies show widespread perennial firn aquifers on the Antarctic Peninsula (Fig 1.5), and more specifically the Wilkins Ice Shelf (Montgomery et al., 2020b; van Wessem et al., 2016, 2020).

In Chapter 4, we present the first hydrological observations of a firn aquifer in Antarctica on the Wilkins Ice Shelf (Montgomery et al., 2020b). We investigated this firn aquifer using slug tests, a borehole dilution test, and groundwater flow modelling and found that it is highly permeable and drains into a nearby rift. Scientists have known about the likely presence of a saturated firn layer on the Wilkins Ice Shelf since the early 1970's from airborne radar, however the in-situ validation of this aquifer leads us to believe it has likely influenced past partial ice shelf breakups through hydrofracture (Braun et al., 2009; Humbert and Braun, 2008; Scambos et

al., 2000). Meltwater stored in firn aquifers increases the potential for hydrofracture because it causes saturation of the vertical firn column and increases the hydrostatic head. With a large hydrostatic head year-round, the aquifer provides enhanced fracturing for whenever stresses change to favor tensile extensions or loss of compression, even in the winter (Scambos et al., 2009).

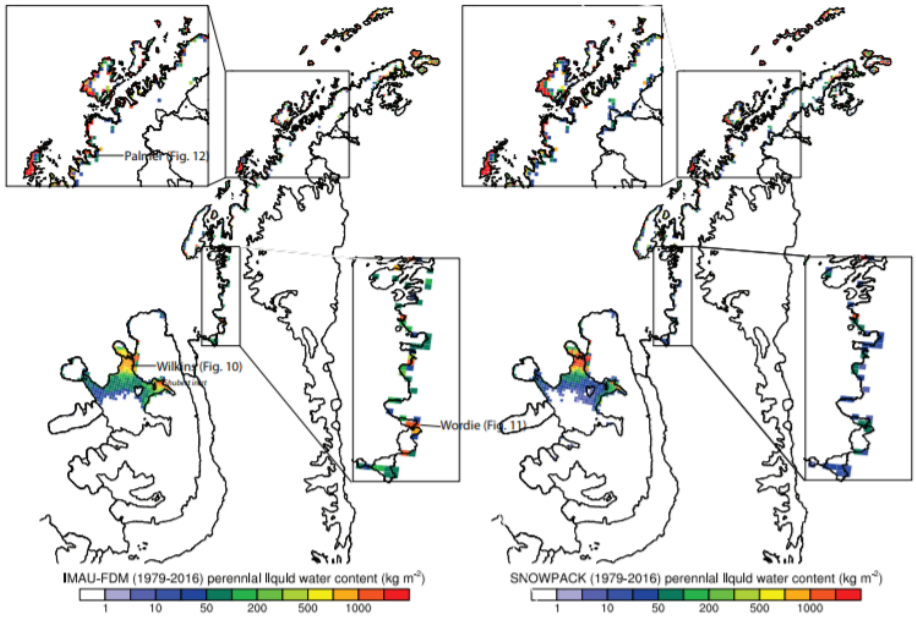

Figure 1.5 - Modelled IMAU-FDM (left row) and SNOWPACK (right row) annual average (1979–2016) vertically integrated liquid water content for PFA points. From van Wessem et al. (2020).

1.3 Summary and Project Overview

The overall goal of this research is to improve our understanding of the components of ice sheet SMB, i.e. accumulation and meltwater runoff and storage. We aim to fill knowledge gaps by providing new in-situ and remotely sensed observation datasets. In Chapter 2, we present

SUMup, a database we created which is the first standardized, publicly available database of surface mass balance observations over both ice sheets and sea ice to benefit the cryospheric community. Researchers can now easily access over 2.5 million cryospheric measurements simultaneously instead of having to source each dataset individually which increases efficiency and scientific progress. In Chapter 3, we derive a new dataset of accumulation measurements using airborne radar observations over almost a decade temporally across the snowiest and most data-sparse regions of Greenland. These large-scale observational datasets provide a foundation for future measurements to be added onto and to evaluate global, regional, and local models. In Chapter 4, we present the first hydrological observations from a firn aquifer on the Antarctic Ice Sheet and explore how it could have led to past ice shelf breakups and future ice shelf destabilization. Currently, there are only two observed sites of firn aquifers on polar ice sheets making this observation extremely rare and important for the community. With continued warming, meltwater will play an increasingly important role in ice sheets and ice shelves and their stability so it is essential to monitor these meltwater features. Finally, in Chapter 5, I summarize results from the preceding chapters and present ongoing and future research ideas.

2 The SUMup Dataset: Compiled measurements of surface mass balance components over ice sheets and sea ice with analysis over Greenland

This chapter is adapted and reformatted from:

Montgomery, L., Koenig, L., & Alexander, P. (2018). The SUMup dataset: compiled measurements of surface mass balance components over ice sheets and sea ice with analysis over Greenland. *Earth System Science Data*, *10*(4), 1959–1985. https://doi.org/10.5194/essd-10-1959-2018

2.1. Introduction and Background

Earth's polar regions are warming at an accelerated rate. As increased air temperatures, and associated feedbacks with radiative heating, persist the ice cover is changing particularly at the ice/atmosphere interface (e.g. Vaughan et al., 2003; Serreze and Francis, 2006; Hall et al., 2013). This change is evident by declining Arctic sea ice extent (e.g Ritcher-Menge et al., 2016) and the recent acceleration of total mass loss from the Greenland Ice Sheet (GrIS) and Antarctic ice sheets (AIS), (e.g. Velicogna et al., 2014; IMBIE Team, 2018), that contributed ~11 mm to global sea levels between 1992 and 2011 (Shepherd et al., 2012). Surface change is particularly evident over the GrIS. Surface mass balance is defined as snow accumulation, including snow fall, water vapor redeposition and positive wind redistribution, minus ablation, including melt discharge, negative wind redistribution, evaporation and sublimation (van den Broeke et al., 2017). In this paper, we use the terminology of accumulation and negative accumulation as we cannot, with our measurements, separate out the components of wind redistribution, sublimation, evaporation or melt. The GrIS's surface mass balance is dominated by melt, now accounting for

more than half of its mass loss (e.g. van Angelen et al., 2013; van den Broeke et al., 2017; Enderlin et al., 2014; Hofer et al., 2017). To understand this change, and the processes driving the change, it is vital to compile measurements from the past and present, and continue to collect them in the future.

In 2012, at the Surface Mass Balance and Snow on Sea Ice Working Group (SUMup) meeting, the modeling and remote sensing communities clearly stated to observationalists that the lack of easy to access, standardized, in-situ measurements hindered scientific achievement. They also emphasized the need for spatially extensive measurements and annual to sub-annual accumulation measurements to coincide with the spatial and temporal scales covered by modeling and remote sensing methods. A public, annual to decadal, standardized time-series of measurements was recommended (Koenig et al., 2013). Modeling and remote sensing studies require validation measurements (e.g. Fettweis et al., 2017; Arthern et al., 2006; Burgess et al., 2010; Kuipers Munneke et al. 2015; Koenig et al., 2016), ideally with the model's same spatial (typically ten's of km) and temporal (typically sub-annual) resolutions. These observations are needed over large polar regions, which are difficult for an individual researcher to compile. Today, most field measurements for validation are dispersed across multiple data centers/datasets in differing formats. Some previous Arctic and Antarctic studies have compiled large sets of measurements, generally accumulation measurements, (e.g. Mock 1967a; Mock 1967b; Ohmura and Reeh, 1999; Vaughan and Russell, 1997; Favier et al., 2013; US ITASE, Mayewski et al., 2013; Wang et al., 2016; Machguth et al., 2016b; Thomas et al., 2017; Matsuoka et al., 2018) though most cover only a small region of the ice sheet, are not annually resolved and/or are not publicly available through a data distribution center.

Here, we present the July 2018 SUMup dataset and its three subdatasets: density, accumulation, and snow depth on sea ice. This data paper serves to fully describe the dataset and includes analysis of the data over the GrIS demonstrating how this dataset increases our knowledge of surface mass balance processes by compiling previously dispersed measurements into a standardized dataset. Uses of SUMup include model validation, remote sensing validation and algorithm development, and long-term monitoring efforts. SUMup measurements should not be used to assess individual measurement errors or establish errors on specific retrieval methods. This is because (1) the spatial/temporal variability of snow depth on sea ice is naturally large due atmospheric processes, including accumulation and aeolian processes, further increased by sea ice characteristics such as age, drift, and ridging (e.g. Warren et al., 1999; Sturm et al., 2002) , and (2) the spatial/temporal variability of density and accumulation on land ice is also large due to atmospheric processes, including accumulation, temperature, solar radiation and aeolian process, further increased by ice elevation, topography, melt and water flow processes (e.g. Alley, 1988; Courville et al., 2007; Laepple et al., 2016; Vandercrux et al., 2018). The field measurements in SUMup were not designed to and cannot control for this naturally occurring variability.

2.2 The SUMup Dataset

2.2.1 Overview

The SUMup dataset is an expandable, community-based dataset of field measurements of surface mass balance components that is consistent in format, properly described through metadata, and publicly available. The July 2018 SUMup dataset contains three subdatasets that consist of measurements of snow/firn density (doi:10.18739/A2JH3D23R), snow accumulation on land ice

(doi:10.18739/A2DR2P790), and snow depth on sea ice (doi:10.18739/A2WS8HK6X). The SUMup dataset is a living document, meant to be expanded as new measurements are taken or previous measurements discovered. The current release of the July 2018 SUMup dataset expands and replaces the previous three smaller releases of July 2013, July 2015, and July 2017. The measurements compiled in SUMup are from the polar regions and most date from 1950 to present day. Some ice cores and radar data contained both post- and pre-1950 accumulation measurement and we did not exclude the pre-1950 data in order to keep the records intact. Pre-1950 accumulation estimates represent ~2% of the accumulation subdataset.

Figure 2.1 shows the locations of density and accumulation measurements represented by the July 2018 SUMup dataset. Snow depth on sea ice locations are not shown on this map due to the broad spatial sampling. Density and accumulation measurements are often co-located over the ice sheets where ice cores were collected (Fig. 2.1).

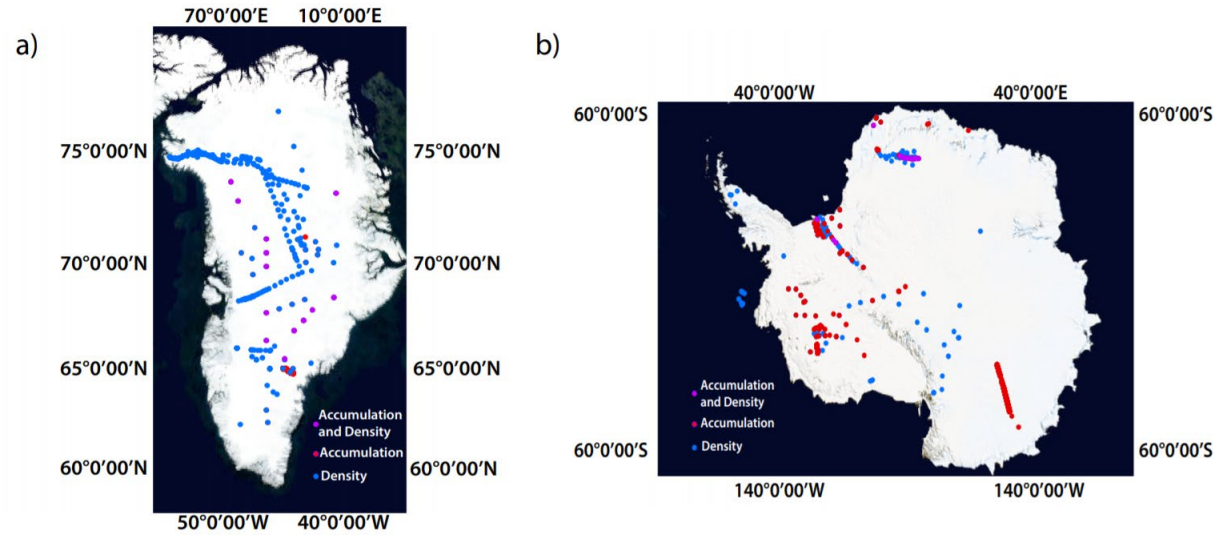

Figure 2.1 - a) Measurement locations for accumulation (red), snow density (blue) or both (purple) for the SUMup dataset on the GrIS. Snow depth on sea ice data for the Arctic are not shown. b) Same as above but for the AIS. Locations on sea ice, those in the Bellingshausen Sea, include both snow density and snow depth on sea ice measurements.

2.2.2 Sources

SUMup measurements were collected, formatted, and compiled primarily through two methods: 1) searching data archives that traditionally host cryospheric data which included Pangaea (https://www.pangaea.de/), the Arctic Data Center (https://arcticdata.io/), NOAA's National Climate Data Center (https://www.ncdc.noaa.gov/) and the National Snow and Ice Data Center (https://nsidc.org/) and 2) by asking members of the cryospheric community to contribute field measurements. Keyword searches for the first method includes searching for the words "density", "accumulation", and "snow depth on sea ice". For point measurements, annually and sub annually accumulation measurements are included. For data from spatially extensive methods (e.g. from radar isochrones), near-annually resolution is required. Various data types are compiled into the SUMup dataset including hand-written notes, technical reports, and digital files. Each measurement in the SUMup dataset contains a citation to the original source of the data. Based on keyword searches, data for this release, July 2018, should include most relevant measurements available in the data archives listed above posted before May 2018. It is possible, however, that datasets can be missed by keyword searches and the community is encouraged to contact the authors directly about any missing datasets that should be included in future releases of SUMup. Specifically, we are working to standardize data from the Japanese Antarctic Research Expedition (JARE) to add in a future release of SUMup.

New and unique data sources are included in the SUMup dataset. Notably, the snow density subdataset includes snow pit data from Carl Benson's Greenland traverses in the early 1950's and data from 1955 that previously had not been digitally scanned (Benson, 2013; Benson, 2017). The 1955 notebooks are only archived in the National Snow and Ice Data Center paper archives. The SUMup dataset also includes snow accumulation measurements from

Summit Station, Greenland's stake network called the Bamboo Forest (Dibb et al., 2004) and corresponding density measurements at monthly temporal resolution (Dibb et al., 2007). Additionally, more widely used data sources are included, such as, US International Trans-Antarctic Scientific Expedition (US ITASE, Mayewski et al., 2013) ice cores, the Program for Arctic Regional Climate Assessment (PARCA, Mosley-Thompson et al., 2001) ice cores and The Greenland Inland Traverse (GrIT, Hawley et al., 2014) snow pits and ice cores. Section 2.4 provides more details on the specific sources for each of the three subdatasets including the complete list of all citations.

2.2.3 Contributing to the Dataset

The SUMup dataset will continue to expand on an annual basis as new measurements are taken and/or old measurements are discovered. Beyond expanding the current subdatasets, we expect to add additional subdatasets on surface mass balance processes which may include, but are not limited to, snow/ice albedo, snow temperature, and short-wave/long-wave radiation measurements. The community is encouraged to contribute data or suggest missing data sources/types to add to SUMup by contacting the authors directly.

2.2.4 Structure and MetaData

Each measurement contains common variables including the date taken, latitude, longitude, surface elevation if on land, the measurement itself, error associated with the measurement, the method in which the measurement was taken, and a citation for which the measurement can be sourced back to. By convention, negative latitudes represent south and negative longitudes represent west. For measurements that did not specify a specific month and day for the measurement, but provided only the year ('yyyy'), the date was entered as 'yyyy0000'. A fill

value of -9999 was used for unknown or unmeasured parameters. Measurements can be separated into direct measurements, when the instrument measures the desired parameter directly, and derived measurements, when the instrument measures a parameter related to the primary parameter and uses a known relationship equation to derive the desired measurement. In this paper, we refer to *both direct and derived measurements* as measurements. Measurement methods are fully listed in each dataset's metadata by number. For clarity, in the density dataset, methods (defined in the readme files) 1-4, 6-9, and 13 are direct measurements (e.g. density cutters, ice core sections, etc.) while methods 5 and 10-12, and 14-15 are derived measurements (e.g. neutron density probe, X-ray microfocus computer tomography, Gamma ray attenuation, etc.). In the accumulation dataset, methods 1 and 3 are direct measurements (e.g. ice core sections and stake measurements) while method 2 is derived (radar isochrones). All snow depth on sea ice measurements are direct measurements. Uncertainties of measurements were only recorded if provided with the original measurement. More detail on general uncertainty for measurement methods used in SUMup is available for density cutters (Conger and McClung, 2009), neutron density probe (Morris, 2008), density and conductivity mixed permittivity (DECOMP) (Wilhelms, 2005), and gamma ray attenuation (Wilhelms, 1996). These can be applied to measurements as appropriate for individual scientific application.

If any of the original measurements/metadata were unclear or non-existent, the original author of the data was contacted to clarify inconsistencies or questions. Snow density measurements that exceeded a physically plausible range from <0 kg m^3 and >1000 kg m^3 were rejected. Specific details on measurement methods and citations for each subdataset are included in the SUMup metadata files hosted at the Arctic Data Center and described below.

2.2.4.1 Snow Density

The snow/firn density subdataset of SUMup is the largest, containing over 2,100,000 unique measurements of density at different depths (Fig. 2.1). Table 1 describes the parameters for each density measurement. The measurement methods include density cutters of different sizes (generally from 100 - 1000 cm^3) used in snow pits, gravitational methods used on ice core sections, neutron-density methods performed in boreholes, X-ray microfocus computer tomography performed on snow samples, gamma-ray attenuation in boreholes, pycnometers used on snow samples, optical televiewer (OPTV) borehole logging, and DECOMP. The majority of the observations (~76%) come from Greenland ice cores or snow pits (Renaud, 1959; Ohmura, 1991; Ohmura, 1992; Alley, 1999; Bolzan and Strobel, 1999(a-g); Miller and Schwager, 2000(a,b); Wilhelms, 2000(a-d); Bolzan and Strobel, 2001(a,b); Mosley-Thompson et al., 2001; Bales et al., 2001; Conway, 2003; Dibb and Fahnestock, 2004; Dibb et al., 2007; Harper et al., 2012; Benson, 2013; Miège et al., 2013; Hawley et al., 2014; Koenig et al., 2014; Baker, 2016; Chellman, 2016; Machguth et al., 2016a; Mayewski and Whitlow, 2016(a-d); Schaller et al., 2016; Benson, 2017; Schaller et al., 2017; Cooper et al., 2018; Macferrin et al., in review). Antarctic measurements comprise ~23% of the snow density subdataset and are predominantly from ice cores (Graf et al., 1988a-q; Wagenbach et al., 1994b-d; Gerland and Wilhelms, 1999; Graf et al., 1999n-y; Oerter et al., 1999a-h; Oerter et al., 2000a-j; Graf et al. 2002a-o; Oerter, 2002; Schlosser and Oerter, 2002c; Graf and Oerter, 2006z-au; Albert, 2007; Oerter, 2008p-ae; Fernandoy et al., 2010a-c; Kreutz et al., 2011; Lewis et al., 2011; Koenig and Brucker, 2011; Mayewski et al., 2013; Hubbard et al., 2013; Medley et al., 2013; Schaller et al., 2017). The depth of the density measurements were recorded using two different methods, either the top and bottom depth or a midpoint depth. While a midpoint can be determined uniquely from the top

and bottom depths the top and bottom cannot always be determined from the midpoint and researchers need to determine how to standardize or interpolate the depths for their specific applications.

Table 2.1 - The parameters for each snow density measurement in the SUMup dataset with a brief description and the unit of measurement.

Column	Description	Unit
Date Taken	Date the data was taken	yyyymmdd
Latitude	Latitude of measurement	Decimal degree
Longitude	Longitude of measurement	Decimal degree
Start Depth	Top depth of the measurement in m from the snow/air interface (snow surface).	m
Stop Depth	Bottom depth of the measurement in m from the snow/air interface (snow surface).	m
Midpoint Depth	Midpoint depth of the measurement in m from the snow/air interface (snow surface).	m
Density	Snow density measurement	g/cm^3
Error	Uncertainty in density measurement	g/cm^3
Elevation	Elevation above sea level	m
Method	How the measurement was collected (see metadata for more details)	-
Citation	Cited source of data (see metadata for more details)	-

2.2.4.2 Snow Accumulation on Land Ice

The snow accumulation on land ice subdataset of SUMup contains over 230,000 unique measurements (Fig. 2.1). Table 2 describes the parameters for each accumulation measurement. The measurement methods include ice cores and/or boreholes, snow pits, radar isochrones, and stake measurements. Arctic measurements are predominantly from ice cores and stake measurements and include one radar near-annual transect in southeast Greenland (Bolzan and

Strobel, 1999(a-g); Bolzan and Strobel, 2001(a,b); Mosley-Thompson et al., 2001; Dibb and Fahnestock, 2004; Miège et al., 2013). The Antarctic measurements are predominantly from ice cores and include two radar transects, one in West Antarctica and one in East Antarctica (Wagenbach et al., 1994a; Graf et al., 1999a-m; Scholsser and Oerter, 2002a-b; Spikes et al., 2005; Graf and Oerter, 2006a-y; Anschütz and Oerter, 2007a-f; Banta et al., 2008; Oerter, 2008a-o; Fernandoy et al., 2010a-c; Ferris et al., 2011; Verfaillie et al., 2012; Burgener et al., 2013; Mayewski et al., 2013; Medley et al., 2013; Philippe et al., 2016). In most instances accumulation (in water equivalent, WE) was provided in the original measurement, however, the Summit Station, Greenland bamboo forest measurements consist of weekly surface height change at 100 stakes along with snow density (Dibb and Fahnestock, 2004). We multiplied the height change by the coincident snow density and averaged across all stakes to get accumulation measurements for SUMup. Similarly, the Bolzan and Strobel data (1999 a-g; 2001 a,b) provided a snow pit depth, year, and density that were converted to accumulation. Most of the accumulation measurements are annually resolved with the major exceptions being the radar measurements, which are approximately decadal, and bamboo forest data, which is approximately monthly.

Table 2.2 - The parameters for each snow accumulation measurement on land ice in the SUMup dataset with a brief description and the unit of measurement.

Column	Description	Unit
Date Taken	Date the data was taken	yyyymmdd
Latitude	Latitude of measurement	Decimal degree
Longitude	Longitude of measurement	Decimal degree
Start Year	First year of measurement if accumulation is not annual	year
End Year	Last year of measurement if accumulation is not annual	year

Year	Year of accumulation if accumulation is annual	year
Accumulation	Accumulation in m of water equivalent per year	m WE/a
Error	Uncertainty in measurement	m WE/a
Elevation	Elevation above sea level	m
Radar Horizontal Resolution	Horizontal resolution of radar data along track	m
Method	How the measurement was collected (see metadata for more details)	-
Name	Name of field campaign (see metadata for more details)	-
Citation	Cited source of data (see metadata for more details)	-

2.2.4.3 Snow Depth on Sea Ice

The snow depth on sea ice subdataset is the sparsest within SUMup with ~92,000 unique measurements. Table 3 describes the parameters for each snow depth measurement. The measurement methods include rulers, magnaprobes, avalanche probes, and snow corers. The Arctic measurements span from 1990-2018 and cover areas off the coast of Finland (Eero Rinne, personal communication), near Kotzebue Sound, and Utqiagvik, Alaska (Turner et al., 2018a-b), Eureka and Nunavut, Canada from the Enviornment and Climate Change Canada campaign (ECCC 2014) (King et al., 2015), near Ellesmere Island from the CryoSat-2 Validation Experiment (CryoVEX) (Haas et al., 2017), Elson Lagoon from the Bromine, Ozones, and Mercury Experiment (BROMEX) (Webster et al., 2014), and Prudhoe Bay, Alaska from the Ice and Climate Experiment (ICEX 2011)(Gardner et al., 2012). The Antarctic observations are from the Sea Ice Mass Balance in the Antarctic (SIMBA) dataset which was collected from the research vessel/ice breaker *N.B. Palmer* in September and October 2007 in the Bellingshausen Sea (Lewis et al., 2011). We note that large, standardized datasets of radar-derived snow depth on sea ice are available through the IceBridge Sea Ice Freeboard, Snow Depth and Thickness

product and similar products derived from the IceBridge Snow Radar (Kreutz et al., 2017; Kwok et al., 2017). These snow depths from Operation IceBridge are no longer included in the SUMup dataset as of July 2015, but are included in a separate archive due to their size.

Table 2.3 - The parameters for each snow depth on sea ice measurement in the SUMup dataset with a brief description and the unit of measurement

Column	Description	Unit
Date Taken	Date the data was taken	yyyymm dd
Latitude	Latitude of measurement	Decimal degree
Longitude	Longitude of measurement	Decimal degree
Distance Along Transect	Distance along a transect of in-situ snow depth measurements over sea ice from the initial Lat, Long. Used for snow-depth measurements where point by point Lat, Long was not recorded.	m
Snow Depth	Snow depth measurement	m
Snow Depth Error	Uncertainty in snow depth measurement	m
Density Taken	If density measurement was taken = 1, if no measurement =0.	-
Sea Ice Thickness	Sea ice thickness measurement	m
Sea Ice Thickness Error	Uncertainty in sea ice thickness measurement	m
Sea Ice Type	1=first year ice, 2=multilayer ice, -9999 = unknown	-
Sea Ice Freeboard	Sea Ice freeboard measurement	m
Sea Ice Freeboard Error	Uncertainty in sea ice freeboard	m
Snow Ice Thickness	Snow ice thickness measurement	m
Snow Ice Thickness Error	Uncertainty in snow ice thickness measurement	m

Radar Horizontal Resolution	Horizontal resolution of radar data along track	m
Method	How the measurement was collected (see metadata for more details)	-
Citation	Cited source of data (see metadata for more details)	-

2.3. Spatial and Temporal Data Analysis

The goal of the SUMup dataset is that it can be broadly used by the scientific community for a variety of research studies. Tables 4 and 5 provide the basic descriptive statistics for each subdataset for the Arctic and Antarctic, respectively. These tables provide a coarse overview of the data, however, when using the SUMup datasets subsetting by location, time, depth, etc will likely be required for specific applications. The minimum value for accumulation in the Arctic is -0.004 m WE/a which represents an ablation value from monthly Bamboo Forest measurements at Summit Station, Greenland. In total, there are 5 months, all occurring in separate years, with small negative accumulation measurements from Summit Station. These negative accumulation measurements are likely due to the ablation processes of sublimation or negative wind redistribution; however, a stake measurement alone cannot determine the underlying process of a surface height change.

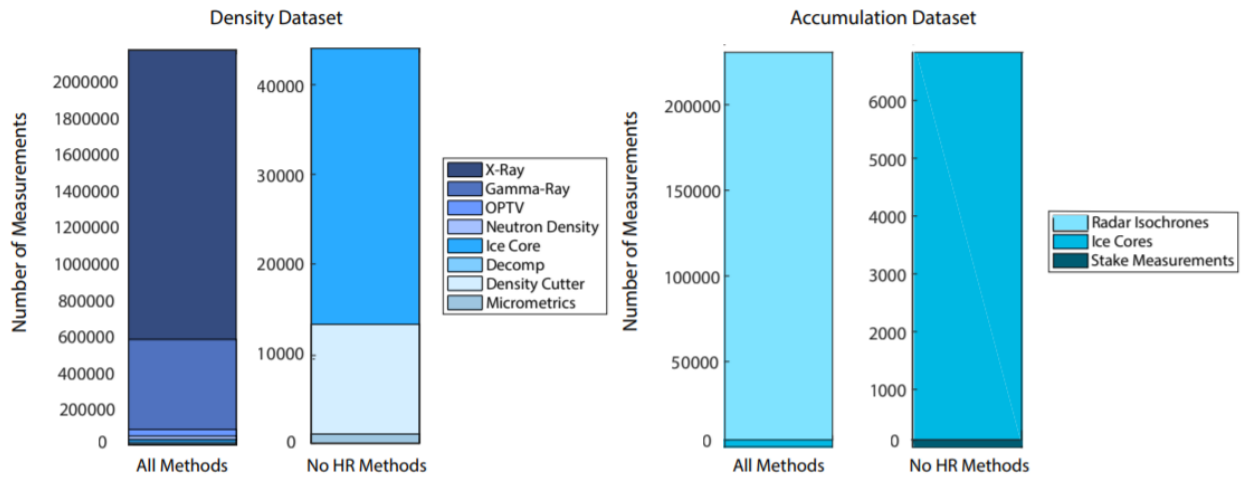

Figure 2.2 - Bar charts showing the measurement methods in the a) density subdataset and b) accumulation subdataset. The left bar in each plot shows the distribution of all methods and the right bar shows the distribution of methods excluding the high-resolution spatial (accumulation) or depth (density) measurements.

Field data collected over the vast polar regions have spatial and temporal sampling bias, as the time, cost and logistics to systematically sample these regions is unreasonable. We describe the SUMup dataset here to elucidate possible bias. All the measurements in SUMup, with the exception of one location, were collected during the spring/summer season for that polar region, roughly April through August for the Arctic and October through February for the Antarctic. Summit Station, Greenland, the only GrIS station with year-round operations, is the one exception in the dataset where temporally-consistent, year-round measurements are taken. Below, we summarize the spatial and temporal distributions of the SUMup dataset by subdatasets. For the two largest subdatasets, snow density and accumulation, we present analysis over the GrIS (Sect. 3.4). This analysis is meant to be an introduction to the dataset and is not exhaustive. We encourage the community to continue to use and more fully exploit this dataset. Figure 2.2 provides a bar graph showing the measurements methods that make up each subdataset showing that measurements techniques with high spatial (e.g. radar isochrones) and

high depth (e.g. neutron probes) resolution dominate the number of measurements in a subdataset, however, they often have limited spatial coverage with respect to the entire region.

Table 2.4 - The descriptive statistics for the all of the Arctic measurements in SUMup including the minimum (min), maximum (max), mean, median, standard deviation (stdev) and number of measurements (N).

Statistic	Snow Density (g cm^{-3})	Accumulation on Land Ice (m WE/a)	Snow Depth on Sea Ice (m)
min	0.0003	-0.004	0.000
max	0.970	2.257	1.2180
mean	0.4717	1.040	0.1852
median	0.3792	1.034	0.1560
stdev	0.2037	0.171	0.1505
N	1642313	144060	89536

Table 2.5 - The descriptive statistics for the all of the Antarctic measurements in SUMup including the minimum (min), maximum (max), mean, median, standard deviation (stdev) and number of measurements (N).

Statistic	Snow Density(g cm^{-3})	Accumulation on Land Ice (m WE/a)	Snow Depth on Sea Ice (m)
min	0.1008	0.0179	0.000
max	0.9379	1.3980	1.900
mean	0.5568	0.1306	0.479
median	0.4252	0.1327	0.430
stdev	0.2272	0.0585	0.363
N	519069	88020	3176

2.3.1 Snow Density

Measurements were compiled of snow/firn density that cover ~306 sites in the Arctic and ~164 sites across Antarctica (Fig. 2.1). The majority of these measurements come from snow pits and ice cores on the GrIS and AIS, however, there are 7 locations of snow density measurements on sea ice in the Bellinghausen Sea. Here, we analyse only the ice sheet measurements.

The density subdataset is dominated (98% of data) by high vertical depth resolution measurements (millimeter scale for ~100 meters) from, X-ray microfocus computer tomography, neutron density methods, gamma-ray attenuation, OPTV, and DECOMP measurements taken on cores or in boreholes at 24 locations in Northern Greenland (Wilhelms, 2000a-d; Miller and Schwager, 2000a-b;, Schaller et al., 2016; Schaller et al., 2017) and 44 locations from Antarctica (Gerland and Wilhelms, 1999; Oerter et al., 1999a-h; Oerter et al., 2000a-j; Graf et al., 2002a-o; Kreutz et al., 2011; Hubbard et al., 2013; Schaller et al., 2017) (Fig. 2.2). Because of the high-depth resolution of these measurements millimeter scale, compared to more typical density measurements at decimeter to meter scale, these data saturate histogram representations of this subdataset. For this reason, we do not use these measurements in the following analysis, thus providing a more realistic overview of the fraction of the density measurements taken throughout time and space.

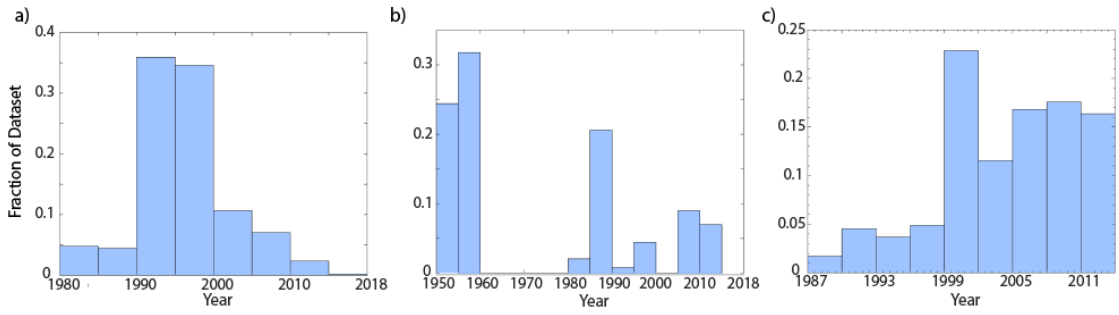

Figure 2.3 - Histograms showing the date taken and associated fraction of the density dataset for A) Antarctica, B) Greenland excluding Summit Station, and C) Summit Station. Please note different time scales on x-axis.

Figure 2.3 provides histograms showing the fraction of density measurements taken by year for Antarctica, Greenland excluding Summit Station, and for Summit Station. (Summit Station was defined as a bounding box of 72N to 73N and 38W to 39W.) Summit Station measurements are plotted separately because this unique site provides the only location on the GrIS with year-round measurements over multiple years. The histograms for Antarctica and Greenland show spikes through time related to major collection campaigns. Antarctic density measurements peak from 1990 to 2000 related to a large amount of ice cores taken in Dronning Maud Land and the Filchner Ronne Ice Shelf (Oerter et al., 1999a-g; Oerter et al., 2000a-i; Graf et al., 2002a-o). Greenland measurements first peak in the early 1950's with measurements from Benson's traverses. They peak again in the late 1980's through the 1990's related to the activities surrounding GISP2 and PARCA ice cores (Alley, 1999; Bolzan and Strobel, 1999(a-g); Mosley-Thompson et al., 2001) and peak for third time in the early 2010's with the Greenland Inland Traverse and the Arctic Circle Traverse cores (Miège et al., 2013; Hawley et al., 2014). Measurements from Summit station steadily increase in time from 1987 to 2014 with a slight peak in the late 1990's and early 2000's related to additional measurements surrounding PARCA and GISP2 projects (Dibb and Fahnestock, 2004; Alley, 1999.

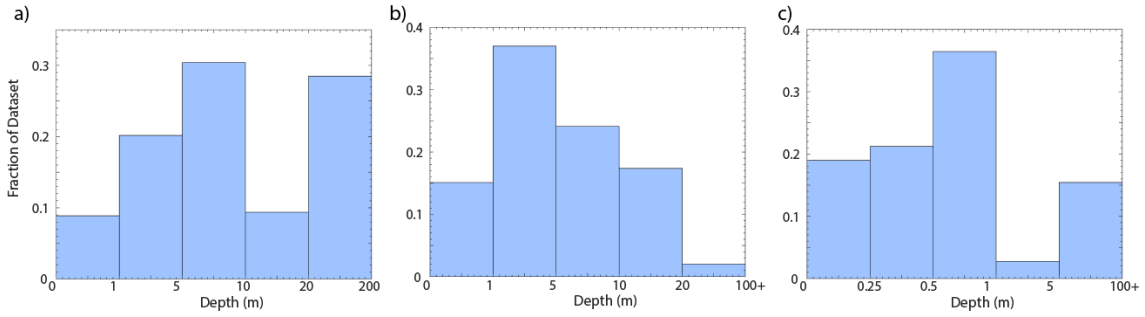

Figure 2.4 - Histograms showing the fraction of the density dataset by mid-point sampling depths for A) Antarctica, B) Greenland excluding Summit Station and C) Summit Station.

Figure 2.4 provides an overview of the distributions of depths sampled by the density subdataset. Overall, the number of measurements decreases with depth. The Antarctic measurements decrease less uniformly with depth which is related to the larger number of deeper ice cores. The majority of Greenland measurements are above 5 meters and there are very few measurements below 20 m demonstrating the large number of shallow cores collected across Greenland. At Summit Station, the majority of the measurements are taken above 1 meter as a result of systematic tasking to dig ~1 m snow pits at approximately monthly intervals since 2003. The deep 100 m plus measurements at Summit come from the GISP2 ice core (Alley, 1999).

2.3.2 Accumulation

Measurements of accumulation over land ice were taken at ~91 locations in Antarctica, and ~36 locations in Greenland. These include two radar traverses that span several hundreds of km in Antarctica, and a 75-km radar traverse in Southeast Greenland. (Fig. 2.1).

62% of the accumulation measurements are from the Arctic, all within Greenland, with <1% of the overall measurements coming from Summit Station. The Antarctic contributes the remaining 38% of the measurements. The accumulation subdataset is dominated (96% of data, Fig. 2.2) by high horizontal spatial resolution (10's of m) radar accumulation measurements taken from 3 ice sheet transects (Fig. 2.1). These data saturate histogram representations of this subdataset and are not used in the following analysis to provide a more realistic overview of the fraction of accumulation measurements taken throughout time and space.

Figure 2.5 provides histograms showing the fraction of accumulation measurements taken by year for Antarctica, Greenland excluding Summit Station, and for Summit Station.

Year, in this case, is defined as the year in which the ice core, snow pit, etc was collected/dug. The histograms for the Antarctic and Greenland show sporadic spikes through time corresponding to major collection campaigns, similar to, yet more exaggerated than in the density subdataset. Antarctic measurements peak in the early 2000's when US ITASE ice cores were collected in West Antarctica (Mayewski et al., 2013). Greenland accumulation measurements peak in the late 1980's with ice cores preparing for the GISP2 core and in the late 1990's when the PARCA ice cores (Mosley-Thompson et al., 2001) were collected. Summit Station has a constant monthly collection of accumulation measurements from August 2003 to August 2016 from the Bamboo Forest measurements (Dibb and Fahnestock, 2004) and represent the only year-round collection of accumulation measurements in the SUMup dataset.

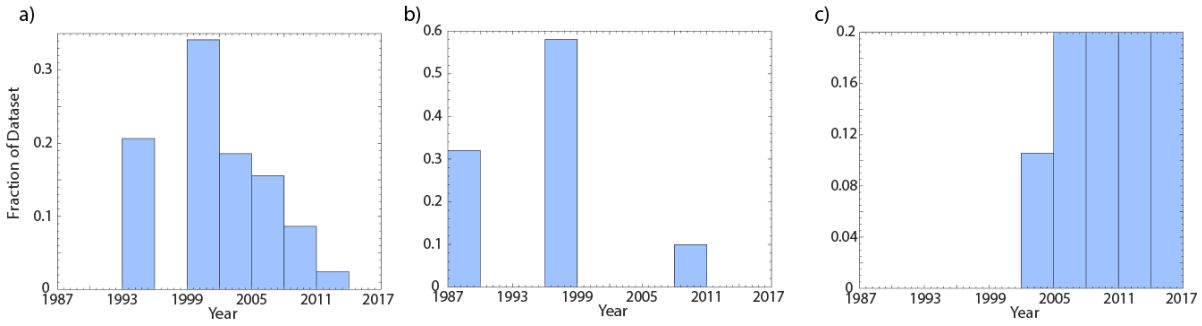

Figure 2.5 - Histograms showing the date taken and associated fraction of the accumulation dataset for each area examined: A) Antarctica, B) Greenland excluding Summit Station, and C) Summit Station.

While understanding the date when accumulation measurements are taken is important, it is also important to understand the year represented by a sample, corresponding to the depth. Figure 2.6 provides the distribution of years when annual accumulation was measured from 1950 to present. Antarctica has a relatively even distribution of accumulation measurements until 2000 when the number of samples decreases. This decrease is due to the fact that many of the cores collected by US ITASE from 2006-2008 in East Antarctica could not be dated to determine

accumulation and also shows that most of the firn cores collected date back to 1950 or later. The Greenland accumulation measurements peak between 1980 and 2000. The mostly shallow ice cores in Greenland, and relatively higher accumulation rates compared to Antarctica, result in less data from 1950 to 1980 in the ice cores. The sharp decline in the 2000's is due to a lack of coring efforts that occurred during that decade in Greenland. Summit Station has a consistent year-round sampling of accumulation from the 2003 to 2016. These systematic measurements significantly outnumber the single measurements per year collected from ice cores at Summit Station that sample the decades before 2000.

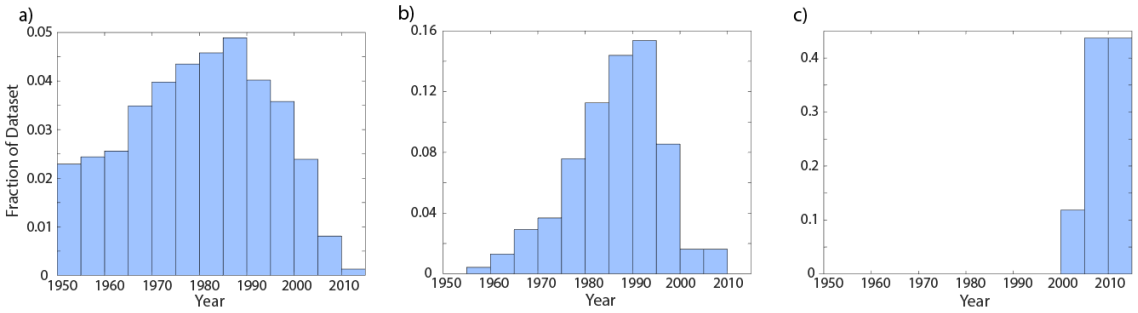

Figure 2.6 - Histograms showing the fraction of accumulation measurements by year for A) Antarctica, B) Greenland excluding Summit Station and for C) Summit Station. Dates are only shown from 1950 forward.

2.3.3 Snow Depth on Sea Ice

The ~92,000 measurements of snow depth on sea ice are mostly from the Arctic representing 97% of the measurements and the Antarctic represents the remaining 3%. The Arctic measurements span from 1990-2018 (Fig. 2.7) while the Antarctic measurements are from 2007. The majority of the observations are from 2010 to 2018, including the CryoVEX 2017, ICEX 2011, BROMEX, and Environment and Climate Change Canada (ECCC) 2014 Snow on Sea Ice campaigns.

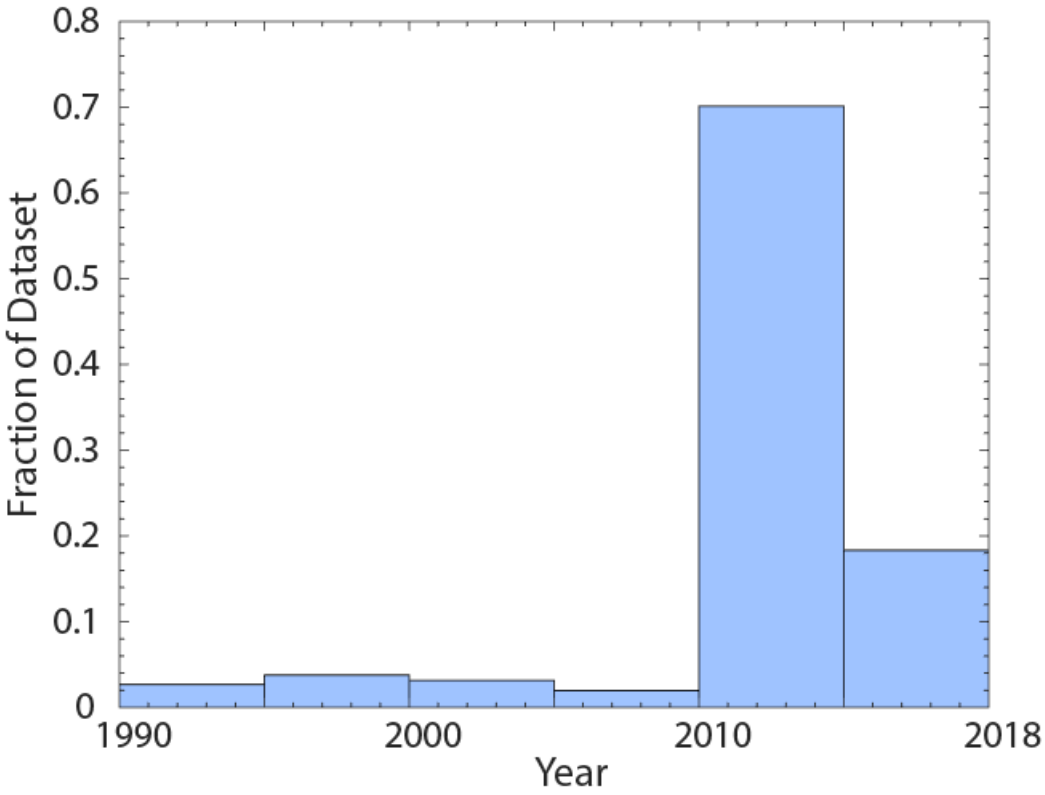

Figure 2.7 - Histogram showing the fraction of snow depth on sea ice measurements by year.

2.3.4 Analysis over the Greenland Ice Sheet

Recent warming over the GrIS, including a melt event in 2012 that covered nearly the entire surface (Nghiem et al., 2012), has increased both snow density and snow accumulation in recent decades (e.g. Morris and Wingham, 2014; Machguth et al., 2016a; Overly et al., 2016). Improved measurements, or models, of density and its evolution with time are needed to reduce uncertainties when converting altimetry measurements into total ice sheet mass balance using altimetry (e.g. Zwally and Li, 2002; Shepherd et al., 2012) and for converting radar isochrones into measurements of accumulation (e.g. Koenig et al., 2016). Many models use mean annual temperature and accumulation to model the spatial and temporal evolution of density (e.g. Herron and Langway, 1980; Reeh et al., 2005; Kuipers Munneke et al. 2015). Some studies, however, show that density models generally underestimate surface (<1 m depth) density

measurements (Koenig et al.., 2016) while other studies point to the importance of the surface boundary condition for density models when comparing to measurements (Kuipers Munneke et al., 2015; Bellaire et al., 2017). Fausto et al. (2018) find mean annual temperature is a poor predictor of snow density from 0-10 cm depth. Here, we look more closely at the density and accumulation measurements within the SUMup dataset over the GrIS and their sampling distributions with respect to temperature, elevation and latitude.

2.3.4.1 Greenland Density distributions with Elevation, Latitude and Temperature

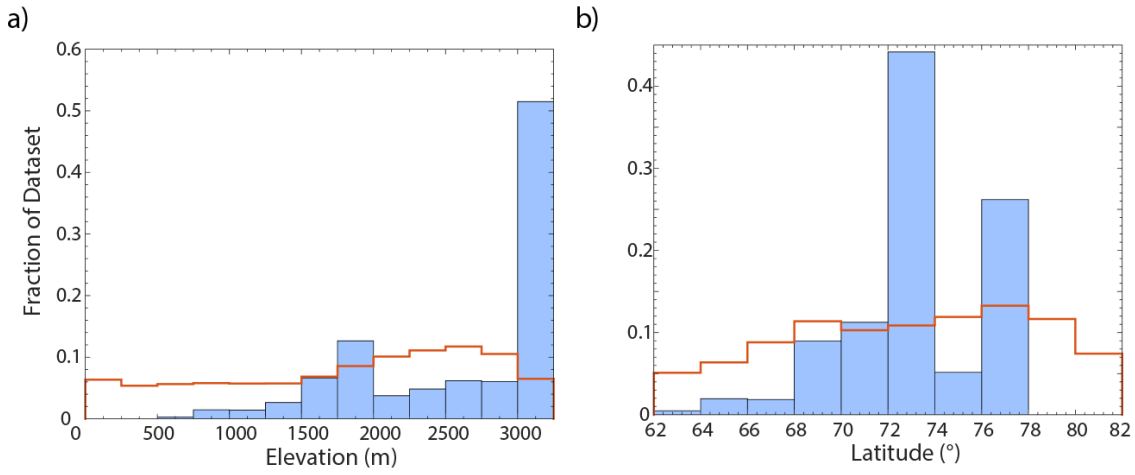

Figure 2.8 - A) Histogram showing the fraction of density subdataset by elevation. Red line is the fraction of elevations for the entire GrIS from CryoSat-2 DEM. B) Histogram showing the fraction of density dataset by latitude. Red line is the fraction of latitudes for the entire GrIS.

Figure 2.8 shows the distribution of density measurements with elevation and latitude compared to the total distribution of elevations and latitudes for the entire GrIS. The fraction of the elevation at 250 m bins (red line of Fig. 2.8) for the Greenland ice sheet is derived from the CryoSat-2 Greenland digital elevation model (DEM; Helm et al., 2014). Figure 2.8 uses similar graphing techniques to those of Fausto et al. (2018) to clearly show sampling bias in the observation dataset. If there were no sampling bias, the fraction of measurements would be

similar to the fraction of values from the DEM. This is not the case. For elevation (Fig. 2.8a) we see that elevations below 3000 m are undersampled, with the exception of the 1750-2000 m bin, and elevations above 3000 m are largely oversampled. The measurements are therefore biased to higher, inland elevations which, if averaged, would likely cause a low bias in sampled densities. Figure 2.8b shows that our dataset is sampled best over central Greenland. More measurements are required from lower elevations and southern (< 70N) and northern (> 78N) latitudes to fill the gaps in the current dataset and reduce spatial bias.

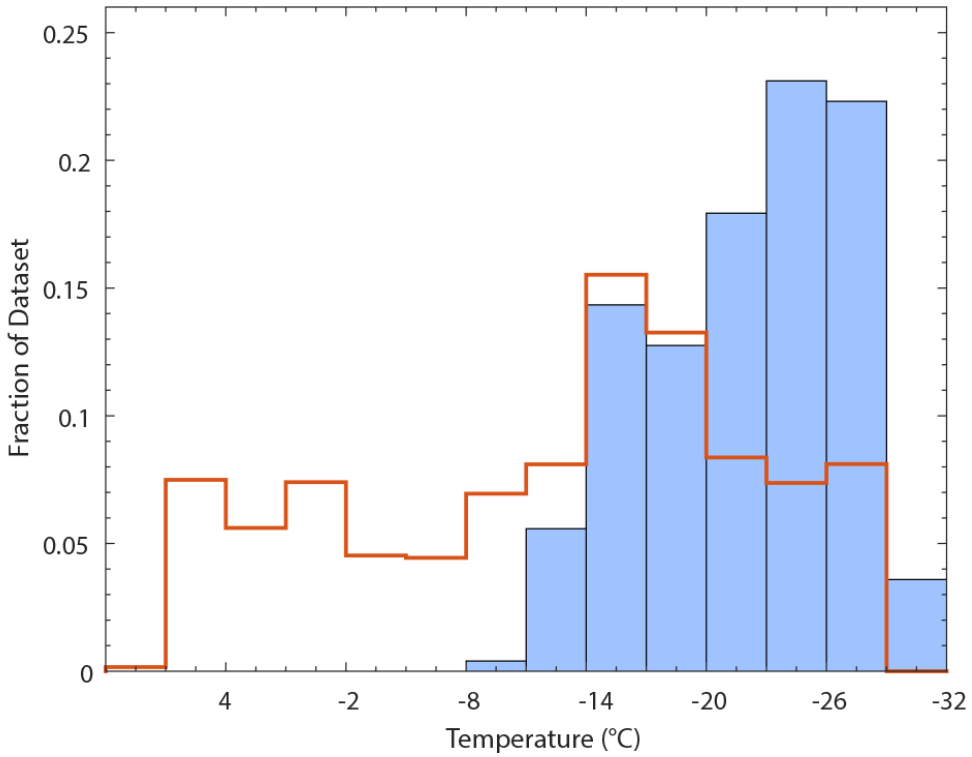

Figure 2.9 - Histogram showing the fraction of the density subdataset by modeled 3m annual air temperature. Red line shows 1990-2015 annual average MAR3.5 model 3m air temperature distribution for each grid cell across the ice sheet.

Because mean annual air temperature is a parameter often used to model density (e.g. Herron and Langway, 1980; Reeh et al.; 2005), Figure 2.9 shows the distribution of density measurements in Greenland in relation to 3 m mean annual air temperature estimated by the Modèle Atmosphérique Régional (MAR) model version 3.5 (Fettweis et al., 2013) with a

horizontal resolution of 25 km. We used the National Centers for Environmental Prediction–National Center for Atmospheric Research Reanalysis version 1 (NCEP-NCARv1) forced MAR 3.5 simulation (run from 1948–2015) to find the mean annual 3 m air temperature for the year the corresponding to when the density measurement was taken. The NCEP-NCAR forcing was chosen because it is more reliable than ERA forcings (Fettweis et al., 2017). The red line in Fig. 2.9 shows the distribution of annual average temperatures (derived from 1990-2015) for the entire GrIS. Figure 2.9 clearly shows a preferential sampling of GrIS regions with lower temperatures. Cold temperatures (-20 deg C and below) are oversampled in the density dataset while temperatures above -14 deg C, which make up ~30% of the GrIS, make up less than 6% of the sampled densities. As with elevation, the density sampling distribution by mean annual temperatures likely results in a low-density bias when trying to characterize the entire GrIS. In general, the density measurements in SUMup across the GrIS oversample cooler, inland regions and undersample coastal, warmer regions.

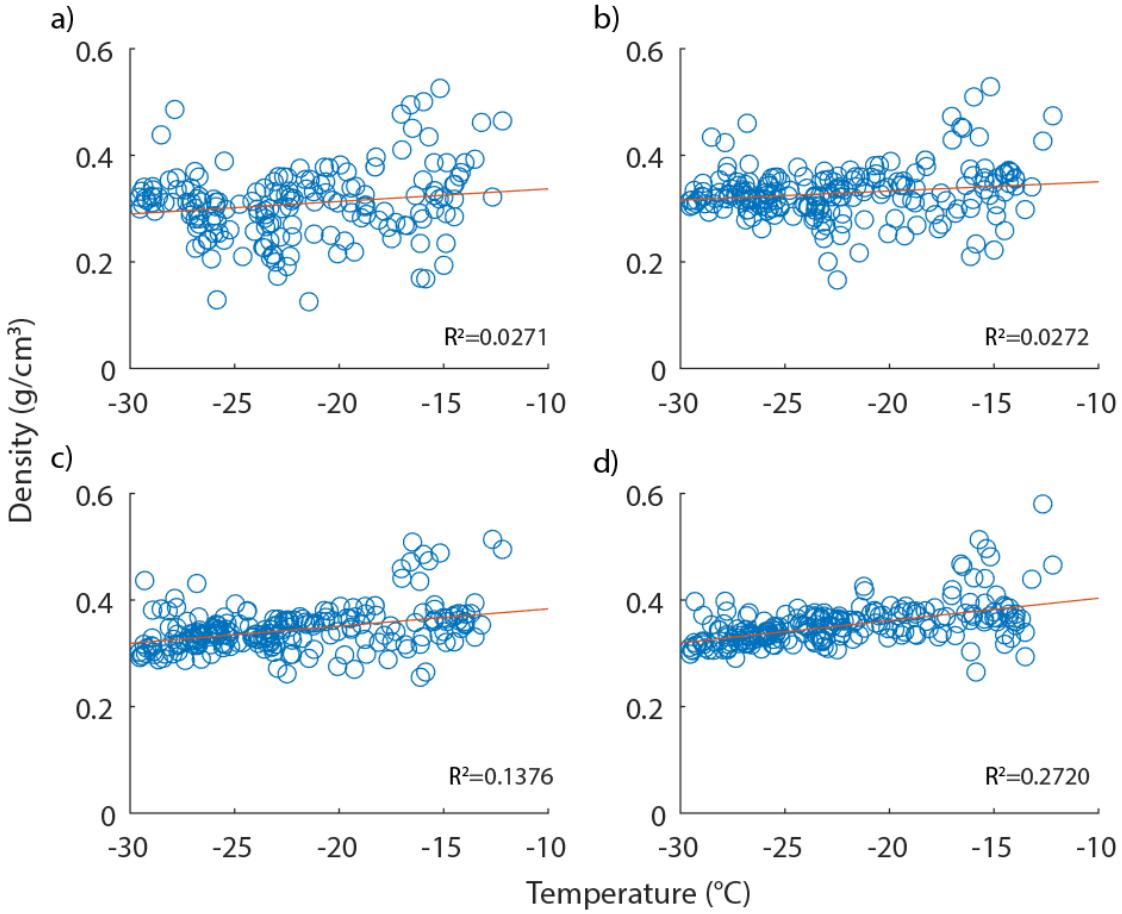

Figure 2.10 - Scatterplot showing the MAR 3.5 modeled mean annual 3 m air temperature in the year the density was measured compared to the mean density in top A) 10 cm, B) 25 cm, C) 50 cm, and D) 100 cm.

Figure 2.10 plots all sites in Greenland with density measurements coincidently sampled to depths of 10, 25, 50 and 100 cm compared to the mean annual temperature. No clear relationship (Pearson Correlation coefficient, R^2 = 0 to 0.137) between mean annual temperature and density is seen in our data until ~1 m depth (R^2=0.272) where higher temperatures correspond to higher density. This result suggests that in the top 1 m of snow/firn on the GrIS, in the colder, more inland areas, temperature may not be the primary variable leading to densification. Solar radiation, layering in firn, and wind processes (e.g. Liston et al., 2007; Hörhold et al., 2011) are likely important in these regions and require snow density models that account for these processes. Due to the spatial sampling bias in this dataset, melt processes are

likely not a primary process in determining snow density for these measurements, however, melt processes will contribute more in the future (Nghiem et al., 2012; McGrath et al., 2015)

2.3.4.2 Accumulation distributions with Elevation and Latitude

Snowfall over the GrIS can also be parameterized by elevation and latitude. Figure 2.11 shows the distributions of the accumulation measurements over the GrIS by elevation and latitude. As with the density measurements the accumulation measurements all come from high elevations on the GrIS (>1750 m) with the highest elevations (>3000 m) being largely oversampled. The sampling across latitudes is the most evenly distributed, however, latitudes above 78 N represent a gap in the dataset. We do not compare the accumulation subdataset with mean annual temperatures here because each year of accumulation has a different mean annual temperature associated with it. We deem it beyond the scope of this analysis and suggest this as a future study that could be researched using the SUMup dataset.

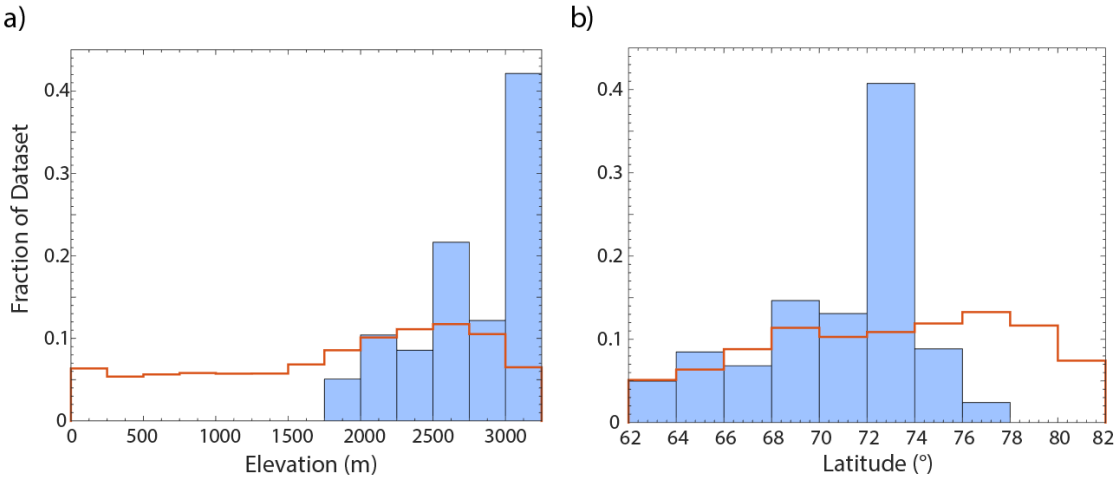

Figure 2.11 - A) Histogram showing the fraction of accumulation subdataset by elevation. Red line is the fraction of elevations for the entire GrIS from CryoSat-2 DEM. B) Histogram showing the fraction of accumulation dataset by latitude. Red line is the fraction of latitudes for the entire GrIS.

2.3.4.3 Year-round density and accumulation measurements from Summit Station.

Summit Station is the only site in the dataset, and on the GrIS, that has been systematically sampled for density and accumulation on a nearly monthly basis. Hence, it is the only location on the GrIS to watch the long-term, decadal, seasonal evolution of snow surface density. Figure 2.12 shows the monthly mean surface density to depths of 10 cm, 25 cm 50 cm and 100 cm. A seasonal cycle is evident in the 10 cm and 25 cm depth mean densities with a decrease (trough) in density in late summer (August/September) and an increase (peak) in April. The decrease in summer density is likely due to surface hoar, a low-density snow crystal formation that is well known to form at Summit Station in the summer when wind speeds are low and humidity relatively high (e.g. Alley and other, 1990; Albert and Schultz, 2002; Dibb and Fahnestock, 2004). As wind speeds increase and water vapor decreases in the winter the surface snow increases in density. The seasonal signal in density is damped out by 1 m depth at Summit Station. Figure 2.12 also shows larger natural variability in average density measurements in the top 50 cm compared to the top 100 cm. This is expected as the deeper snow is more insulated from atmospheric and radiative processes in this dry-snow-zone location.

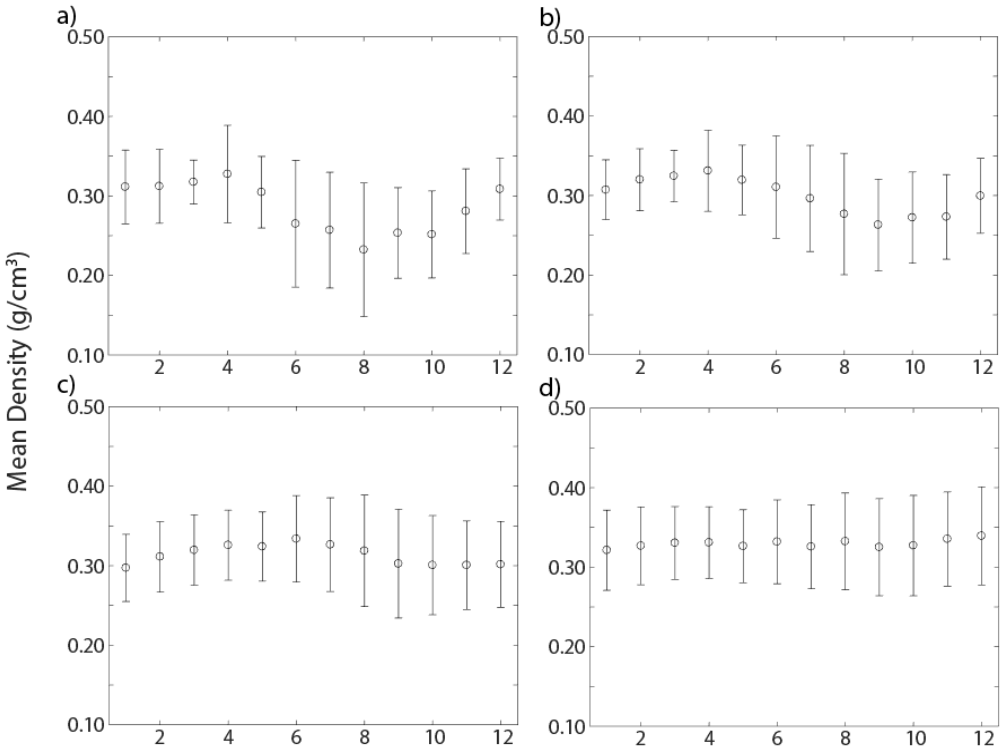

Figure 2.12 - Plot of mean density (circle) and +/- 1 standard deviation (whiskers) for each month at Summit Station, Greenland for a) 10 cm b) 25 cm c) 50 cm d) 100 cm

Figure 2.13 show the monthly mean accumulation at Summit Station. Accumulation is highly variable with slightly lower values in the early Summer months (May/June/July). Dibb and Fahnestock (2004) also showed a similar trend in stake measurements and Summit Station from just 2 years of data and explained that the summer season may not actually be seeing a decrease in accumulation but that thinning layers, densification, may be causing the stake measurements to not rise as much in the summertime compared to the wintertime when a snowfall event occurs. Determining if there is a true decrease in summer accumulation or increase in snow/firn compaction rate at Summit Station requires additional research.

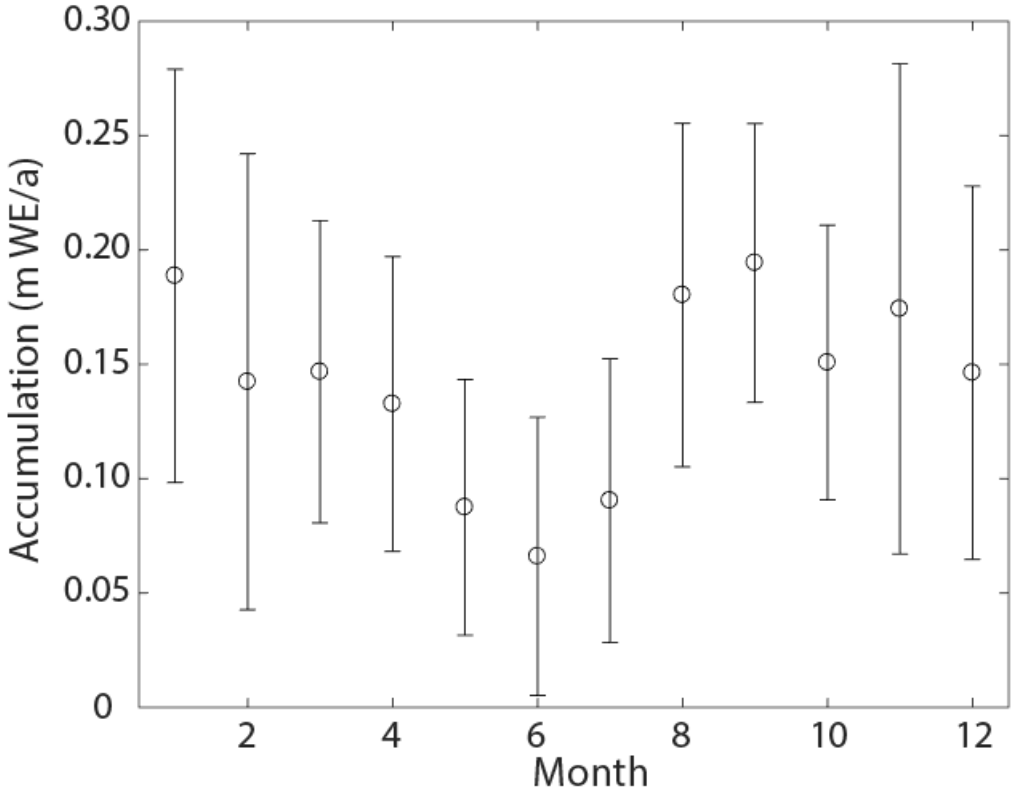

Figure 2.13 - Plot of mean accumulation (circle) and +/- 1 standard deviation (whiskers) for each month at Summit Station, Greenland.

2.4 Data Availability

The SUMup dataset is currently available through the Arctic Data Center. It hosts our three subdatasets in both csv and netcdf formats along with metadata files to further explain the methods and citations. The dataset will be updated annually.

2.5 Discussion and Conclusion

We present and describe the SUMup dataset, an expandable, community-based dataset of field measurements of surface mass balance components that is consistent in format, has clearly defined metadata, and is publicly available. The subdatasets include compiled measurements of snow/firn density (doi:10.18739/A2JH3D23R), accumulation on land ice

(doi:10.18739/A2DR2P790), and snow depth on sea ice (doi:10.18739/A2WS8HK6X) from the Arctic and Antarctica.

As seen in SUMup, the measurements over the GrIS and AIS are sporadic in time and space, peaking during specific field campaigns and lapsing in between which makes monitoring change with and understanding processes from field measurements difficult. This is especially prevalent for parameters like density and accumulation that change with both seasonal and climatic atmospheric conditions. Overall, there are gaps in density and accumulation data from ~2000 forward and from locations on the periphery of the ice sheets. While there currently is a temporal gap in the most recent decades, we note that the GreenTRaCs traverses have collected cores across the GrIS in 2016 and 2017, including at previous PARCA sites. Once these cores are processed, they will be able to help fill some of the time gaps for the GrIS (R. Hawley, personal communication).

Density and accumulation measurements of the GrIS oversample cooler, inland regions and undersample coastal, warmer regions. Oversampling these regions may lead to an underestimation of the total average surface density, especially in the summer season, when the measurements are undersampling regions with significant melt processes that increase density. No clear relationship between mean annual temperature and density is seen in the data until a depth of 1 m where a relationship between higher temperatures and increased density is observed. This suggests that additional parameters, such as wind speed and radiative balance, should be considered when modeling density for the GrIS at SUMup density locations and depths above 1 m. Summit Station, Greenland is the only location with year-round density and accumulation measurements in the dataset, and on the GrIS, and seasonal cycles are evident in accumulation rate and density for depths above 50 cm.

Our analysis of the SUMup dataset shows gaps in ice sheet measurements in the recent decades and in low elevation regions on the periphery of the ice sheets. These are the exact regions where climate change will and has had the largest effects on the Greenland and Antarctic ice sheets (eg. Shepherd et al., 2012; IMBIE Team, 2018; Enderlin et al., 2014) and where additional future measurements are warranted.

We encourage the cryospheric community to contribute additional field data to the SUMup dataset. We also encourage the cryospheric community, including modelers and scientists working in the field of remote sensing to use this dataset for model validation for surface mass balance and satellite- or airborne-sensor algorithm development. SUMup is a dynamic, living dataset and is expected to be expanded and released annually.

2.6 Acknowledgements

LM and LK acknowledge the National Science Foundation grant PLR 1603407 for funding this work. We thank our two anonymous reviewers and our editor, Reinhard Drews, for providing thorough insight and commentary that helped to greatly improve the quality of the manuscript. *Publication of this article was funded by the University of Colorado Boulder Libraries Open Access Fund.*

3 Accumulation rates (2009-2017) in Southeast Greenland derived from airborne snow radar and comparison with regional climate models

This chapter is adapted and reformatted from:

Montgomery, L., Koenig, L., Lenaerts, J. T. M., & Kuipers Munneke, P. (2020). Accumulation rates (2009–2017) in Southeast Greenland derived from airborne snow radar and comparison with regional climate models. *Annals of Glaciology*, 1–9. https://doi.org/10.1017/aog.2020.8

3.1 Introduction

Driven by rising atmospheric temperatures, the Greenland Ice Sheet (GrIS) is losing mass at an accelerated rate (Bevis et al., 2019; Kjeldsen et al., 2016; Hanna et al., 2013, Shepherd et al., 2012; van Angelen et al., 2013; van den Broeke et al., 2009). The total mass loss of the GrIS over the 2010-2018 period is estimated to be 286 ± 20 Gt yr^{-1}, with 49 ± 3 Gt yr^{-1}, coming from Southeast Greenland (Mouginot et al., 2019). In the remainder of the 21st century, it is expected that increased meltwater runoff, and the associated decrease in surface mass balance (SMB), will dominate solid ice discharge as the GrIS's largest contribution to sea level rise (e.g. Enderlin et al., 2014). SMB is defined as snow accumulation and wind-driven snow redistribution (through erosion or redeposition), minus runoff, where accumulation is the difference between snowfall and evaporation/sublimation (Lenaerts et al., 2019). In this study, we ignore redistribution, as it is two orders of magnitude smaller than snowfall integrated across Southeast Greenland (Lenaerts et al., 2012). Although it is not the focus of this study, redistribution likely explains a large portion of the small-scale (<1 km) variability in accumulation (Dattler et al., 2019). Additionally, there is little-to-no runoff expected in the period we observe between the last peak melt and mid-spring. Therefore, we assume SMB to be equal to accumulation in this study.

Southeast Greenland, which we define as the region between 45ºW to 33ºW and 60ºN to 67ºN (Fig. 3.1), encompasses the area with the highest accumulation rates on the GrIS (Shepherd et al., 2019; Berdhal et al., 2018). Regional climate models (RCM) suggest that Southeast GrIS receives ~30% of the total GrIS snowfall (Miège et al., 2013). Therefore, interannual variations in this region strongly influence the total GrIS mass balance, even determining the sign of the total mass balance during some years (Burgess et al., 2010). However, evaluating the rate and pattern of accumulation in climate models is challenging, as there are very few in-situ observations available on the Southeast GrIS (e.g. Ettema et al., 2009; Hanna et al., 2011; Lucas-Picher et al., 2012; van den Broeke, 2016; Fettweis et al., 2017; Montgomery et al., 2018).

Using airborne observations, we can address the lack of in-situ accumulation observations in Southeast Greenland. A first compilation of GrIS accumulation rates derived from NASA Operation IceBridge (OIB) airborne snow radar was presented by Koenig et al. (2016) for the period of 2009 to 2012. Here, we extend the time series of radar-derived accumulation rates to 2017 focusing on Southeast Greenland, using observationally constrained, gridded firn density products to convert radar-derived depth to accumulation. In addition, we compare these radar-derived accumulations to two RCMs, the Modèle Atmosphérique Régional version 3.9 (MAR) and the Regional Atmospheric Climate Model version 2.3p2 (RACMO2). The goal of this work is to understand the magnitude, spatiotemporal variability, and uncertainty of radar-derived accumulation in Southeast Greenland, and to provide an initial assessment of RCM performance in simulating Southeast Greenland SMB.

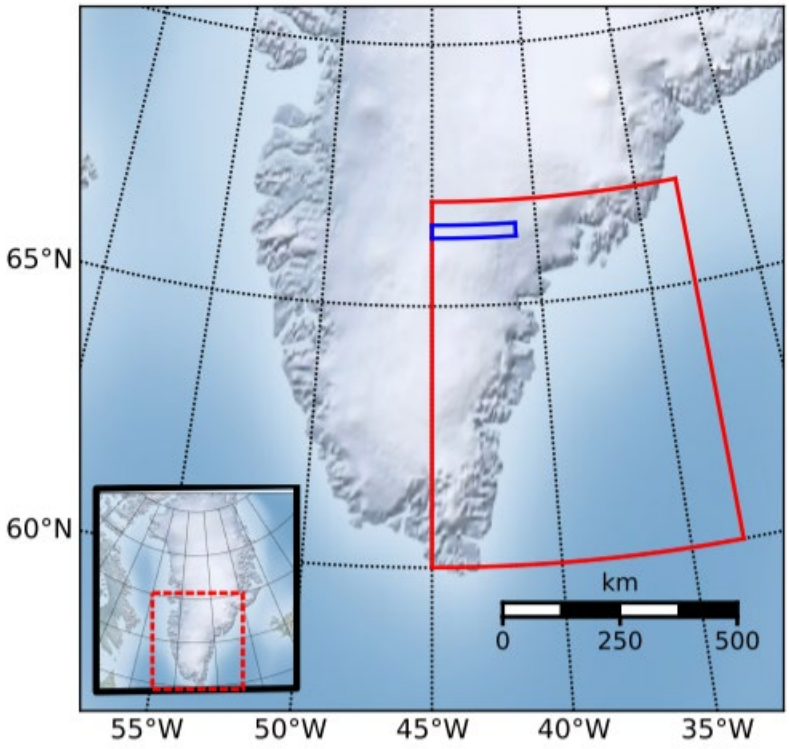

Figure 3.1 – Overview of our bounded study region in Southeast Greenland (red) and flight-line case study region (blue). Inlaid box is a map of Greenland with a box around the zoomed area (dashed red).

3.2 Observations, Instruments, and Models

3.2.1 Operation IceBridge Airborne Snow Radar Data

From 2009-2019, the Center for Remote Sensing of Ice Sheets (CReSIS) at the University of Kansas operated the snow radar onboard the NASA P3-B and DC8 aircraft during OIB missions. We use the radar data from 2009-2017 due to data and model output availability at the time of the study. This radar maps internal annual accumulation layers ranging from 10 cm to >1 m (Panzer et al., 2013). These data, IceBridge snow radar L1B Geolocated Radar Echo Strength Profiles, Version 2, are available from the National Snow and Ice Data Center (NSIDC; Paden et al., 2014). The snow radar detects isochronal layers in the firn and are dated by assuming annual

stratigraphy and counting each layer down from the surface (Medley et al., 2013; Koenig et al., 2016). Annual layering of accumulation can be detected because radar reflection horizons represent contrasts in the material's dielectric permittivity, attributed to isochronous buried sequences, ice crusts, and snow layers (Medley et al., 2013). The radar uses a frequency-modulated continuous wave (FMCW) architecture that operates in the 2–6.5 GHz frequency range with a vertical resolution of ~5 cm (Medley et al., 2013; Panzer et al., 2013). We chose this radar over the other radars aboard OIB because of its high vertical resolution and shallower penetration depth that allow the radar to measure recent accumulation rates (past ~1 to 20 years).

3.2.2 In-Situ Density Observations

The SUMup (SUrface Mass balance and snow depth on sea ice working group) dataset provides snow and firn density profiles and accumulation measurements across the entire GrIS (Montgomery et al., 2018). Density profiles from 306 locations on the GrIS are used to compare modeled to observed densities in the top meter of firn (Fig. 3.2a/b; Renaud, 1959; Ohmura, 1991, 1992; Alley, 1999; Bolzan and Strobel, 1999a–g, 2001a, b; Miller and Schwager, 2000a, b; Wilhelms, 2000a–d; Mosley-Thompson et al., 2001; Bales et al., 2001; Conway, 2003; Dibb and Fahnestock, 2004; Dibb et al., 2007; Harper et al., 2012; Benson, 2013, 2017; Miège et al., 2013; Hawley et al., 2014; Koenig et al., 2014; Baker, 2016; Chellman, 2016; Machguth et al., 2016; Mayewski and Whitlow, 2009a–d; Schaller et al., 2016, 2017; Cooper et al., 2018; MacFerrin et al., 2018a,b). We use thirty-five density profiles from Southeast Greenland to compare with RCM density in the top five meters. Most density profiles were retrieved from firn cores (98%) with average core depths greater than 10 meters while a small fraction were taken from snow pits (2%) with depths less than 2 meters.

3.2.3 MAR and RACMO2 simulated SMB

We use our radar-derived observations to evaluate the accumulation simulated by two RCMs (MAR and RACMO2) over Southeast Greenland. MAR and RACMO2 are forced at their lateral boundaries by a reanalysis data set (ERA-Interim 1979-2018) (Noël et al., 2016; Fettweis et al., 2017; Delhasse et al., 2018). Monthly gridded SMB from MAR (originally 15 km) and RACMO2 (originally 5.5 km) is downscaled to a 1-km spatial resolution, and provide the atmospheric input used to derive density profiles (see Crocus and FDM modelled density section). The RCM SMB products used here are downscaled based on the local regression to elevation from higher resolution digital elevation models (Noël et al., 2016; Fettweis, personal communication, 2019). These downscaled accumulation model products are used to compare with our radar-derived accumulation. Previous studies have shown that both MAR and RACMO2 SMB products compare well to available in-situ observations on the GrIS (Fettweis et al., 2017; Noël et al., 2018), although an evaluation of Southeast GrIS has so far been hampered by the paucity of observations in that region.

3.2.4 Crocus and FDM modelled density

Spatially gridded density profiles are taken from two firn models, Crocus and the Firn Densification Model of the Institute for Marine and Atmospheric research Utrecht (IMAU-FDM v2.3p2), (referred to hereafter as Crocus and FDM, respectively). Crocus model output, available at a horizontal resolution of 15 km, is forced with atmospheric data and mass fluxes from MAR (Fettweis et al., 2017). Crocus is a snow model that simulates energy and mass evolution of a snow cover at a given location and provides vertical density profiles (Brun et al., 1989; Brun et al., 1992). The FDM model output, available at a 5.5 km spatial and 10-daily (instantaneous) temporal resolution, is a time-dependent, one-dimensional model that keeps track

of the density and temperature in a vertical firn column, and is driven by atmospheric input originating from another regional climate model, RACMO2 (Kuipers Munneke et al., 2015; Ligtenberg et al., 2018). Model output prior to our study period is used to understand density differences across the GrIS since the majority of observations from SUMup are not from 2009-2017 (Fig. 3.2). Both densification models can simulate liquid water content, percolation, layer saturation, and refreezing in firn. The FDM can store liquid water through capillary forces, which best simulates the processes occurring in the percolation zone in Southeast Greenland (Ligtenberg et al., 2011). The FDM densification rate in Southeast Greenland is tuned to density observations from 22 dry firn cores (Kuipers Munneke et al., 2015).

3.3 Methods

To derive accumulation rates ($\dot{b}$) from radar observed firn layers we use a combination of two equations following standard methods (Medley et al., 2013; Das et al., 2015; Koenig et al., 2016). Equation 1 shows the water-equivalent accumulation rate, $\dot{b}$, in m w.e. a^{-1} at along-track location, x, using a snow density profile, $\rho(x)$, in kg m^{-3}, with a as the age of the layer in years from the date of radar data collection, and ρ_w as the density of water in kg m^{-3}.

Equation 1:
$$\dot{b}(x) = \frac{z(x)\rho(x)}{a(x)\rho_w}$$

The two way travel time of the radar (TWTT) in seconds is converted to depth, z, using a dielectric mixing model for ice-air mixture from Looyenga (1965) in Equation 2, where c is the speed of light in m s^{-1}, ρ_i is ice density in kg m^{-3}, and ε'_i is the dielectric permittivity of pure ice.

Equation 2:
$$z = \frac{TWTT(x)\rho(x)c}{2\left(\frac{\rho}{\rho i}\left(\varepsilon' i^{\frac{1}{3}}-1\right)+1\right)^{3/2}}$$

Equations 1 and 2 are combined to Equation 3.

Equation 3: $$\dot{b}(x) = \frac{TWTT(x)\rho(x)c}{2a(x)\rho_w(\frac{\rho}{\rho i}\left(\varepsilon'_i{}^{\frac{1}{3}}-1\right)+1)^{3/2}}$$

3.3.1 Selecting Flight Tracks

Any flight tracks that were included our study area, 45ºW to 33ºW and 60ºN to 67ºN, were downloaded from NSIDC and run through a semi-automated layer picker software (detailed in Koenig et al., 2016). The flight track missions that were most often used included "Southeast Coastal", "Southeast Glaciers", "Helheim-Kangerdlugssuaq", but vary depending on the year. Often, accumulation rates could not be derived because the layers were not clearly identifiable due to topography, flight maneuvers, or meltwater percolation disrupting firn stratigraphy. There are no annual accumulation measurements available in SUMup coincident in space and time to compare with our new OIB-derived accumulation. Instead, radar-derived accumulation rates are directly compared to modelled accumulation, because our observations reflect all of the individual components of SMB throughout the winter season (when melt and runoff are absent), i.e. snowfall and sublimation/evaporation.

3.3.2 Density profiles and associated uncertainties

In Southeast Greenland, only 35 observed density profiles, *ρ(x)*, are available from SUMup. Therefore, we seek to increase the coverage of this region using the FDM and Crocus firn models that have gridded density products available. A simple model, such as a semi-empirical firn densification model that assumes a dry firn column, as described by Herron and Langway in 1980, cannot be used to approximate density profiles in Southeast Greenland, because it is a region where liquid water is commonly found in the firn. To assess how these models perform and which to use for our study, we compare their output against observations at corresponding times and locations. The FDM density profiles were linearly interpolated in time to find daily values, since the original data is only output every ten days. There is no FDM model

output available beyond 2016, so an average 2009-2016 density profile was used to derive accumulation for 2017, which provides a conservative estimate. If no day was associated with the measurement in the SUMup dataset, we assigned the date to be May 1st, as in Koenig et al. (2016).

To determine which gridded density product to use to derive accumulation and its associated uncertainty, we examine densities from models compared to observations in the top meter and five meters of snow across Greenland spatially. The comparison of observed and modelled density in the top meter of snow shows us how well surface processes are being represented. In the top meter across all of Greenland for 306 unique locations from the SUMup dataset (Fig. 3.2a), Crocus underestimates densities by 50 kg m^{-3}, similar to the results of a 60 kg m^{-3} underestimation from Alexander et al. (2019). In Southeast Greenland specifically, densities are being underestimated by an average of 80 kg m^{-3} in the top meter of firn, with an average observed value of 362 ± 45 kg m^{-3} and an average Crocus output value 294 ± 29 kg m^{-3}. The FDM shows only a slight overestimation of densities within the top meter by 20 kg m^{-3} across all of Greenland (Fig. 3.2b). In Southeast Greenland, the FDM agrees well with observations, with densities overestimated by 30 kg m^{-3} and an average density value of 343 ± 24 kg m^{-3}. The FDM has less variability than Crocus as well as a lower root mean squared error (RMSE) (0.06 for FDM vs. 0.11 for Crocus, Fig. 3.2c) showing that it better represents densities in the top meter of the GrIS. However, neither model is capturing small scale variation in observed densities likely due to grid resolution (Fig. 3.2c). Our uncertainty is defined as the absolute difference between the modeled density and observed density in the top meter, which is determined to be 19% and 5% for Crocus and FDM, respectively. We use these errors as a measure for the final radar-derived accumulation uncertainty, because this layer comprises most (if not all) of the winter

accumulation.

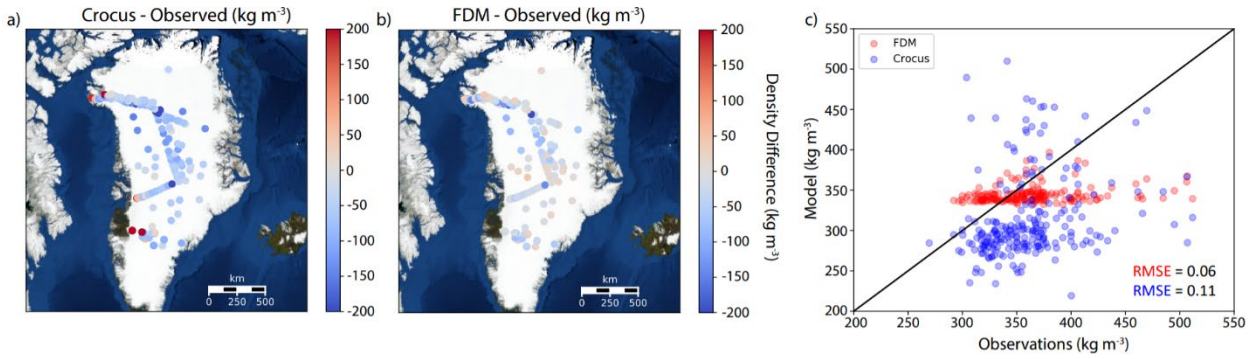

Figure 3.2 - Difference of average density (kg m^{-3}) in the top meter between a) Crocus or b) FDM and SUMup observations across Greenland. c) Scatterplot of Crocus and FDM densities vs. observations.

Further, we analyze the density profiles of both observations and models to the depth of the highest radar-derived accumulation rates we have observed, ~5 meters snow water equivalent. The average density of the top 5 meters of snow/firn from SUMup observations in Southeast Greenland (representing 35 unique cores) is 437 ± 59 kgm^{-3} (Fig. 3.3). Below the top meter in Crocus, the densification rate slows because there is less pore space available to compact and it is compensating for the excessive densification rate above. This compensation of density values allows Crocus to have a low bias for the top 5 meters with an average value of 432 ± 90 kg m^{-3}. The FDM density profile agrees better with the observations overall, showing a similar densification rate, although it still slightly underestimates the average density values (404 ± 50 kg m^{-3}). We use the FDM density profiles to derive accumulations and in our analysis because they are within the uncertainty range of the observations, i.e. ± 1 standard deviation, though we also derive accumulations using the Crocus profiles only to quantify the total uncertainty.

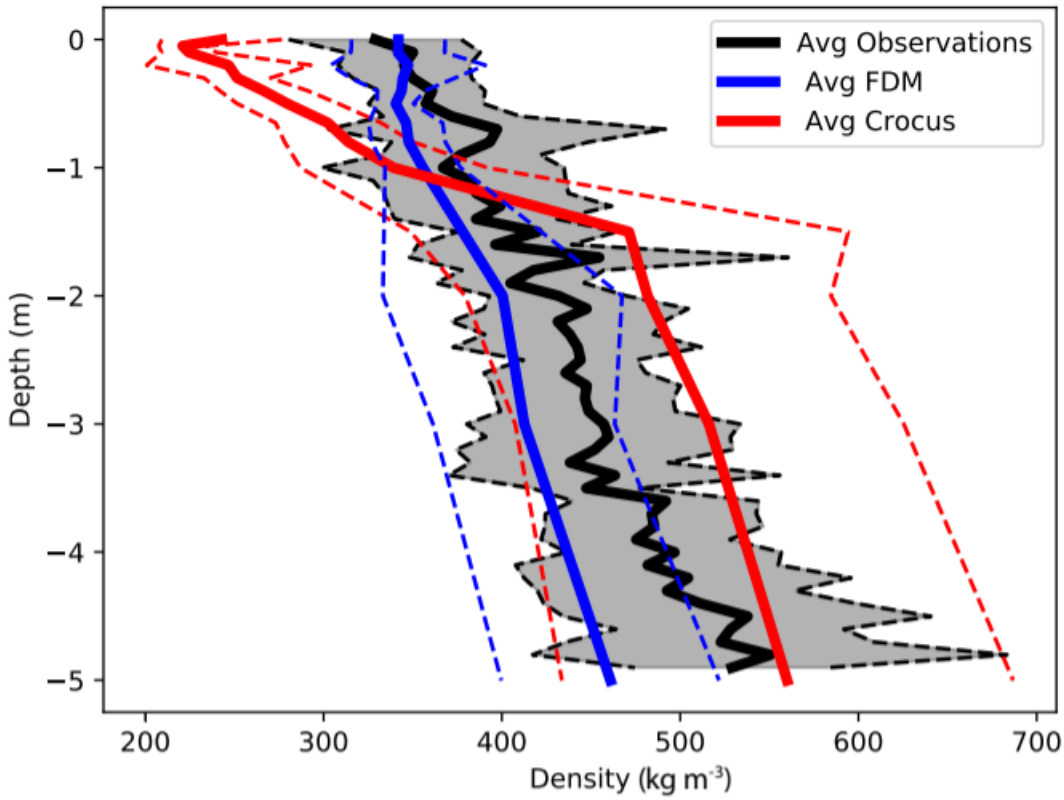

Figure 3.3 - Average density profile of the top 5 meters of all observed SUMup (N=35) cores (black) in Southeast Greenland and co-located FDM (blue), and Crocus (red) in space and time. The standard deviation is shown in the dashed line of the same color.

3.3.3 Determining layer age and total accumulation uncertainty

Depth or layer ages, *a*, are determined by assuming that spatially continuous isochronal layers are annually resolved. An automated layer picker (Koenig et al., 2016) was used to find the peak density gradients to determine layers ages that were verified and adjusted manually as necessary using a graphical user interface. The first layer would represent 10 months instead of the full year in our study. This is because it encompasses the springtime measurement from the snow radar aboard OIB (often taken in April/May) back to the previous years melt, causing a peak in the density gradient in July ±1 month (Koenig et al., 2016). The second source of error

occurs during manual adjustment of the picked layers and is estimated to be a maximum of ±3 range bins, or ~ 8 cm (Koenig et al., 2016). In our study, this accounts for a range of 7 to 13% errors (10% on average) depending on accumulation rates, which is similar to the mean error of 7% found in Koenig et al. (2016). Combining this with the errors from the density models we get a total error range on the radar-derived accumulation of 11% (FDM) to 21% (Crocus) depending on the firn model used. The results we show are only representative of the radar-derived accumulations using the FDM density profiles.

3.4 Results

3.4.1 Radar derived accumulation rates

A time series of accumulation rates and their uncertainties were derived from OIB snow radar from 2009 to 2017 (Fig. 3.4). Average radar-derived accumulation across all of Southeast Greenland for each year ranges from 0.5 to 1.2 m w.e. with higher values near the coast and decreasing values as you move inland. The year-to-year variable acquisition of observations, is due to the variations in flight lines and data quality. An increase in spatial coverage from 2009 to 2011 can be explained by a greater number of flights and adjustments to the radar antenna leading to better data quality (Koenig et al., 2016). Resulting from the improved data quality, the percentage of measurements that were able to be derived from all flight lines increased from ~40% to 70% in those years. From 2012 to 2014, there was less coverage, with only one flight line obtained in 2013 and three in 2014, likely due to unfavorable flying conditions in those seasons, along with only ~22-46% of the data of sufficient quality. 2015 and 2017 provide more complete spatial coverage, with more consistent flight paths as well as ~58% to 65% of the radar data containing discernable layers. In 2016, there was reduced radar performance on many

flights leading to a lack of quality data (36%). The number of flights and area covered varies by year (Supplementary Table 1, Fig. 3.4), with peak coverage in 2011 (70%) and 2015 (65%).

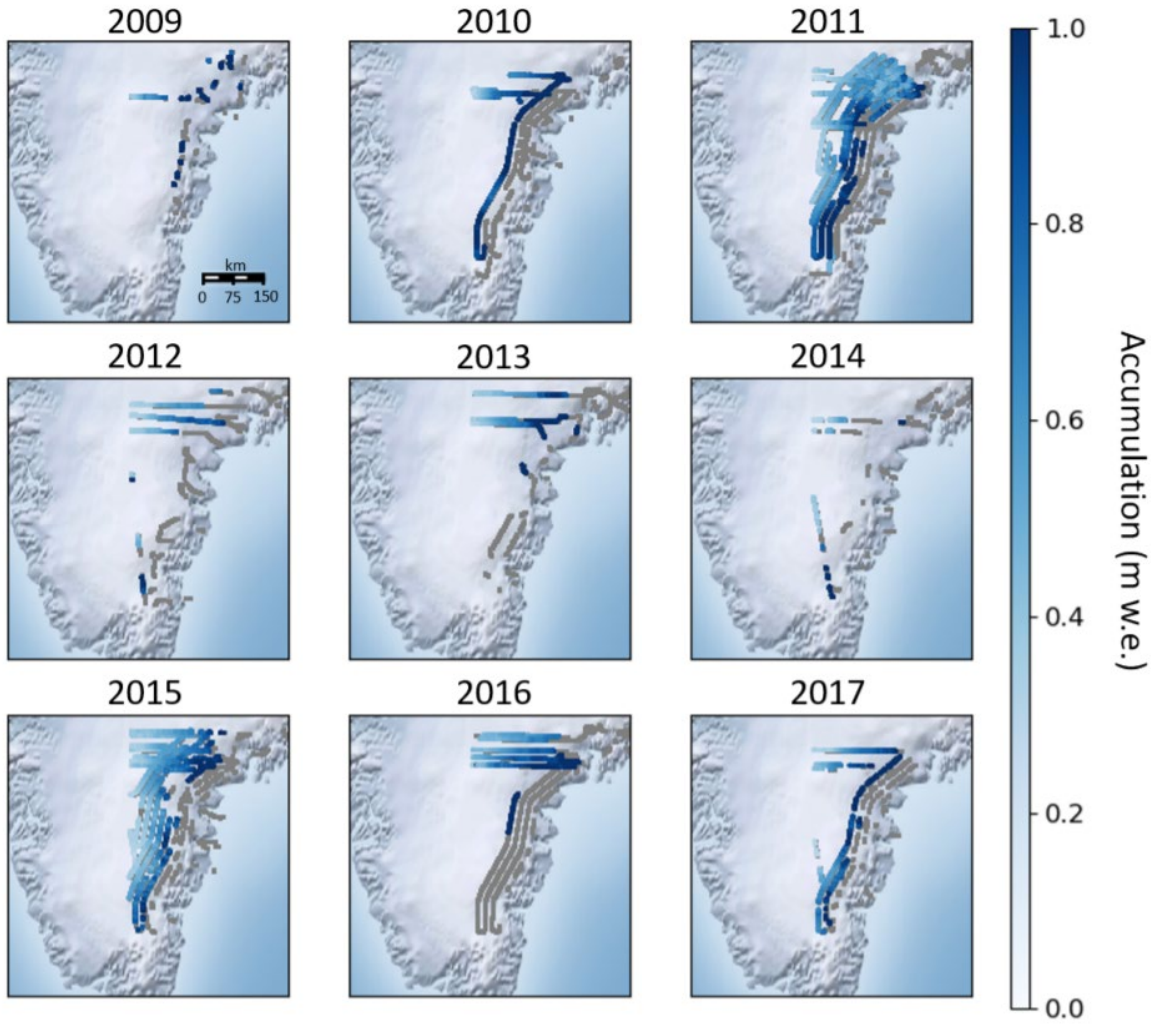

Figure 3.4 - Annual Accumulation (m w.e.), derived from OIB Snow Radar, from 2009 to 2017. Flight tracks that were not discernable for accumulation layers are in grey.

3.4.2 Comparison with RCMs: interannual variability

With a data set of radar-derived accumulation rates spanning almost 10 years, we can analyze the interannual variability and compare that with RCMs (Fig. 3.5). Since there is no single OIB flight line that is consistently flown every year from 2009-2017, we focus our

analysis to an area (45°W to 41°W and 66.3°N 66.55°N, Fig. 3.1) that contains a partial set of flight lines each year (except 2009), and match these observations in space and time with the closest MAR and RACMO2 grid points. Accumulation from RACMO2 follows a similar pattern of interannual variations, although it had a relatively large bias of -0.18 m w.e (44%). In contrast, MAR shows a more constant accumulation rate from 2010 to 2017. However, its multi-annual mean is closer to the observations, with an average bias of -0.13 m w.e. (29%). Over this time period, RACMO2 captures the interannual trends ($r^2 = 0.86$) while MAR does not ($r^2 = 0.08$), showing very little interannual variability. To assess how representative the 2010-2017 period is for the longer-term accumulation record (1979-2017), and considering the above model biases, we analyze the 30-year mean and variability in accumulation across the same area from RCMs (Fig. 3.5b). For both RACMO2 and MAR, the standard deviations of the 2010-2017 accumulation (RACMO2: 0.408 ± 0.039; MAR: 0.45 ± 0.024) fall within the 1979-2017 variability (RACMO2: 0.43 ± 0.063; MAR: 0.47 ± 0.068). This implies that the RCM analysis in this study area is consistent with interannual patterns spanning multiple decades.

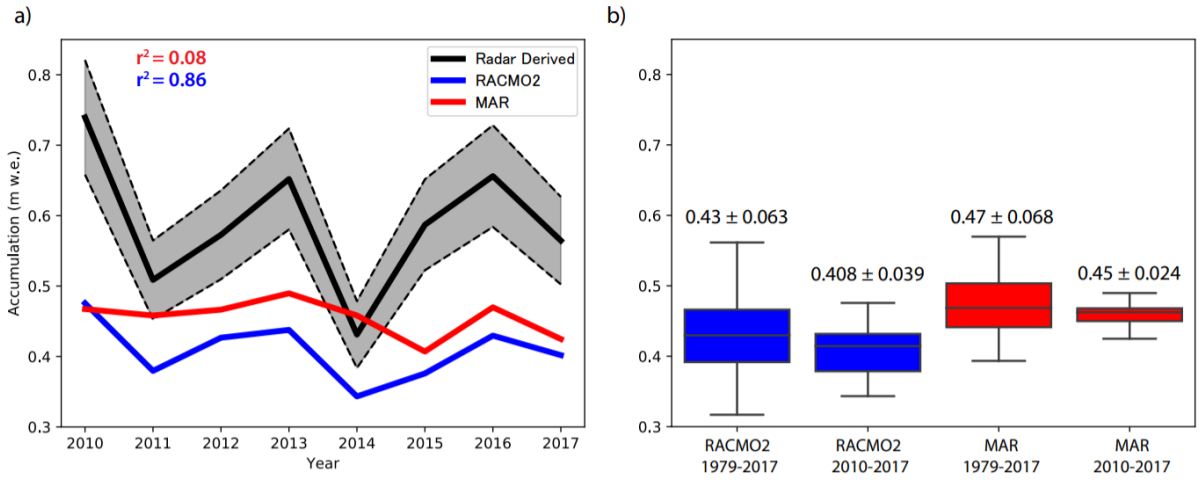

Figure 3.5 – a) Inter-annual variability of radar-derived accumulation rates (black) from 2010-2017 of area overflown each year compared with MAR (red) and RACMO2 (blue). Uncertainty

of observations (11%) shown in dashed lines of the same color. b) Box plot of RACMO2 and MAR accumulations from 1979-2017 showing the middle 50% of data (2nd and 3rd quartiles), the line inside the box represents the median values, and the whiskers show the greatest/least values within 1.5 times the interquartile range of the upper and lower quartile.

3.4.3 Comparison with RCMs: spatial variability

Radar-derived accumulation rates from each 10-month period were compared to downscaled 1 km MAR and RACMO2 accumulation covering the same period. The years of 2011 and 2015 had the best spatial coverage and are shown in Fig. 3.6i. RACMO2 underestimates accumulation rates in Southeast Greenland with a mean bias of -0.51 m w.e. across the entire region in 2011 and -0.41 m w.e. in 2015. In 2011, accumulation is overestimated towards the lower elevations (< 1500 m) but this is dominated by accumulation underestimation everywhere else. MAR closely matches accumulation rates in 2011 with a mean bias of -0.09 m w.e. and in 2015 the mean bias is -0.22 m w.e. averaged across Southeast Greenland. This good agreement in 2011 reflects the low spatial heterogeneity compared to observations. Scatterplots show a similar pattern as the difference plots, showing that both MAR and RACMO2 underestimate accumulation in Southeast Greenland (Fig. 3.6ii). The root mean square errors (RMSE) for RACMO2 during 2011 (0.26) and 2015 (0.29) are greater than those from MAR for the same years (0.17 and 0.23). When considering the 11% uncertainty of the radar-derived accumulation, the RMSE of each year decreases, except for MAR in 2011 where the RMSE is the same (RACMO2 2011: 0.18, RACMO2 2015: 0.12, MAR 2011: 0.17, MAR 2015: 0.08). However, the uncertainty does not fully account for the difference in radar-derived vs. modelled accumulation and therefore it must be attributed to a physical process in the models.

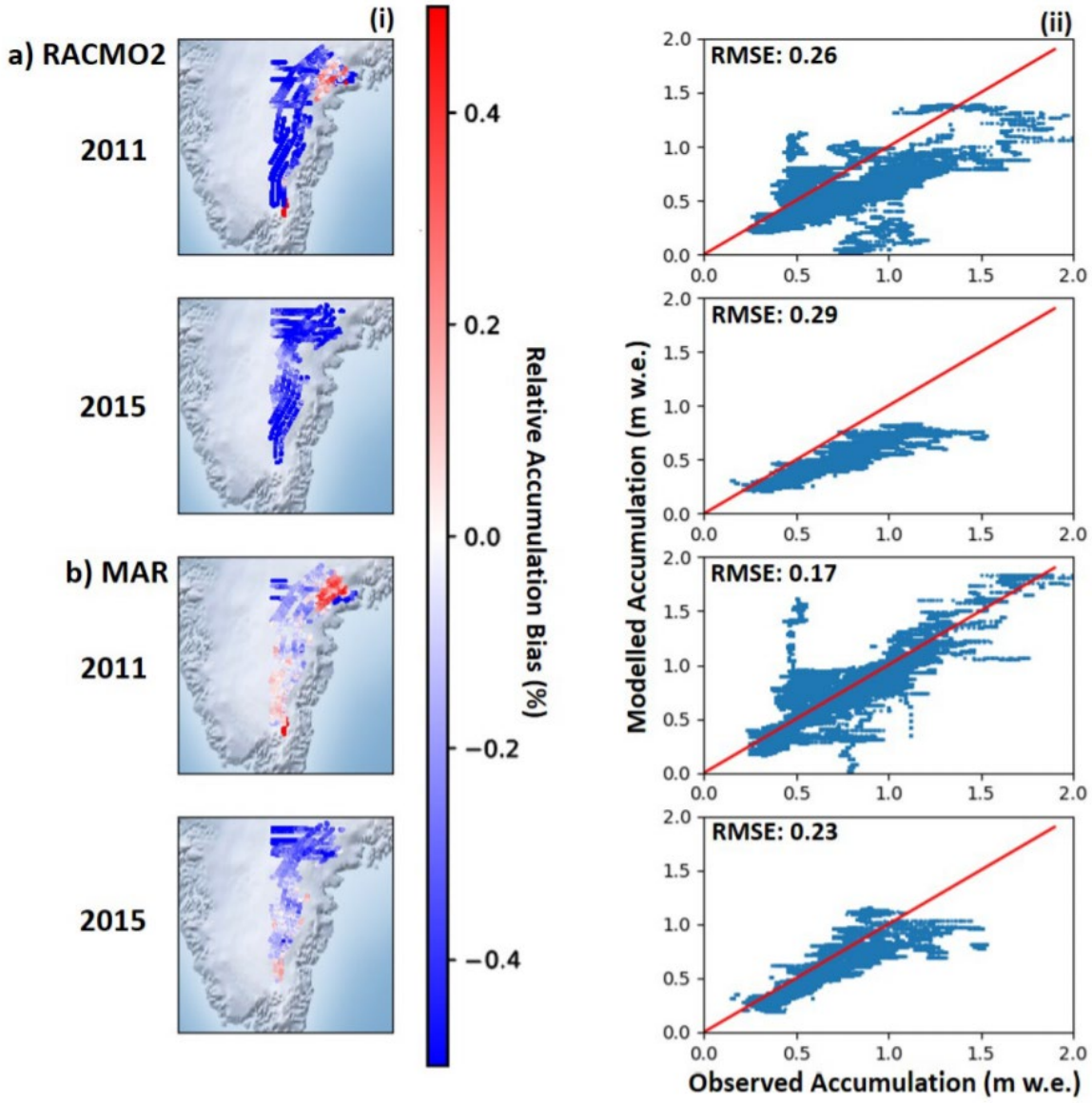

Figure 3.6 – a) (i) Relative difference between OIB derived accumulation and RACMO2 for 2011 and 2015, and (ii) Scatterplots showing radar-derived accumulation vs. RACMO2. b) Shows the same analysis except with MAR.

3.5 Discussion

Annual accumulation can be derived from OIB airborne radar in Southeast Greenland. However, in general, only the most recent layer or ~10 months can be detected in the percolation zone

where melt and refreezing obscures the stratigraphy below the last year's snowfall. A future increase and inland progression of surface melt on the GrIS implies that this technique's potential to yield reliable long-term accumulation records will be progressively more challenging in the future. We can reduce the spatial uncertainty of these derived measurements by attaining more in-situ observations along OIB flightline tracks.

This study provides a record of OIB radar-derived accumulation in Southeast Greenland that has been extended from Koenig et al., (2016) to include 2009 to 2017. Compared to that earlier study, we have also updated some of the methods and data sets. Firstly, we use an updated version of MAR (v3.9.2) as well as RACMO2 to compare RCM accumulation with OIB radar-derived accumulation. Secondly, we use FDM density profiles to derive accumulation, which best represent Southeast Greenland. The resulting differences between our results and Koenig et al. (2016) illustrate that realistic density profiles are essential to convert radar-derived depth to accumulation. This is highlighted by our comparison of Crocus and FDM with observations, yielding a total uncertainty associated only to density choice of 5% (FDM) to 19% (Crocus). The FDM density profiles show better agreement with observations, likely because the FDM physics are designed for use over ice sheets, while the Crocus model is developed for Alpine snow conditions. FDM profiles are also tuned to measurements from the GrIS ice sheet (Kuipers Munneke et al., 2015). Along with the density estimate, the layer picking software is a source of uncertainty in deriving accumulation rates and has been quantified by Koenig et al. (2016) to be ~8 cm from manual adjustment of layers or an average of 10% uncertainty in our study. Our overall uncertainty of 11% on radar-derived accumulation is reasonable compared to other studies, which yield uncertainties of 14-15% (Koenig et al. (2016); Medley et al. (2013)). The biases between models and observations as well as the uncertainties can be constrained by

collecting additional coincident observations of accumulation and density in Southeast Greenland. These observations are also necessary to provide an independent estimate of Southeast Greenland accumulation, as RCMs are currently the only tool available to provide GrIS SMB at this spatial resolution.

To assess future changes in accumulation and SMB, we must be able to differentiate between interannual variability and longer-term trends in RCMs. Interannual variability of accumulation in Southeast Greenland is driven by synoptic patterns associated to the strength and location of the Icelandic Low situated to the east of Greenland (Berdahl et al., 2018). On average, the large-scale southwesterly atmospheric circulation brings moisture to the southern coast of Greenland, where the steep slopes of the ice sheet act as efficient barriers to the flow, and orographic precipitation is abundant. Over the 2010-2017 time period (2009 is excluded because no flightlines overlap our case study region in that year), our case study shows that RACMO2 captures the interannual trends better than MAR, while MAR better represents the absolute magnitude of radar-derived accumulation. Over a 30 year period from 1979-2017, accumulation is examined from MAR and RACMO2 to show that variability of the study period (2010-2017) is within that of the longer-term from both RCMs (Fig. 3.5b). On the other hand, the 8-year time period we observe is too short to discern a significant long-term trend. We would need OIB data from a longer time period, similar to that of the RCMs (>30 years), to attempt to isolate long-term trends from interannual variability.

In order to quantify how much accumulation Southeast Greenland contributes to the GrIS's total SMB, and how it may impact changes in SMB in the future, spatial variability of accumulation in RCM's is vital to understand. When comparing modelled mean bias to observations in our flightline case study (Fig. 3.5a), accumulation is underestimated by both

MAR and RACMO2. This result could be due to the specific to this study area chosen, and unfortunately we are unable to expand this assessment to other regions, since this is the only region that has coverage in most years. However, our comparison of the spatial variability in models and observations (Fig. 3.6i) suggests that this result is valid for the larger Southeast Greenland region. As other SMB components (including melt, sublimation, and blowing snow redistribution) are at least two orders of magnitudes smaller than snowfall (mm vs. m) in Southeast Greenland (Box and Steffen, 2001; Lenaerts et al., 2012), the biases in the RCMs must be attributed to biases in snowfall.

RACMO2 has a high snowfall bias near the coast, while MAR has a larger bias in the interior (Fig. 3.7). These patterns are consistent with the relative differences shown in Figure 3.6, where RACMO2 shows underestimation inland and MAR shows an overestimation. Our MAR results contrast with those of Koenig et al. (2016), who found that an earlier verison of MAR (MAR3.5.2) overestimated accumulation in all of Southeast Greenland. With updated physics (increase in the cloud life time (Fettweis et al., 2017; Delhasse et al., 2018) and employed at higher resolution (15 km vs. 25 km), MARv3.9 shows good agreement across most of the region, though still slightly underestimates accumulation. The majority of the radar-derived accumulations are taken closer inland than where RACMO2 has dominant snowfall events, closer to the coast (Fig. 3.7). These biases are due to the fact that we are working with model accumulation downscaled to 1 km, which better resolves accumulation than the original grids, but still cannot take into account the mountainous topography in Southeast Greenland. The bias towards higher snowfall on the coast in RACMO2 is likely due to the representation of orographic precipitation in the model, i.e. when moist easterly air masses collides with coastal mountains and precipitate as they are lifted, resulting in high coastal precipitation and drier

conditions further inland. RACMO2 resolves topographical features that have to do with orographic precipitation, while MAR cannot, because downscaled 1km RACMO2 has a higher original horizontal resolution (5.5km) than downscaled 1km MAR (15 km).

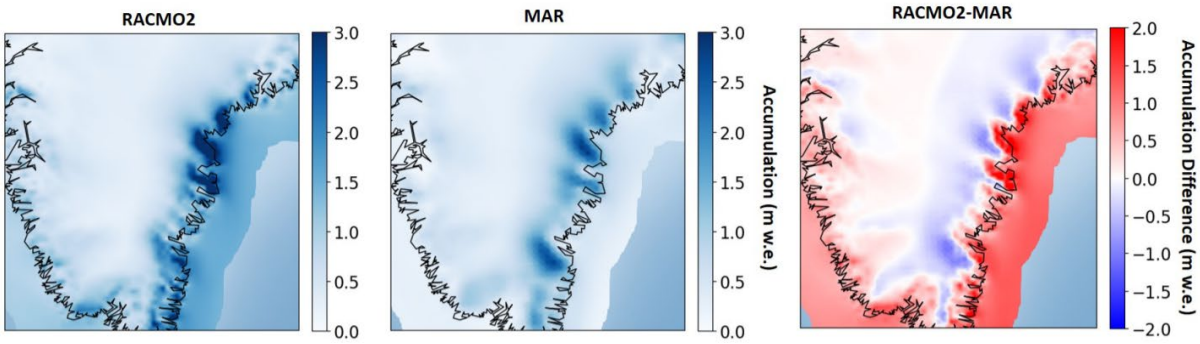

Figure 3.7 – Average annual snowfall (m w.e.) from 2009-2017 in a) RACMO2, b) MAR, c) RACMO2-MAR.

Our results corroborate previous work, which has shown that of RACMO2 overestimates accumulation at lower elevations and MAR overestimates accumulation at higher elevations. On the Q-transect on the Qagssimiut ice lobe in South Greenland, RACMO2 shows a wet bias towards the coast that is likely the dominant source of error (Hermann et al., 2018). Similarly, in RACMO2, Antarctica has a bias of orographic precipitation in coastal areas, likely because it does not compute precipitation prognostically (i.e. snow falls in the same grid cell that it is created) (Lenaerts et al., 2017). Schmitt et al., 2018 emphasized the same concern about overestimation of accumulation due to high orographic forcing in RCMs and attributes some of the error to the precipitation scheme in hydrostatic models, recommending use of WRF or HARMONIE as a non-hydrostatic alternative. Our results further verify these model biases, leading to the conclusion that RCMs must be improved to be better representative of the current climatological conditions since observations will continue to be sparse across the majority of the ice sheet. We propose future work of comparing radar-derived accumulations using a diagnostic,

non-hydrostatic, high resolution model to diagnose the different precipitation schemes and see if we can reduce the error in accumulation. Additionally, we recommend that model development target orographically forced precipitation at the coast, as it a large source of error in SMB calculations that could influence total SMB of the GrIS.

3.6 Conclusions

A dataset of annual accumulation was derived from OIB snow radar for 2009-2017 in Southeast Greenland where there were very few in-situ measurements available. Our estimated uncertainty of this new dataset is 11%, which results from the uncertainty associated with the semi-automated layer picking software, and uncertainty in the FDM density profiles used to derive the accumulation. We find that density profiles vary widely in the top meter of firn and can widely affect accumulation rates, especially in the high-accumulation area of Southeast Greenland. This data set can be used to validate RCMs in Southeast Greenland, an area of high variability and uncertainty. RACMO2 consistently underestimates accumulation rates across the entire region in 2011 and 2015 (the years with the best spatial coverage), but was able to capture interannual variability in a case study region. MAR shows better agreement with accumulation rates in 2011 and 2015 across Southeast Greenland, though shows little interannual variability. The pattern observed in the relative differences can be explained by the snowfall component of each model which is biased higher towards the coast in RACMO2 and inland in MAR. In-situ observations in this region will always be sparse, so we must rely on RCMs in the future to assess changing SMB. This study points to the need of focused model development of precipitation schemes to more accurately portray high accumulation regions on the GrIS.

3.7 Data Availability

This new accumulation dataset is available at the Arctic Data Center (doi:10.18739/A2J96095Z).

3.8 Acknowledgements

Lynn Montgomery and Lora Koenig acknowledge the National Science Foundation (PLR 1603407) and the NASA Earth and Space Science Fellowship (80NSSC17K0383). Peter Kuipers Munneke is funded by the Netherlands Earth System Science Centre (NESSC). We thank Xavier Fettweis for assistance with MAR model output and Brice Noël for discussion about RACMO2 output. We also thank the Associate Chief Editor Dustin Schroeder, the Scientific Editor Michelle Koutnik, and the two anonymous reviewers for their comments and suggestions, which greatly helped us in improving our paper.

4 Hydrologic properties of a highly permeable firn aquifer in the Wilkins Ice Shelf, Antarctica

This chapter is adapted and reformatted from:

Montgomery, L., Miège, C., Miller, J., Scambos, T. A., Wallin, B., Miller, O., et al. (2020). Hydrologic properties of a highly permeable firn aquifer in the Wilkins Ice Shelf, Antarctica. *Geophysical Research Letters*. https://doi.org/10.1029/2020GL089552

4.1 Introduction

Ice shelves, extensions of ice sheets and glaciers that have thinned sufficiently to become afloat on the ocean, are prevalent around the Antarctic Ice Sheet (AIS) and play a role in restraining ice-sheet discharge into the ocean (Siegert et al., 2019). More than 80% of Antarctica's ice discharge is released through ice shelf outflow and basal melting making them an integral control on the mass balance of the AIS (Rignot et al., 2013; Pritchard et al., 2012). Observations show that there are extensive surface hydrologic systems and meltwater storage on ice shelves in Antarctica (Bell et al., 2017; Kingslake et al., 2017; Lenaerts et al., 2017; Phillips et al., 1998) that can potentially accelerate their disintegration (Banwell et al., 2013; Scambos et al., 2004; Scambos et al., 2000). However, the meltwater volume, residence time, storage characterics and lateral/vertical movement remain not well understood despite being critical to estimate impacts on mass balance, ice dynamics and sea-level changes (e.g., Smith et al., 2020; Lenaerts et al., 2019; Bell et al., 2018).

Firn aquifers, well documented in mountain glaciers (e.g., Fountain and Walder, 1998) and more recently discovered in Greenland and Svalbard (Forster et al., 2014; Christianson et al.,

2015), form when meltwater produced at the surface percolates into the firn and fills the available pore space above the firn-ice transition without refreezing during winter. Firn aquifers are located where there is sufficient pore space volume in the firn column for meltwater to be stored and high accumulation which provides insulation that permits the saturated subsurface layer to remain at 0°C (Kuipers Munneke et al., 2014; Forster et al., 2014). In Greenland these conditions occur in the southeast, south, and northwest sectors where accumulation rates are ~1-5 meters water equivalent (m w.e.) per year and melt rates are >650 mm $WEyr^{-1}$ (Montgomery et al., 2020a; Bell et al., 2018; Noël et al., 2018). For the AIS, areas with similar surface melt and snow accumulation signatures are rare, though recent modelling studies show widespread perennial firn aquifers on the Wilkins Ice Shelf (WIS) and elsewhere on the Antarctic Peninsula (van Wessem et al., 2020; van Wessem et al., 2016). These aquifers can contribute to sea level rise if connected to the ocean by slowly draining into crevasses (Koenig et al., 2014) and are especially important to understand on ice shelves where meltwater storage is likely a precursor to hydrofracture and ice shelf breakups (Bell et al., 2018; Scambos et al., 2000).

In December 2018, we conducted fieldwork on the WIS using a combination of borehole drilling, hydrological tests, and ground-penetrating radar profiles. We used hydrological and geophysical measurements combined with a groundwater flow model to quantify lateral water flow and assess the hydrologic balance of the aquifer. Further, these results can be used in future studies to examine the impact of firn aquifers on ice shelf stability.

4.2 Study Site

Our field site is located on the southwestern portion of the Wilkins Ice Shelf on the Antarctic Peninsula (Fig. 1a). Measurements were taken ~50 km from the edge of the ice shelf (-70.80S, -71.71W) from 3-12 December 2018. Average (2010-2017) annual accumulation and melt rates

simulated from two regional climate models (MAR and RACMO2) at the field site are 590-800 mm WEyr^{-1} and 250-425 mm WEyr^{-1} (Fig. 1c; Table S1) (Noël et al., 2018; Agosta et al., 2019; Datta et al., 2019; Datta et al., 2018). A 17 km long rift in the ice shelf was observed ~5 km from our field site (Fig. 1b).

Analysis of NASA Operation IceBridge 2014 radio-echo-sounding profiles collected over the WIS using the Multichannel Coherent Radar Depth Sounder (MCoRDS; CReSIS., 2020), indicated a bright reflector in the upper firn similar to high-amplitude reflections associated to firn aquifers for the Greenland ice sheet (Forster et al., 2014; Miège et al., 2016). Based on the separation of the snow surface reflection and the bright sub-surface return, we anticipated the top of the firn aquifer to be ~13 m below the surface (Fig. S1; Studinger et al., 2014). MCoRDS processing steps to retrieve aquifer extent and depth to water are discussed in detail in Miège et al., (2016) and Brangers et al., (2020).

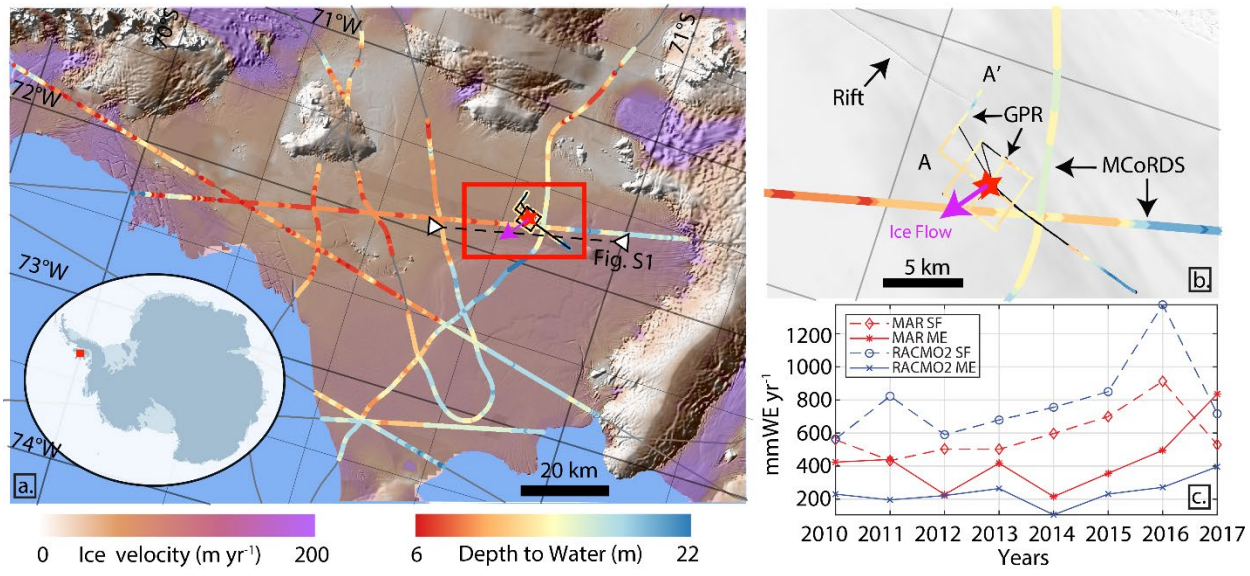

Figure 4.1 - a) Field site location (black star in red square) on the Wilkins Ice Shelf. The depths to the water table (blue-orange color bar) are derived from the MCoRDS radar system (CReSIS,

2020), a part of NASA's Operation IceBridge flight on 16 November 2014 (Fig. S1). Background is a hillshaded DEM (REMA; Howat et al., 2019). **b)** Close-up of our fieldsite (black star; image is from Landsat 8, 24 February 2020) with Operation IceBridge (OIB) aquifer detections (large circles) along with water-table estimates from our GPR surveys (small circles) around camp and across an adjacent ice shelf rift. Black lines show areas with GPS data only. The magenta arrow represents the direction of surface velocity based on an 8-day continuous GPS record. **c)** Time-series of annual snowfall (SF) and melt (ME) for 2010-2017 as simulated by both RACMO2 and MAR at the field site.

4.3 Methods

4.3.1. Borehole drilling and firn/ice cores

We used a custom-built lightweight electrothermal drill to drill three boreholes located ~1 m apart reaching depths of 14 m, 20 m and 35 m to estimate density, stratigraphy, and use for other hydrological tests. Drill specifications are in the supplemental material of Miller et al. (2018). To determine gravimetric density, core sections (average diameter of 55 mm) were weighed and measured immediately after collection. The average uncertainties of these density measurements ranged from 9-11% similar to previous studies (Text S5; Conger and McClung, 2009; Fornasini, 2008). We anticipate some meltwater to have drained during extraction and prior to weighing but cannot quantify the added uncertainty to the density measurements. The stratigraphy was recorded and two main facies were identified: firn and ice lenses (Figs. 2a, S2). No section of the retrieved core had temperatures substantially different from 0°C within the aquifer (accuracy ~±0.5°C).

4.3.2 Hydraulic conductivity estimate

Slug tests are used to measure the hydraulic conductivity in the saturated zone of an aquifer. Before the slug tests, we placed a pressure transducer (HOBO Onset© U20-001-02) with an operational range between 0 and 400 kPa and a maximum error of 3 cm of water, at the bottom of the borehole which allowed us to record the water-level changes (Fig. S3a). To perform a slug test we measured the time it took to displace a small volume of water by inserting/removing a solid cylinder (1187.7 cm^3) into the water-filled part of the borehole and measuring the response time for the water level to return to its initial level (Fig. S3c). We use present measurements from six slug tests (with the least noise) from December 9-11, 2018 in the 20 m borehole.

4.3.3. Borehole Dilution Test

We used a saline dilution method in the 35 m borehole to estimate discharge through the aquifer and locate the base of the flow zone. This method is established for traditional groundwater studies (Pitrak et al., 2007) and was recently adapted for estimating water discharge within firn aquifers in the Greenland Ice Sheet (Miller et al., 2018). The method consists of injecting a saline solution of a known conductivity into the borehole and monitoring the conductivity variation over time throughout the borehole to estimate horizontal flow through permeable firn. A description of the method is in the Supplementary Material (Text S1; Fig. S4). After injecting and homogenizing the salt solution in the borehole, vertical conductivity profiles were recorded with a vertical spacing of 30 cm in the water-filled part of the borehole: every 30 minutes for the first four profiles, followed by two profiles taken an hour apart, then two more profiles taken 2 hours apart (Fig. 2b). One additional profile was taken the following morning. The total duration

of the experiment was ~17 hours. This borehole dilution test also allows us to estimate specific discharge and linear velocity with depth (Figs. 2b,c).

4.3.4. Geophysical surveys and water-table elevation estimates

We used ground-penetrating radar (GPR) to survey the top ~50 m of the firn/ice column and identify the water-table depth around the drilling site and rift. We also surveyed ~35 km of surface topography using a GPS receiver. Limited post-processing was required because the water table was easily identified as a high-reflective high-amplitude signal. Post-processing included shifting the traces vertically to align the surface with the first break position of the signal, geolocation, adjustment for surface elevation, and removing the mean trace for the profiles from each trace within the profiles to enhance layering details. We converted from two-way-travel time to depth using mean density from the cores above the water table and a relationship linking permittivity and density (Kovacs et al., 1995). Details of the GPR method are in the Supplemental Material (Text S2).

We also conducted an 8-day continuous GPS survey (1-second epochs) at the drill site (3-11 December 2018) to determine the short-term ice flow vector and tidal range (Fig. S5). Ice flow speed was 92.8 m d^{-1} with near-zero diurnal variation. The daily range of vertical ice motion, roughly equal to tidal motion, was 0.8 to 1.3 m.

Both GPS-receiver signals were processed using the precise point positioning (PPP) web-based processor hosted by the Canadian Spatial Reference Service (CSRS - https://webapp.geod.nrcan.gc.ca/geod/tools-outils/ppp.php).

4.3.5. Flow-rate modeling

We use SEEP2D (Jones, 1999), a 2-D finite element flow model within the Groundwater Modelling System package, to simulate water flow within the aquifer, based on the results of the slug tests, GPR, and firn core measurements to determine if the aquifer is in steady state and constrain recharge estimates. SEEP2D solves the steady-state (i.e. all recharge that reaches the aquifer is discharged into the rift) groundwater flow equation (Freeze and Cherry, 1979) that is based on mass balance, and utilizes Darcy's Law calculated as

$$\frac{Q}{A} = -K\frac{\partial H}{dx}$$

where Q is groundwater flow ($m^3\ s^{-1}$), A is cross-sectional area (m^2), K is the hydraulic conductivity ($m\ s^{-1}$), and $\partial H/\partial x$ is the slope of the water table. Details of SEEP2D model setup and assumptions are in the Supplemental Material (Text S3).

We ran SEEP2D simulations with the following recharge scenarios:

1. High Recharge (*MAR and RACMO2*): 100% of surface meltwater (425 mmWE yr^{-1}), MAR; and (250 mmWE yr^{-1}), RACMO2 recharges the aquifer, with no refrozen melt in the firn.
2. Medium Recharge *(RACMO2)*: 50% of surface meltwater (125 mmWE yr^{-1}) recharges the aquifer, 50% of meltwater is refrozen.
3. Low Recharge (*RACMO2*): 25% of surface meltwater (62.5 mmWE yr^{-1}) recharges the aquifer, 75% of meltwater is refrozen.
4. Low Recharge (*MAR*): 10% of surface meltwater (42.5 mmWE yr^{-1}) recharges the aquifer, 90% of meltwater is refrozen.

Recharge scenarios were chosen to represent a wide range of possible climactic conditions on the ice shelf. We compare these steady state output conditions (water table slope and aquifer thickness) to our observations to determine if these scenarios are plausible. One test of plausibility is to compare the amount of refrozen meltwater in the simulation to the column fraction of ice lenses in the firn core density profile.

4.4 Results

4.4.1 Firn Core Characteristics

The deepest firn core was collected at 35 m, below the estimated firn-ice transition of ~29.6 m (when the specific discharge reaches 0 – Fig. 2c). The average firn density above the aquifer was 650 kg m^{-3} and within the aquifer was 850 kg m^{-3} (Fig. 2a). Two shallower firn cores were collected one meter away from the deepest firn core and show small-scale spatial variability in density above the aquifer with an average densities of 627 and 669 kg m^{-3} (Fig. S2), which agree within 9-11% uncertainty. The three firn cores also show variability in ice lenses, with an ice fraction above the aquifer varying from 17.9% to 20.3%, and an average of 18.1%. We measured the depth to water table which ranged from 13.39-13.46 m, averaging 13.43 m, proving a homogeneous water table depth at the site. We compare this measured depth with the GPR depth converted from two-way-travel time and find a good agreement (± 20 cm).

4.4.2 Hydraulic Conductivity

We derived values of hydraulic conductivity from slug tests ranging from 1.0×10^{-4} to 1.7×10^{-4} with a geometric mean of $1.4 \pm 1.2 \times10^{-4}$ m s^{-1}. These correspond to permeabilities ranging from 1.8×10^{-11} m^2 to 3.1×10^{-11} m^2, and averaging $2.6 \pm 2.2 \times 10^{-11}$ m^2. Water level change values ranged from 10 to 15 cm (Fig. S3). The slug tests indicate a highly permeable aquifer (similar to

unconsolidated sand) with similar hydraulic conductivity values to that of the firn aquifer found in Southeast Greenland (Miller et al., 2017).

4.4.3 Borehole Dilution Test

A time-series of conductivity profiles from the 35 m borehole after the saline solution was injected is shown in Fig. 2b. We note that this conductivity represents a vertical profile of salinity and not hydraulic conductivity. The background conductivity is below detection, until ~30 m where it increased to 75 μS cm^{-1}. After the conductivity reached 200 μS cm^{-1} in the water-filled borehole (Text S1), we observed a gradual decrease of the conductivity above 20 m until background levels were reached. Below 20 m, the conductivity did not reach background levels during our experiment time. The decrease in conductivity over time in the profiles indicates lateral water flow which dominates the freshening process in the borehole. We consider diffusion rates to be negligible in this process as they are ~30 times smaller than the inferred advection of water. The decrease in dilution rate with depth (and therefore lateral flow) is primarily due to decreasing porosity. The profile reaches pore close-off at ~30 m, eliminating any dilution or lateral flow (Fig. 2a).

The vertical specific discharge (Text S4) profile derived from the salt dilution indicates where and the rate at which water flows laterally in the borehole profile into connected pores in the surrounding aquifer (Fig. 2c). The bottom depth of the specific discharge profile where flow ceases (29.6 m) agrees with the bottom depth of the aquifer we found through coring (~29 m). The average specific discharge is 1.9×10^{-6} m s^{-1} with a maximum value of 1.6×10^{-5} m s^{-1} at the top of the aquifer due to high porosity values which results in a standard deviation (σ) of $2.8\times10^{-}$

^{6} m s^{-1}. However if we omit the maximum outliers, specific discharge σ decreases to 1.1×10^{-6} m s^{-1}.

We also calculated the average linear velocity profiles using uniform porosities ranging from 0.1 to 0.3 (Fig. 2d; Text S4; Koenig et al., 2014). The density measurements in the region just above the aquifer suggest that the porosity is near the high end of this range at the top of the aquifer (Fig. 2a). The average linear water velocity ranged from 0.6-1.7 m d^{-1} depending on the porosity. Our maximum linear velocity value was 14.1 m d^{-1} assuming a porosity of 0.1. The calculated values of linear water velocity are substantially larger than the measured ice motion (0.25 m d^{-1}), therefore, the water flow is faster than the surrounding ice flow.

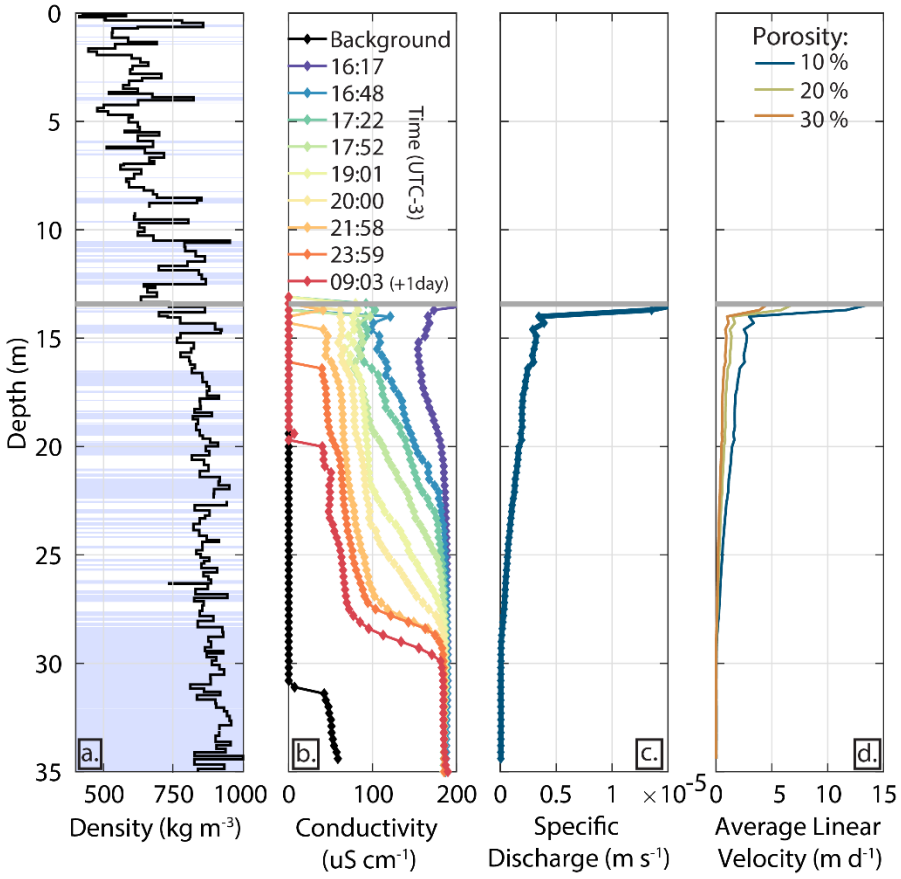

Figure 4.2: Firn characteristics and dilution test results. **a)** Core properties (density and stratigraphy) through the firn aquifer. Blue bands indicate ice layers, white indicates porous firn; grey line corresponds to the water table. The base of the aquifer is indicated by the lowest ice-dominated ~29-35m. **b)** Salt dilution time series. Black line shows the background characteristics of the aquifer, including a non-zero salinity within the basal ice layer. Color lines and their start times (UTC -3) represent successive conductivity vertical profiles after salt added to the borehole (Dec 10-11, 2018). **c)** Resulting specific discharge estimated from the dilution rate. **d)** Average linear velocity interpreted from the dilution rate assuming different porosities.

4.4.4 GPR Survey of the Rift

The combined GPR-GPS radar profile from the field site across the southern terminus of the ice shelf rift (~ 5 km) indicates the surface of the ice shelf is initially ~17 m above the WGS84 ellipsoid height and rises to ~20 m within a few hundred meters of the rift location (3.8 km along the profile) before tipping downward towards the rift (Figs. 1b, 3a). This profile shape is typical of rifts in ice shelves (.e.g., Fricker et al., 2005). A survey of Landsat imagery (www.earthexplorer.usgs.gov) showed that the rift appeared in late 2009, shortly after a series of major disintegration events on the Wilkins Ice Shelf (Humbert et al., 2010). Rifts (breaks through the entire ice shelf) generally occur when tensile stresses exceed the tensile strength of the ice plate (Braun et al., 2009; Scambos et al., 2009). The rift was filled with snow at the southern end.

The profile reveals firn and ice lenses parallel to the ice shelf surface (Fig. 3a), and a continuous strong reflector at the same depth (±1 m) as the aquifer's upper surface at the core site. No layering is observed below the bright layer, consistent with the radar attenuation

expected for an aquifer layer. As the profile approaches the rift, it shows the inferred aquifer surface deepening, and crossing the firn ice layering. The inferred aquifer surface intersects the rift at an ellipsoidal height of about 0 m, close to local sea level (Fig. 3b). Decreasing aquifer height and consequently decreasing hydraulic head towards the rift strongly implies lateral movement of water towards the rift and drainage through its side walls.

4.4.5 Groundwater Flow Modelling

To quantitatively evaluate that water is flowing into the rift (thereby removing some of the annual recharge to the aquifer) and constrain the parameters in which the aquifer system would be in steady state, we use the SEEP2D groundwater flow model. Table S2 shows the results of the SEEP2D modelling.

First, we present two extreme scenarios of a steady state aquifer where all surface melt, ranging from 250 mm WEyr^{-1} to 425 mmWE yr^{-1} depending on the RCM used, recharges the aquifer. The $\partial H/\partial x$ (gradient) and A (thickness) parameters required for the high recharge scenario contribution would be physically impossible compared to our observations because the water table of the aquifer is not 26-46 m (Table S2) above the firn-ice transition (i.e., we see no ponding). Further, the presence of refrozen melt layers in the upper firn suggests that the aquifer is not being recharged by all surface meltwater.

We also examine a recharge scenario where 125 mm WEyr^{-1} (50%) of surface melt recharges the aquifer, using RACMO2 melt input. The other half of the melt input refreezes or densifies the snowpack, which could explain the ice layers in the stratigraphy above the aquifer. However, steady state is only reached if the hydraulic conductivity is twice the observed value,

the $\partial H/\partial x$ has a 13 m gradient over 3800 m distance, or if the aquifer is twice as thick. Major dynamical or structural changes would have to occur in a short distance for this scenario to be plausible.

Our final scenarios present low meltwater recharge values ranging from 42.5 to 62.5 mmWE yr^{-1}, consequently leading to 75-90% of the melt input refreezing in the firn above. With this small amount of melt recharging to the aquifer, our model output matches closely with field measurements (Fig. 3b). However, the ice fraction above the aquifer measured at our study site is too small to represent this amount of refrozen meltwater per year (i.e., no thick ice layers).

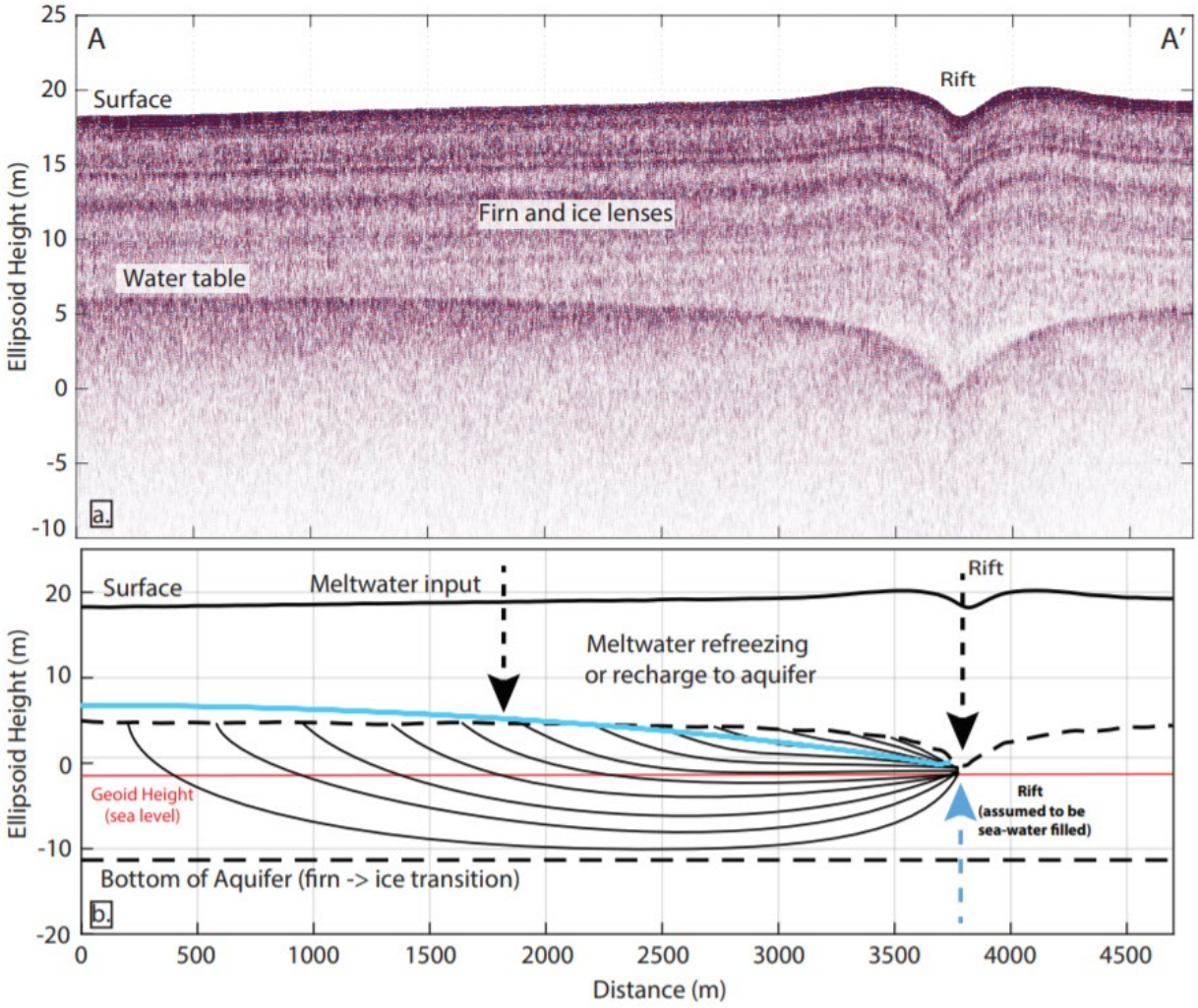

Figure 4.3. GPR profile across the rift and analysis of water flow and drainage of the firn aquifer layer **a)** GPR profile taken across a 5 km transect of the WIS. The high-reflective high-amplitude internal reflector ranging between 12-17 m below the surface is inferred to be the top of the firn aquifer. This begins to slope downward into an ice shelf rift 3.8 km from the start of the profile. Layering above the aquifer reflector represents ice layers within porous firn. **b)** Schematic showing structure of aquifer and processes occurring in the snowpack. Solid black lines within the aquifer show flowlines resulting from meltwater input. Teal line shows the water table from the RACMO2 Low Recharge Scenario.

4.5 Discussion and Conclusions

We provide the first measurements of hydraulic conductivity, density, and specific discharge of a firn aquifer on an ice shelf in Antarctica. We also show that the water in this firn aquifer at this field site likely is discharging into a nearby rift. These measurements were performed at only one location, but allow us some insight into the meltwater storage in the WIS. Further field experiments spatially distributed (i.e., seismic refraction, magnetic resonance, hydrological tests, and firn stratigraphy and density profiles) would be necessary to fully quantify the overall structure and age of the aquifer, various drainage divides, and the magnitude of the total discharge into the rift.

The average hydraulic conductivity value for the WIS aquifer (from slug tests, $1.4 \times 10^{-4} \pm 1.2$ m s^{-1}) is of the same magnitude but potentially below what was measured in Greenland ($2.7 \times 10^{-4} \pm 1.6$ m s^{-1}). In turn, the specific discharge from dilution tests, (1.9×10^{-6} ms^{-1}, $\sigma = 2.8 \times 10^{-6}$ m s^{-1}) is also less than the value (4.3×10^{-6} m s^{-1}, $\sigma = 2.5 \times 10^{-6}$ m s^{-1}) from Greenland. This results from the smaller surface slope relative to the Helheim study area (~0 versus 0.8 degrees;

Forster et al., 2014) and also suggests that there is less recharge on the ice shelf. The lower recharge rates can be explained by the lower melt rates compared to the Helheim Glacier region. In fact, both the modelled WIS accumulation and melt rates are less than half of the values in the southeastern Greenland region (590-800 and 250-425 (Fig. 1c) vs. 1400-1650 and 730 mm $WEyr^{-1}$; Miege et al., 2016). Miller et al. (2017, 2018) found that the Greenland firn aquifer was highly permeable and had evidence of direct meltwater flow. This meltwater likely flowed into nearby crevasses and possibly down to the bed of the ice sheet into the ocean (Poinar et al., 2017). Similarly, we find that the WIS firn aquifer is highly permeable and is likely discharging into the nearby rift.

Our hydrological modelling results indicate that while plausible, it is unlikely that the WIS aquifer is in steady state with all meltwater discharged to a nearby rift. The high recharge scenario was deemed implausible because hydraulic gradients rose above the ice shelf surface. The medium recharge scenario provided a more plausible ratio of recharge to refreeze and approximately accounts for the ice fraction of 18% observed in the core above the aquifer. To achieve steady state, this scenario either requires a water table slope or hydraulic conductivity that is two times greater than our observed values. Since we had to extrapolate our single hydraulic conductivity measurement value throughout the entire system, variability of K in the system could explain the discrepancy. It is also possible that refreezing at the base of the aquifer accounts for some of the unexplained water mass. The low recharge scenarios both match the observed water table (Fig. 3b), though this implies that 75-90% of the meltwater input densifies or is refrozen in the firn column above the aquifer, which does not agree with the observed ice fraction above the aquifer (Fig. 2a). However, meltwater is required to bring the firn to an isothermal state above the aquifer to allow recharge after the winter season, which varies

annually based on seasonal snow thickness and temperature, and could explain some excess meltwater (Miller et al., 2020).

We assume that our study site on the WIS firn aquifer is slowly draining into a large rift that was formed in 2009. Earlier observations using airborne radar show a highly reflective high-amplitude internal reflector near the surface (1966 and 1975 surveys; OIB surveys in 2014 shown in Fig. 1) absent of any observed widespread surface flooding, even in the highest-melt years (Braun et al., 2009; Scambos et al., 2000; Vaughan et al., 1993). The presence and thickness of an aquifer is controlled primarily by the summer meltwater flux and the annual net snowfall and rainfall, and to a lesser extent by freezing at the base of the aquifer column (Montgomery et al., 2017). Without surface flooding or complete re-freeze seen from satellite imagery for several decades (Barrand, 2013; Braun et al., 2009; Scambos et al., 2000; Vaughan et al., 1993), the WIS has apparently maintained a near-balanced system with respect to water table height and therefore snowfall and recharge conditions. However, the specific dynamics of the past WIS aquifer are unknown, including if it was in steady state and has always had cracks in the ice shelf with which to evacuate water.

Firn aquifers offer sufficient water storage capacity to contribute to ice shelf disintegration events, as evidenced by the partial break-ups of the northern and northwestern WIS in 1993, 1998, and 2008-2009 where the bright reflector from airborne radar was present (Braun et al., 2009; Humbert and Braun, 2008; Scambos et al., 2000). Our study supports this conclusion, identifying the WIS aquifer as having high permeability and the drainage of the aquifer into the adjacent rift. However, the stability of an aquifer-bearing ice shelf will be dependent on the volume of the aquifer and relationship to lateral flow of water within the aquifer. Discharge from firn aquifers has been modelled to be able to cause hydrofracturing to

the bed of ice sheets with enough inflow of meltwater (Poinar et al., 2017). If a series of low melt years or high snowfall years decreased the relative height of the top of the aquifer column, the potential for hydrofracture is greatly reduced. The year-round availability of water at depth allows for enhanced fracturing whenever stresses change to favor tensile extensions or loss of compression, even in the winter (Scambos et al., 2009). With complete saturation of the vertical firn column, the hydrostatic head for hydrofracture is at a maximum value and has the potential to cause destabilization of ice shelves and iceberg calving through hydrofracturing (Bell et al., 2017; Pollard et al., 2015; Scambos et al., 2009; Scambos et al., 2003). Continued and improved monitoring of firn aquifers would lead to better understanding of the role these aquifers play in ice-shelf disintegration.

4.6 Acknowledgments, Samples, and Data

This work was supported by a NSF grant ANT-1745116. C.M. was partly supported by NSF Grant ARC-1604058. We appreciate constructive and thorough reviews by Elizabeth Case, Jonny Kingslake, Annie Putman and Baptiste Vandecrux, which greatly improved this manuscript. We thank our Editor Mathieu Morlighem for handling our manuscript. We acknowledge and express our gratitude to the British Antarctic Survey for outstanding field and logistics support, including our exceptional field guide, Tom Lawfield. We also thank Tri Datta, Christoph Kittel, and Brice Noël for providing model output from MAR and RACMO2. We thank Michelle Koutnik for lending us her conductivity probe. We acknowledge UNAVCO for lending us two GPS receivers. We acknowledge the use of data and/or data products from CReSIS generated with support from the University of Kansas, NASA Operation IceBridge grant NNX16AH54G, NSF grants ACI-1443054, OPP-1739003, and IIS-1838230, Lilly Endowment Incorporated, and Indiana METACyt Initiative. *REMA DEM (Fig. 1) is provided by the Byrd*

Polar and Climate Research Center and the Polar Geospatial Center under NSF-OPP awards 1543501, 1810976, 1542736, 1559691, 1043681, 1541332, 0753663, 1548562, 1238993 and NASA award NNX10AN61G. Computer time provided through a Blue Waters Innovation Initiative. DEMs produced using data from DigitalGlobe, Inc. Geospatial support for this work provided by the Polar Geospatial Center under NSF-OPP awards 1043681 and 1559691. Any use of trade, firm, or product names is for descriptive purposes only and does not imply endorsement by the U.S. Government. All data used in this manuscript can be found at https://www.usap-dc.org/view/dataset/601390.

4.7 Supplemental Material

4.7.1 Supplemental Material Texts

Text S1. Details of Borehole Dilution test

We prepared a solution of 11500 uS/cm by adding 20 g of salt to 1 L of water (melted snow) targeting a resulting conductivity of 200 uS/cm once mixed in the water filled borehole (Figure S4a). Prior to injecting the solution, we ran an initial conductivity vertical profile to record the background specific conductivity with depth in the water-filled part of the borehole. We then placed a conductivity probe (HOBO Onset© U24-002-C) operating in its low range between 100 and 10000 uS/cm at the mid-point of the water-filled borehole and monitored the water conductivity for an hour as the water and salt were being mixed in the borehole (Figure S4). Any use of trade, firm, or product names is for descriptive purposes only and does not imply endorsement by the U.S. Government. For mixing the saline solution within the water-filled borehole, we lowered a small submersible pump (Proactive 12-V Tornado pump) and positioned it about one meter above the borehole base. The water pumped at the base of the borehole was

released just above the water table via a 1.27-cm diameter plastic tubing to create a vertical water movement. We injected the saline solution from the surface using a 0.635-cm diameter plastic tube and flushed the solution using fresh water to make sure all saline water was injected. After injection, we turned the pump on and mixed the saline solution in the borehole for an hour until the column had a homogeneous conductivity of 200 uS/cm (Figure S4b).

Text S2. GPR Methods

The control unit, manufactured by Malå (a RAMAC system), is operated with a 250-MHz antenna. The antenna was towed on a sled behind the snowmobile (Figure S5). The average travel speed was 1.5 - 2.5 ms^{-1} with a scanning rate of 1 second and a depth range set around 500 ns. This resulted in a stacked, or averaged, GPR trace being collected every 2 m on average. For simultaneous geolocation of the GPR traces, we used a dual-frequency Trimble© R7 GPS receiver in kinematic mode with a sampling interval of 1 seconds (~1.5-2.5 m). A GPS Zephyr GeodeticTM antenna was installed on a metal mast located at the back of the snowmobile, 1 m above the snow surface. For gaining positioning accuracy, we processed the GPS data using the precise point positioning (PPP) web-based processor hosted by the Canadian Spatial Reference Service (CSRS - https://webapp.geod.nrcan.gc.ca/geod/tools-outils/ppp.php). The travel time to depth conversion was done using a permittivity value of 2.32 which corresponds to an average density of 620 kg/m3 observed above the water table (upper 13.4 meters) using an empirical relationship from Kovacs et al., 1995. Using the nearest GPR trace to the three core sites, the depth of the high-reflective layer in the GPR profile was in good agreement (+/- 20 cm) with the water table measured directly at the borehole site.

Text S3. SEEP2D Model Setup and Assumptions

We simulated flow along a 2D vertical cross section 3800 meters long with nodal spacing of approximately 6 meters horizontally and 4 meters vertically. The thickness (A) of the aquifer varied in space and was delineated by our GPR measurements of the water table, and observations of the firn-ice transition for core samples (Figure 3b). We derived specified recharge fluxes (Table S2) from melt estimates from MAR3.9 (7.5 km resolution) or RACMO2.3p2 (5.5km resolution) 2010-2017 averaged surface melt at our field site. No flow boundaries were used for the bottom and upstream side of the domain. Along the downstream boundary, where discharge occurs, we used a no flow boundary below sea level to approximate the presumed occurrence of a freshwater-salt water interface. A specified head (-0.28 meters ellipsoid height, Figure 3b) was used based on the water table height on the downstream boundary above sea level. Although aquifer properties may vary along the cross section, a heterogeneous simulation is not justified given the limited available field data.

Our simulations utilized the following assumptions:

1) the hydraulic conductivity is uniform throughout our study region

2) the bottom elevation of the aquifer is homogeneous,

3) any melt water that is not recharged to the aquifer is refrozen in the unsaturated zone overlying the aquifer. (i.e. we assume sublimation and evaporation of the melt water to be negligible).

4) The rift is partially filled with seawater (to the geoid height) and the density gradient between the freshwater of the aquifer and seawater in the rift causes a hydraulic barrier where no discharge can occur.

Assumption 1 is justified based on homogeneous hydraulic conductivity in a firn aquifer in Greenland (Miller et al., 2017).

Note: Assumption 4) is implemented in SEEP2D by only allowing for water to discharge above the geoid height (Figure 3b). In reality, there may be diffuse flow into seawater, however a more complex boundary is not currently warranted due to a lack of direct observations.

Text S4. Definition of Specific Discharge and Linear Velocity

The specific discharge, representing the flow of water per unit area of porous media (m^3/m^2 s), is calculated at each depth using the specific conductivity measurements from the borehole dilution test (derived from Darcy's Law)

$$q = \frac{\pi r}{2t\alpha} \ln(\frac{C}{C_0})$$

where q is the specific discharge (length/time), r is the borehole radius (length), t is time, α is a formation factor accounting for the amplification of the velocity field by the borehole, commonly taken to be equal to 2 (Pitrak et al., 2007), and C/C_0 is the relative concentration at a given time.

Additionally, the linear velocity (V, the velocity through connected pores), is calculated by

$$V = \frac{q}{n}$$

using three porosity estimates from Koenig et al (2014), where q is the specific discharge and n is the porosity (Cherry and Freeze, 1979).

Text S5. Uncertainty of Density Measurements

Average uncertainty of density measurements for all three cores was calculated using an error propagation formula for products and division based on Fornasini (2008) using an uncertainty of ± 0.002 m for length measurements, ± 0.003 g for weight measurements, ± 0.002 m for diameter measurements, and an error of ± 1% for intactness. There is additional uncertainty in the water-saturated aquifer layer (~13-29 m) from water drainage from cores on the way up the borehole or while taking the measurements of length, diameter, weight, and intactness, however we are unable to quantify the mass loss.

4.7.2 Supplemental Figures

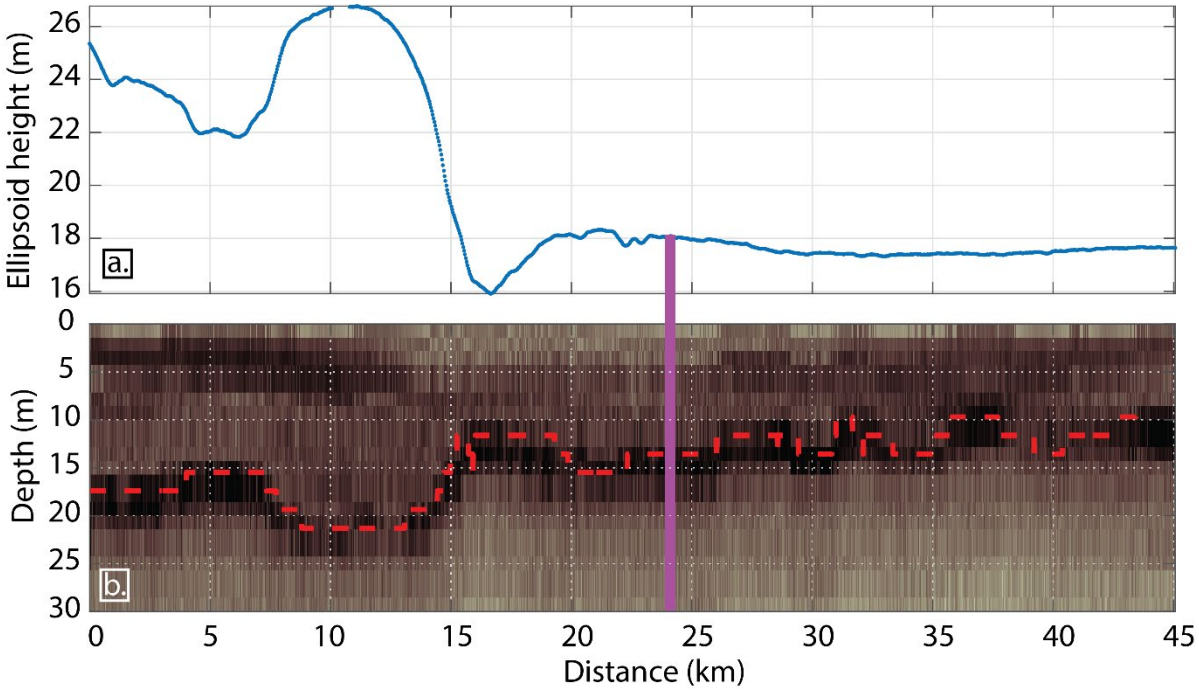

Figure 4.S1. Inset a. shows the elevation profile (Ellipsoid height) for the OIB flight trajectory in the vicinity of our field site, using the Airborne Topographic Mapper data (Studinger, 2014). Inset b. represents the MCoRDS radar data collected simultaneously to the ATM data. We interpret the bright reflector, (dash red line) found between 10 and 25 meters, to be the water table. The purple vertical bar represents the closest location to our field site (1.8 km apart). The

vertical precision of depth is limited to the vertical sample interval (also referred to as bin size) of ~1.9 m for a bandwith of 180-230 MHz, when converting from two-way travel time to depth using a permittivity value of 2.4 (corresponding to an average density of ~650 kg m^{-3}). The MCoRDS and GPR trajectories intersect at two locations: 71.7543°W&70.8162°S and 71.7701°W&70.7944°S (see Figure 1b) with absolute depth-to-water differences of 0.6 and 1.2 meters, respectively.

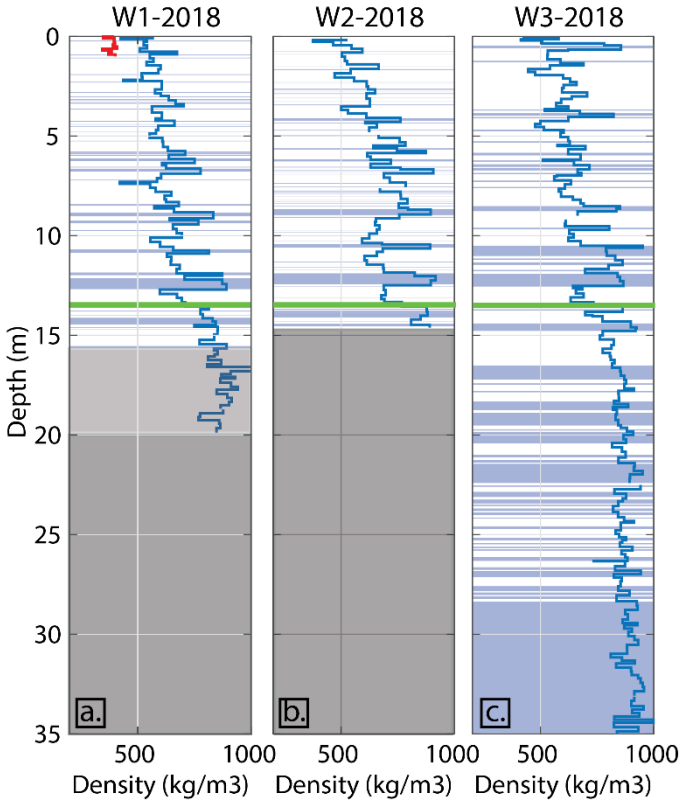

Figure 4.S2. Density (blue line from coring, red line from pit) and stratigraphy (blue = ice lens, white = firn) for the three cores collected at our field site, the horizontal spacing between each core location is about 1 meter. The water table is represented by a green horizontal line. The light

gray rectangle at W1 indicates that only the density was recorded. The dark gray rectangles at W1 and W2 indicate no measurements were taken.

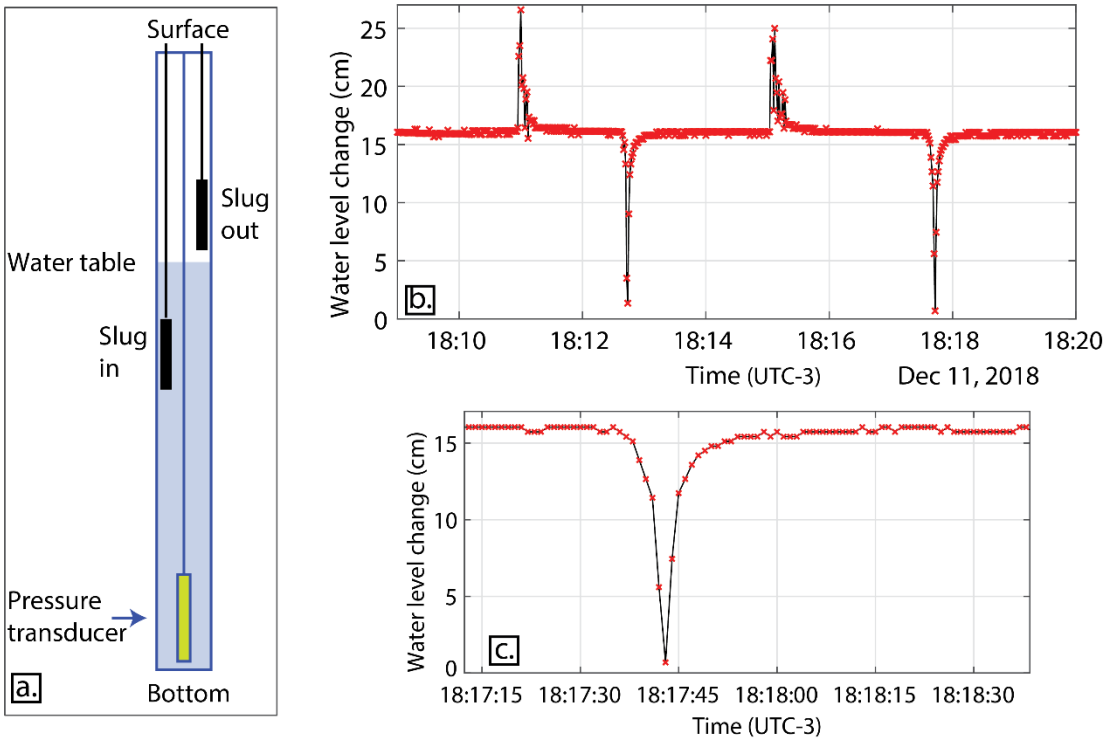

Figure 4.S3. a) Slug test set-up (not at scale). b) Illustration of the water-level changes over time as the slug is inserted and removed from the borehole. c) Close up within the water-level time-series showing one the drawdown and recovery of the water table when removing the slug.

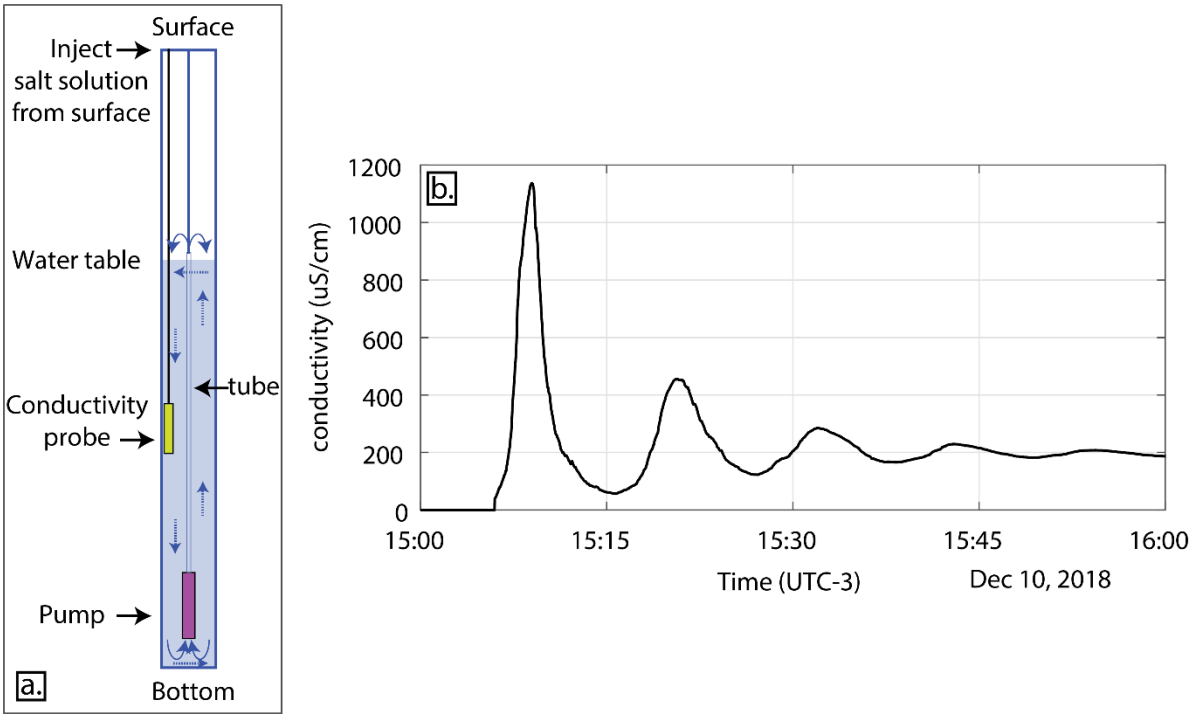

Figure 4.S4. a) Dilution test setup (not at scale). b) Homogenization of salt concentration in the borehole water column after injection at the surface, using a pump placed at the bottom. This step happened prior to logging the evolution of the salt concentration of the water column.

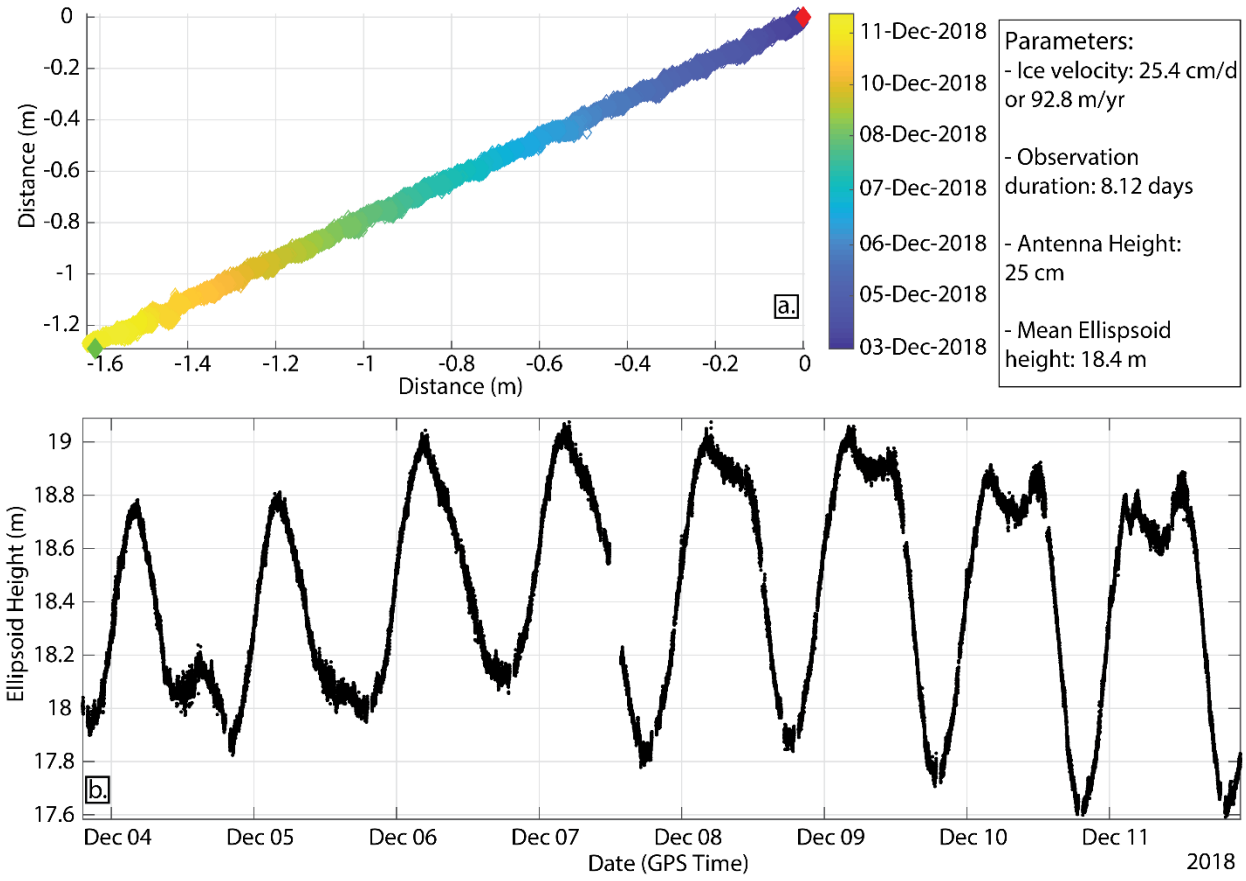

Figure 4.S5. An 8-day continuous stationary GPS survey at the drill site to determine a short-term ice flow vector and the tidal range for part of the tidal cycle after processing the GPS data using with PPP online processor hosted by the Canadian Spatial Reference Service.

4.7.3 Supplemental Tables

Table 4.S1.

	MAR SF	MAR ME	RACMO2 SF	RACMO2 ME
2010	559.74	424.35	563.79	230.49
2011	432.88	440.23	822.64	195.90
2012	503.48	228.02	590.23	222.07
2013	502.34	417.50	678.66	264.36
2014	597.04	215.68	755.65	105.64
2015	699.45	356.39	850.20	231.27
2016	912.56	495.76	1375.38	271.88
2017	529.57	836.10	716.75	396.34

Table 4.S1. Values of snowfall (SF) and melt (ME) shown in Figure 1c in the manuscript from MAR and RACMO2 at the closest grid point to our field site at -70.80S, -71.71W.

Table 4.S2.

	Q	K	$\frac{\partial H}{\partial x}$	Deviation from Observed Slope
Observed	?	1.38×10^{-4}	$-\frac{5}{3800}$	-
High Recharge (MAR)	425	1.38×10^{-4}	$-\frac{46}{3800}$	9x
High Recharge (RACMO2)	250	1.38×10^{-4}	$-\frac{26}{3800}$	5x
Medium Recharge (RACMO2)	125	1.38×10^{-4}	$-\frac{13}{3800}$	2x
Low Recharge (RACMO2)	62.5	1.38×10^{-4}	$-\frac{6}{3800}$	1x
Low Recharge (MAR)	42.5	1.38×10^{-4}	$-\frac{5}{3800}$	1x

Table 4.S2. SEEP2D modelling of recharge scenarios using different amounts of recharge input/discharge output (Q, mmWE yr^{-1}) to determine if the steady state slope of the water table (∂H/∂x, m/m) outcome is plausible. Hydraulic conductivity (K) is in units of m s^{-1}). The final

column shows the multiplicative factor by which the scenario deviates from the observed slope value.

5 Conclusions

5.1 Synopsis and Chapter Summaries

In this dissertation, I use in-situ and remotely sensed observations to improve our understanding of accumulation and melt processes, or surface mass balance, of ice sheets. One major issue I identify, is that accumulation observations, which are essential to quantify SMB, are lacking on both ice sheets. I address this by (1) compiling the SUMup database (Chapter 2) and (2) deriving 8 years of new accumulation measurements from airborne radar over an extremely data-sparse region in Southeast Greenland (Chapter 3). Another issue I identify is the growing impact of meltwater features in coastal areas and ice shelves in Antarctica. We enhance the understanding of these meltwater processes by presenting the first in-situ geophysical and hydrological observations from a firn aquifer on the Wilkins Ice Shelf in Antarctica (Chapter 4). Overall, my research has provided ample new observations and analysis to benefit the cryospheric community in better understanding the past, present, and future conditions of both the Greenland and Antarctic Ice Sheets.

5.1.1 The SUMup Database

In Chapter 2, I describe how we compiled and analyzed the Surface Mass Balance and Snow on Sea Ice Group (SUMup) database; a standardized, formatted, community-based dataset with subdatasets of density, accumulation, 10 m borehole temperatures, and snow depth on sea ice measurements. Uses of SUMup include model evaluation, remote sensing validation and algorithm development, and long-term monitoring efforts. We analyze the 2017 SUMup subsatasets and determine temporal and spatial gaps in measurements on the GrIS. Density and accumulation measurements on the GrIS were relatively oversampled in cooler, inland regions and undersampled in coastal, warmer regions. In addition, we found a lack of observations after

2000 compared to previous decades. Later analysis outside of this paper showed that on the AIS the majority of the measurements are taken in western Antarctica. As more data has been added to SUMup over the last few years, some of these spatial and temporal gaps have been reconciled and we are currently working to compile the 2020 SUMup database for release later this year.

5.1.2 Radar Derived Accumulation Observations in Southeast Greenland

In Chapter 3, I address the issue of the paucity of in-situ accumulation observations by using airborne radar to derive annual accumulation over 8 consecutive years (2009-2017) in Southeast Greenland, a region whose high snowfall heavily influences the sign of the Greenland Ice Sheet total mass balance. In order to derive this dataset of accumulation observations, we use gridded density profiles from two firn densification models, Crocus and the Firn Densification Model of the Institute for Marine and Atmospheric research Utrecht, due to a lack of in-situ density observations. We find that density varies widely in the top meter of firn, which can greatly affect resulting accumulation rates, especially in high-accumulation areas. Our accumulation dataset can be used to evaluate regional climate models and understand model biases. We compare our derived accumulations to model output from two regional climate models, the Modèle Atmosphérique Régional version 3.9 (MAR) and the Regional Atmospheric Climate Model version 2.3p2 (RACMO2). We also find that RACMO2 consistently underestimates accumulation rates across the region, but is able to capture interannual variability, while MAR shows better agreement with mean accumulation rates albeit with underestimated interannual variability. Our study broadly highlights the need for more focused model development and improvement on precipitation schemes in high accumulation areas, in order to better understand and quantify SMB on the Greenland Ice Sheet.

5.1.3 Hydrological Observations from a Firn Aquifer in the Wilkins Ice Shelf, Antarctica

In Chapter 4, I examine meltwater storage and flow in a firn aquifer on the Wilkins Ice Sheet in Antarctica and its impact on ice shelf stability. This meltwater is being stored perennially within the snowpack and the saturated layer is being recharged each summer with meltwater from the surface. Through slug tests, we determine that the aquifer was highly permeable, measuring a hydraulic conductivity ranging from 1.0×10^{-4} to 1.7×10^{-4} m s^{-1} with a geometric mean of $1.4 \pm 1.2 \times10^{-4}$ m s^{-1}. We also found that the aquifer is slowly draining into a nearby rift through hydrological tests, ground penetrating radar, and groundwater flow modelling. From the groundwater flow modeling, we constrained meltwater recharge estimates and determined that the aquifer is likely not in steady state, which means that the amount of meltwater recharging the aquifer is not draining out. From previous satellite and airborne imagery we assume that the aquifer has been present since the 1970's. We speculate that the presence of this aquifer could have influenced past ice shelf breakups through hydrofracture and influence future ice shelf stability in the region.

5.2 Outlook

From this research, multiple new questions arise about surface mass balance processes, three of which I highlight in this section:

1. Where can we expand our knowledge of accumulation using OIB snow radar?,
2. What measurements do we need to take in order to better understand the age, structure, and flow of meltwater in the Wilkins Ice Shelf firn aquifer?
3. Can we use snow models to simulate firn aquifer formation and predict where they will appear in the future?

Firstly, we want to further explore where we can expand our knowledge of accumulation using OIB snow radar. In Chapter 3, we derived a novel dataset of accumulation methods from OIB airborne radar in Southeast Greenland. This method of deriving accumulation has also been recently implemented in regions of northern Greenland (e.g. Ryan et al., 2020) to compare with mapping snowfall rates from Cloud-Sat. In the future, it could be used to derive accumulation across all OIB flightlines on both ice sheets. These datasets would be extremely useful to compare with regional climate models with few in-situ observations and to determine any biases that may be in models.

Secondly, in Chapter 4, we presented the first hydrological measurements from a firn aquifer found in the Wilkins Ice Shelf, Antarctica. The majority of these measurements were taken at one location limiting the conclusions we could draw from the data. To better understand the structure of the aquifer and lateral meltwater motion through it, multi-year observations of local conditions are needed including a full geophysical suite of experiments including seismic refraction, magnetic resonance, hydrological tests, and firn stratigraphy and density profiles. In addition, further observations closer to and into the rift are required to determine the magnitude of drainage from the aquifer. However, in-situ measurements are difficult to obtain as it is challenging to go into the field. To supplement these measurements and provide a higher temporal scale of data, data can be used from Sentinel-1 to determine the extent of the aquifer over time (Brangers et al., 2020).

A third and final direction for future work is to model firn aquifer formation and life cycles using snow models. Firn aquifers provide a unique storage method for meltwater retention which reduces meltwater runoff from mass loss of the GrIS. Observations of these stored systems are sparse and therefore it is essential that we are able to simulate them using snowpack

models which can assist in quantifying current and future mass balance estimates. Previous studies have used various snow/firn models (such as SNOWPACK) to simulate meltwater percolation, refreezing, and retention processes (Steger et al., 2017; Verjans et al., 2019) such as aquifers. We plan to build on this work to better understand how different percolation schemes influence water retention in firn and evaluate how to better simulate firn aquifers in ice sheet snowpacks.

In our future simulations, we plan to implement a bucket scheme and a new meltwater percolation scheme based on Richard's Equations which allows for more saturation and should improve the accuracy of the density profiles and liquid water content quantities (Wever et al., 2014). Once our method is validated with all sites of known aquifers in Greenland based on observations, we can expand our method to a recent aquifer found on the Wilkins Ice Shelf in Antarctica. With limited observations there, uncertainties will be high, though with a proven method we may be able to identify more about the structure, extent, and volume of the aquifer. We can also run SNOWPACK for the entire GrIS and see where aquifers may be at present, especially in regions where we have not discovered them due to lack of observations. Additionally, we can run SNOWPACK with forcings from different climate scenarios to determine where firn aquifers are likely to form in the future and how much liquid water will be able to be retained in the firn.

Beyond the goal of understanding surface mass balance processes, there is a need to expand our niche knowledge of ice sheets in the scope of the broad Earth-atmosphere system. In order to advance scientific progress in geosciences, we must look to larger interdisciplinary research combining many sub disciplines of geology, atmospheric science, oceanography, as well as social sciences, health, and communication. In the end, the Earth system is dynamic and

chaotic, and scientists must work collaboratively to inform current and future generations of climatic change.

6 References

Agosta, C., Amory, C., Kittel, C., Orsi, A., Favier, V., Gallée, H., et al. (2019). Estimation of the Antarctic surface mass balance using the regional climate model MAR (1979–2015) and identification of dominant processes. *The Cryosphere*, *13*(1), 281–296. https://doi.org/10.5194/tc-13-281-2019

Albert, M. (2007). Snow and Firn Permeability: Characteristics of Snow Megadunes and their Potential Effects on Ice Core Interpretation [Data set]. U.S. Antarctic Program Data Center (USAP-DC), via National Snow and Ice Data Center (NSIDC). https://doi.org/10.7265/N5639MPD

Albert, M. R., & Shultz, E. F. (2002). Snow and firn properties and air–snow transport processes at Summit, Greenland. *Atmospheric Environment*, *36*(15), 2789–2797. https://doi.org/10.1016/S1352-2310(02)00119-X

Alexander, P. M., Tedesco, M., Koenig, L., & Fettweis, X. (2019). Evaluating a Regional Climate Model Simulation of Greenland Ice Sheet Snow and Firn Density for Improved Surface Mass Balance Estimates. *Geophysical Research Letters*, *46*(21), 12073–12082. https://doi.org/10.1029/2019GL084101

Alley, R. B., Saltzman, E. S., Cuffey, K. M., & Fitzpatrick, J. J. (1990). Summertime formation of Depth Hoar in central Greenland. *Geophysical Research Letters*, *17*(13), 2393–2396. https://doi.org/10.1029/GL017i013p02393

Alley, Richard B. (1988). Concerning the Deposition and Diagenesis of Strata in Polar Firn. *Journal of Glaciology*, *34*(118), 283–290. https://doi.org/10.3189/S0022143000007024

Alley, Richard B. (1999). GISP2 Stratigraphy [Data set]. https://doi.org/10.1594/PANGAEA.56103

van Angelen, J. H., M. Lenaerts, J. T., van den Broeke, M. R., Fettweis, X., & van Meijgaard, E. (2013). Rapid loss of firn pore space accelerates 21st century Greenland mass loss: 21ST CENTURY GREENLAND SMB. *Geophysical Research Letters*, *40*(10), 2109–2113. https://doi.org/10.1002/grl.50490

van Angelen, J. H., van den Broeke, M. R., Wouters, B., & Lenaerts, J. T. M. (2014). Contemporary (1960–2012) Evolution of the Climate and Surface Mass Balance of the Greenland Ice Sheet. *Surveys in Geophysics*, *35*(5), 1155–1174. https://doi.org/10.1007/s10712-013-9261-z

Anschütz, H., & Oerter, H. (2007a). Accumulation rate of firn core DML67C04_02 (FB0402) [Data set]. https://doi.org/10.1594/PANGAEA.609883

Anschütz, H., & Oerter, H. (2007b). Accumulation rate of firn core DML68C04_03 (FB0403) [Data set]. https://doi.org/10.1594/PANGAEA.609904

Anschütz, H., & Oerter, H. (2007c). Accumulation rate of firn core DML71C05_01 (FB0501) [Data set]. https://doi.org/10.1594/PANGAEA.609905

Anschütz, H., & Oerter, H. (2007d). Accumulation rate of firn core DML72C05_02 (FB0502) [Data set]. https://doi.org/10.1594/PANGAEA.609906

Anschütz, H., & Oerter, H. (2007e). Accumulation rate of firn core DML73C05_03 (FB0503) [Data set]. https://doi.org/10.1594/PANGAEA.609907

Anschütz, H., & Oerter, H. (2007f). Accumulation rate of firn core DML74C05_04 (FB0504) [Data set]. https://doi.org/10.1594/PANGAEA.609908

Arthern, R. J., Winebrenner, D. P., & Vaughan, D. G. (2006). Antarctic snow accumulation mapped using polarization of 4.3-cm wavelength microwave emission. *Journal of Geophysical Research: Atmospheres*, *111*(D6). https://doi.org/10.1029/2004JD005667

Baker, Ian. (2016). NEEM Firn Core 2009S2 Density and Permeability [Data set]. NSF Arctic Data Archive. https://doi.org/10.18739/A2Q88G

Bales, R. C., McConnell, J. R., Mosley-Thompson, E., & Csatho, B. (2001). Accumulation over the Greenland ice sheet from historical and recent records. *Journal of Geophysical Research: Atmospheres*, *106*(D24), 33813–33825. https://doi.org/10.1029/2001JD900153

Banta, J. R., McConnell, J. R., Frey, M. M., Bales, R. C., & Taylor, K. (2008). Spatial and temporal variability in snow accumulation at the West Antarctic Ice Sheet Divide over recent centuries. *Journal of Geophysical Research: Atmospheres*, *113*(D23). https://doi.org/10.1029/2008JD010235

Banwell, A. F., MacAyeal, D. R., & Sergienko, O. V. (2013). Breakup of the Larsen B Ice Shelf triggered by chain reaction drainage of supraglacial lakes: LARSEN B CHAIN REACTION LAKE DRAINAGE. *Geophysical Research Letters*, *40*(22), 5872–5876. https://doi.org/10.1002/2013GL057694

Barrand, N. E., Vaughan, D. G., Steiner, N., Tedesco, M., Kuipers Munneke, P., van den Broeke, M. R., & Hosking, J. S. (2013). Trends in Antarctic Peninsula surface melting conditions from observations and regional climate modeling: ANTARCTIC PENINSULA MELT TRENDS. *Journal of Geophysical Research: Earth Surface*, *118*(1), 315–330. https://doi.org/10.1029/2012JF002559

Bell, R. E., Chu, W., Kingslake, J., Das, I., Tedesco, M., Tinto, K. J., et al. (2017). Antarctic ice shelf potentially stabilized by export of meltwater in surface river. *Nature*, *544*(7650), 344–348. https://doi.org/10.1038/nature22048

Bell, R. E., Banwell, A. F., Trusel, L. D., & Kingslake, J. (2018). Antarctic surface hydrology and impacts on ice-sheet mass balance. *Nature Climate Change*, *8*(12), 1044. https://doi.org/10.1038/s41558-018-0326-3

Bellaire, S., Proksch, M., Schneebeli, M., Niwano, M., & Steffen, K. (2017). Measured and Modeled Snow Cover Properties across the Greenland Ice Sheet. *The Cryosphere Discussions*, 1–22. https://doi.org/10.5194/tc-2017-55

Benedek, C., & Willis, I. (2020). *Winter drainage of surface lakes on the Greenland Ice Sheet from Sentinel-1 SAR Imagery* (preprint). Ice sheets/Greenland. https://doi.org/10.5194/tc-2020-70

Benson, C. (2013). Greenland Snow Pit and Core Stratigraphy (Analog and Digital Formats) Boulder, Colorado USA: National Snow and Ice Data Center.

Benson, C. (2017). Greenland Snow it and Core Stratigraphy. Carl S. Benson Collection. Coll. 2010011. Roger G. Barry Archives and Resource Center. National Snow Data Center. [Accessed June 2017].

Berdahl, M., Rennermalm, A., Hammann, A., Mioduszweski, J., Hameed, S., Tedesco, M., et al. (2018). Southeast Greenland Winter Precipitation Strongly Linked to the Icelandic Low Position. *Journal of Climate*, *31*(11), 4483–4500. https://doi.org/10.1175/JCLI-D-17-0622.1

Bevis, M., Harig, C., Khan, S. A., Brown, A., Simons, F. J., Willis, M., et al. (2019). Accelerating changes in ice mass within Greenland, and the ice sheet's sensitivity to atmospheric forcing. *Proceedings of the National Academy of Sciences*, *116*(6), 1934–1939. https://doi.org/10.1073/pnas.1806562116

Bolzan, J. F., & Strobel, M. (1999a). Oxygen isotope data from snowpit at GISP2 Site 13 [Data set]. https://doi.org/10.1594/PANGAEA.55510

Bolzan, J. F., & Strobel, M. (1999b). Oxygen isotope data from snowpit at GISP2 Site 15 [Data set]. https://doi.org/10.1594/PANGAEA.55511

Bolzan, J. F., & Strobel, M. (1999c). Oxygen isotope data from snowpit at GISP2 Site 31 [Data set]. https://doi.org/10.1594/PANGAEA.55512

Bolzan, J. F., & Strobel, M. (1999d). Oxygen isotope data from snowpit at GISP2 Site 37 [Data set]. https://doi.org/10.1594/PANGAEA.55513

Bolzan, J. F., & Strobel, M. (1999e). Oxygen isotope data from snowpit at GISP2 Site 51 [Data set]. https://doi.org/10.1594/PANGAEA.55514

Bolzan, J. F., & Strobel, M. (1999f). Oxygen isotope data from snowpit at GISP2 Site 57 [Data set]. https://doi.org/10.1594/PANGAEA.55515

Bolzan, J. F., & Strobel, M. (1999g). Oxygen isotope data from snowpit at GISP2 Site 73 [Data set]. https://doi.org/10.1594/PANGAEA.55516

Bolzan, J. F., & Strobel, M. (2001a). Oxygen isotope data from snowpit at GISP2 Site 44 [Data set]. https://doi.org/10.1594/PANGAEA.59995

Bolzan, J. F., & Strobel, M. (2001b). Oxygen isotope data from snowpit at GISP2 Site 571 [Data set]. https://doi.org/10.1594/PANGAEA.59996

Bowling, J. S., Livingstone, S. J., Sole, A. J., & Chu, W. (2019). Distribution and dynamics of Greenland subglacial lakes. *Nature Communications*, *10*(1). https://doi.org/10.1038/s41467-019-10821-w

Box, J. E., & Steffen, K. (2001). Sublimation on the Greenland Ice Sheet from automated weather station observations. *Journal of Geophysical Research: Atmospheres*, *106*(D24), 33965–33981. https://doi.org/10.1029/2001JD900219

Brangers, I., Lievens, H., Miège, C., Demuzere, M., Brucker, L., & De Lannoy, G. J. M. (2020). Sentinel-1 Detects Firn Aquifers in the Greenland Ice Sheet. *Geophysical Research Letters*, *47*(3). https://doi.org/10.1029/2019GL085192

Braun, M., Humbert, A., & Moll, A. (2009). Changes of Wilkins Ice Shelf over the past 15 years and inferences on its stability. *The Cryosphere*, *3*(1), 41–56. https://doi.org/10.5194/tc-3-41-2009

van den Broeke, M. R., Enderlin, E. M., Howat, I. M., Kuipers Munneke, P., Noël, B. P. Y., van de Berg, W. J., et al. (2016). On the recent contribution of the Greenland ice sheet to sea level change. *The Cryosphere*, *10*(5), 1933–1946. https://doi.org/10.5194/tc-10-1933-2016

van den Broeke, M., Bamber, J., Ettema, J., Rignot, E., Schrama, E., van de Berg, W. J., et al. (2009). Partitioning Recent Greenland Mass Loss. *Science*, *326*(5955), 984–986. https://doi.org/10.1126/science.1178176

van den Broeke, Michiel, Box, J., Fettweis, X., Hanna, E., Noël, B., Tedesco, M., et al. (2017). Greenland Ice Sheet Surface Mass Loss: Recent Developments in Observation and Modeling. *Current Climate Change Reports*, *3*(4), 345–356. https://doi.org/10.1007/s40641-017-0084-8

Brun, E., Martin, E., Simon, V., Gendre, C., & Coléou, C. (1989). An energy and mass model of snow cover suitable for operational avalanche forecasting. *Journal of Glaciology*, *35*, 333–342. https://doi.org/10.1017/S0022143000009254

Brun, E., David, P., Sudul, M., & Brunot, G. (1992). A numerical model to simulate snow-cover stratigraphy for operational avalanche forecasting. *Journal of Glaciology*, *38*, 13–22. https://doi.org/10.1017/S0022143000009552

Burgener, L., Rupper, S., Koenig, L., Forster, R., Christensen, W. F., Williams, J., et al. (2013). An observed negative trend in West Antarctic accumulation rates from 1975 to 2010: Evidence from new observed and simulated records. *Journal of Geophysical Research: Atmospheres*, *118*(10), 4205–4216. https://doi.org/10.1002/jgrd.50362

Burgess, E. W., Forster, R. R., Box, J. E., Mosley-Thompson, E., Bromwich, D. H., Bales, R. C., & Smith, L. C. (2010). A spatially calibrated model of annual accumulation rate on the Greenland Ice Sheet (1958–2007). *Journal of Geophysical Research: Earth Surface*, *115*(F2). https://doi.org/10.1029/2009JF001293

Chellman, N. (2016). Core Atmospheric and Snow Measurements at Summit Greenland Environmental Observatory: Snow Pit [Data set]. NSF Arctic Data Archive. https://doi.org/10.18739/A2888F

Chen, J., & Mueller, V. (2018). Coastal climate change, soil salinity and human migration in Bangladesh. *Nature Climate Change*, *8*(11), 981–985. https://doi.org/10.1038/s41558-018-0313-8

Cherry, J., & Freeze, R. A. (1979). *Groundwater*. Englewood Cliffs, NJ: Prentice Hall.

Christianson, K., Kohler, J., Alley, R. B., Nuth, C., & Pelt, W. J. J. van. (2015). Dynamic perennial firn aquifer on an Arctic glacier. *Geophysical Research Letters*, *42*(5), 1418–1426. https://doi.org/10.1002/2014GL062806

Chu, V. W. (2014). Greenland ice sheet hydrology: A review. *Progress in Physical Geography: Earth and Environment*, *38*(1), 19–54. https://doi.org/10.1177/0309133313507075

Church, J. A., Clark, P. U., Cazenave, A., Gregory, J. M., Jevrejeva, S., Levermann, A., et al. (2013). Sea Level Change. In: Climate Change 2013: The Physical Science Basis. Contribution of Working Group I to the Fifth Assessment Report of the Intergovernmental Panel on Climate Change [Stocker, T.F., D. Qin, G.-K. Plattner, M. Tignor, S.K. Allen, J. Boschung, A. Nauels, Y. Xia, V. Bex and P.M. Midgley (eds.)]. Cambridge University Press, Cambridge, United Kingdom and New York, NY, USA.

Conger, S. M., & McClung, D. M. (2009). Comparison of density cutters for snow profile observations. *Journal of Glaciology*, *55*(189), 163–169. https://doi.org/10.3189/002214309788609038

Conway, H. (2003). Roosevelt Island Ice Core Density and Beta Count Data [Data set]. U.S. Antarctic Program Data Center (USAP-DC), via National Snow and Ice Data Center (NSIDC). https://doi.org/10.7265/N55718ZW

Cooper, M. G., Smith, L. C., Rennermalm, A. K., Pitcher, L., Ryan, J. C., Yang, K., & Cooley, S. W. (2018). Direct measurements of ice density down to 1m depth in the Greenland Ice Sheet ablation zone during July 2016 from shallow ice cores [Data set]. *In supplement to: Cooper, MG et al. (accepted): Near surface meltwater storage in low-density bare ice of the Greenland ice sheet ablation zone. The Cryosphere Discussions, 1-25, https://doi.org/10.5194/tc-2017-107*. https://doi.org/10.1594/PANGAEA.886747

Courville, Z. R., Albert, M. R., Fahnestock, M. A., Cathles, L. M., & Shuman, C. A. (2007). Impacts of an accumulation hiatus on the physical properties of firn at a low-accumulation polar site. *Journal of Geophysical Research: Earth Surface*, *112*(F2). https://doi.org/10.1029/2005JF000429

CReSIS. 2020. MCoRDS Data, Lawrence, Kansas, USA. Digital Media. http://data.cresis.ku.edu/. (n.d.).

Cuffey, K., & Paterson, W. S. B. (2010). *The physics of glaciers* (4th ed). Burlington, MA: Butterworth-Heinemann/Elsevier.

Das, I., Scambos, T. A., Koenig, L. S., Broeke, M. R. van den, & Lenaerts, J. T. M. (2015). Extreme wind-ice interaction over Recovery Ice Stream, East Antarctica. *Geophysical Research Letters*, *42*(19), 8064–8071. https://doi.org/10.1002/2015GL065544

Datta, R. T., Tedesco, M., Agosta, C., Fettweis, X., Kuipers Munneke, P., & van den Broeke, M. R. (2018). Melting over the northeast Antarctic Peninsula (1999–2009): evaluation of a high-resolution regional climate model. *The Cryosphere*, *12*(9), 2901–2922. https://doi.org/10.5194/tc-12-2901-2018

Datta, R. T., Tedesco, M., Fettweis, X., Agosta, C., Lhermitte, S., Lenaerts, J. T. M., & Wever, N. (2019). The Effect of Foehn-Induced Surface Melt on Firn Evolution Over the Northeast Antarctic Peninsula. *Geophysical Research Letters*, *46*(7), 3822–3831. https://doi.org/10.1029/2018GL080845

Dattler, M. E., Lenaerts, J. T. M., & Medley, B. (n.d.). Significant Spatial Variability in Radar-Derived West Antarctic Accumulation Linked to Surface Winds and Topography. *Geophysical Research Letters*, *n/a*(n/a). https://doi.org/10.1029/2019GL085363

Delhasse, A., Fettweis, X., Kittel, C., Amory, C., & Agosta, C. (2018). Brief communication: Impact of the recent atmospheric circulation change in summer on the future surface mass balance of the Greenland Ice Sheet. *The Cryosphere*, *12*(11), 3409–3418. https://doi.org/10.5194/tc-12-3409-2018

Dibb, J. E. (2017). Personal Communication.

Dibb, J. E., & Fahnestock, M. (2004). Snow accumulation, surface height change, and firn densification at Summit, Greenland: Insights from 2 years of in situ observation. *Journal of Geophysical Research: Atmospheres*, *109*(D24). https://doi.org/10.1029/2003JD004300

Dibb, J. E., Whitlow, S. I., & Arsenault, M. (2007). Seasonal variations in the soluble ion content of snow at Summit. Greenland: Constraints from three years of daily surface snow samples. *Atmospheric Environment*, *41*(24), 5007–5019. https://doi.org/10.1016/j.atmosenv.2006.12.010

Dunmire, D., Lenaerts, J. T. M., Banwell, A. F., Wever, N., Shragge, J., Lhermitte, S., et al. (2020). Observations of Buried Lake Drainage on the Antarctic Ice Sheet. *Geophysical Research Letters*, *47*(15). https://doi.org/10.1029/2020GL087970

Enderlin, E. M., Howat, I. M., Jeong, S., Noh, M.-J., Angelen, J. H. van, & Broeke, M. R. van den. (2014). An improved mass budget for the Greenland ice sheet. *Geophysical Research Letters*, *41*(3), 866–872. https://doi.org/10.1002/2013GL059010

Ettema, J., van den Broeke, M. R., van Meijgaard, E., van de Berg, W. J., Bamber, J. L., Box, J. E., & Bales, R. C. (2009). Higher surface mass balance of the Greenland ice sheet revealed by high-resolution climate modeling. *Geophysical Research Letters*, *36*(12). https://doi.org/10.1029/2009GL038110

Fausto, R. S., Box, J. E., Vandecrux, B., van As, D., Steffen, K., MacFerrin, M. J., et al. (2018). A Snow Density Dataset for Improving Surface Boundary Conditions in Greenland Ice Sheet Firn Modeling. *Frontiers in Earth Science*, *6*. https://doi.org/10.3389/feart.2018.00051

Favier, V., Agosta, C., Parouty, S., Durand, G., Delaygue, G., Gallée, H., et al. (2013). An updated and quality controlled surface mass balance dataset for Antarctica. *The Cryosphere*, *7*(2), 583–597. https://doi.org/10.5194/tc-7-583-2013

Fernandoy, F., Meyer, H., Oerter, H., Wilhelms, F., Graf, W., & Schwander, J. (2010a). Annual means of d18O, density, and accumulation rates of firn core DML641C02_01 [Data set]. *In supplement to: Fernandoy, F et al. (2010): Temporal and Spatial variation of stable-isotope ratios and accumulation rates in the hinterland of Neumayer station, East Antarctica. Journal of Glaciology, 56(198), 673-687, https://doi.org/10.3189/002214310793146296*. https://doi.org/10.1594/PANGAEA.753157

Fernandoy, F., Meyer, H., Oerter, H., Wilhelms, F., Graf, W., & Schwander, J. (2010b). Annual means of d18O, density, and accumulation rates of firn core DML651C02_03 [Data set]. *In supplement to: Fernandoy, F et al. (2010): Temporal and Spatial variation of stable-isotope ratios and accumulation rates in the hinterland of Neumayer station, East Antarctica. Journal of Glaciology, 56(198), 673-687, https://doi.org/10.3189/002214310793146296*. https://doi.org/10.1594/PANGAEA.753158

Fernandoy, F., Meyer, H., Oerter, H., Wilhelms, F., Graf, W., & Schwander, J. (2010c). Annual means of d18O, deuterium, density, and accumulation rates of firn core NM02C02_02 [Data set]. *In supplement to: Fernandoy, F et al. (2010): Temporal and Spatial variation of stable-isotope ratios and accumulation rates in the hinterland of Neumayer station, East Antarctica. Journal of Glaciology, 56(198), 673-687, https://doi.org/10.3189/002214310793146296*. https://doi.org/10.1594/PANGAEA.753159

Ferris, D. G., Cole-Dai, J., Reyes, A. R., & Budner, D. M. (2011). South Pole ice core record of explosive volcanic eruptions in the first and second millennia A.D. and evidence of a large eruption in the tropics around 535 A.D. *Journal of Geophysical Research: Atmospheres*, *116*(D17). https://doi.org/10.1029/2011JD015916

Fettweis, X., Franco, B., Tedesco, M., van Angelen, J. H., Lenaerts, J. T. M., van den Broeke, M. R., & Gallée, H. (2013). Estimating the Greenland ice sheet surface mass balance contribution to future sea level rise using the regional atmospheric climate model MAR. *The Cryosphere*, *7*(2), 469–489. https://doi.org/10.5194/tc-7-469-2013

Fettweis, Xavier, Box, J. E., Agosta, C., Amory, C., Kittel, C., Lang, C., et al. (2017). Reconstructions of the 1900–2015 Greenland ice sheet surface mass balance using the regional climate MAR model. *The Cryosphere*, *11*(2), 1015–1033. https://doi.org/10.5194/tc-11-1015-2017

Fornasini, P. (2008). *The Uncertainty in Physical Measurements*. New York, NY: Springer New York. https://doi.org/10.1007/978-0-387-78650-6

Forster, R. R., Box, J. E., van den Broeke, M. R., Miège, C., Burgess, E. W., van Angelen, J. H., et al. (2014). Extensive liquid meltwater storage in firn within the Greenland ice sheet. *Nature Geoscience*, *7*(2), 95–98. https://doi.org/10.1038/ngeo2043

Fountain, A. G., & Walder, J. S. (1998). Water flow through temperate glaciers. *Reviews of Geophysics*, *36*(3), 299–328. https://doi.org/10.1029/97RG03579

Fricker, H. A., Bassis, J. N., Minster, B., & MacAyeal, D. R. (2005). ICESat's new perspective on ice shelf rifts: The vertical dimension. *Geophysical Research Letters*, *32*(23). https://doi.org/10.1029/2005GL025070

Gardner, J., Richter-Menge, J., Farrell, S., & Brozena, J. (2012). Coincident multiscale estimates of Arctic sea ice thickness. *Eos, Transactions American Geophysical Union*, *93*(6), 57–58. https://doi.org/10.1029/2012EO060001

Gerland, S., & Wilhelms, F. (1999). Continuous density log of icecore BER11C95_25 [Data set]. *Supplement to: Gerland, Sebastian; Oerter, Hans; Kipfstuhl, Sepp; Wilhelms, Frank; Miller, Heinz (1999): Continuous density log of a 181 metre long ice core from the summit of Berkner Island, Antarctica. Annals of Glaciology, 29, 215-219, https://doi.org/10.3189/172756499781821427*. https://doi.org/10.1594/PANGAEA.227732

Goelzer, H., Nowicki, S., Payne, A., Larour, E., Seroussi, H., Lipscomb, W. H., et al. (2020). The future sea-level contribution of the Greenland ice sheet: a multi-model ensemble study of ISMIP6. *The Cryosphere*, *14*(9), 3071–3096. https://doi.org/10.5194/tc-14-3071-2020

Graf, W., & Oerter, H. (2006a). Annual means of density, d18O, and accumulation rates of snow pit BER01S90_01 [Data set]. *In supplement to: Graf, Wolfgang; Moser, Heribert; Reinwarth, Oskar; Kipfstuhl, Sepp; Oerter, Hans; Minikin, Andreas; Wagenbach, Dietmar (1994): Snow-accumulation rates and isotopic content (2H, 3H) of near-surface firn from the Filchner-Ronne Ice Shelf, Antarctica. Annals of Glaciology, 20, 121-128, hdl:10013/epic.11645.d001*. https://doi.org/10.1594/PANGAEA.548700

Graf, W., & Oerter, H. (2006b). Annual means of density, d18O, and accumulation rates of snow pit BER01S90_01 [Data set]. *In supplement to: Graf, Wolfgang; Moser, Heribert; Reinwarth, Oskar; Kipfstuhl, Sepp; Oerter, Hans; Minikin, Andreas; Wagenbach, Dietmar (1994): Snow-accumulation rates and isotopic content (2H, 3H) of near-surface firn from the Filchner-Ronne Ice Shelf, Antarctica. Annals of Glaciology, 20, 121-128, hdl:10013/epic.11645.d001*. https://doi.org/10.1594/PANGAEA.548700

Graf, W., & Oerter, H. (2006c). Annual means of density, d18O, and accumulation rates of snow pit BER02S90_02 [Data set]. *In supplement to: Graf, Wolfgang; Moser, Heribert; Reinwarth, Oskar; Kipfstuhl, Sepp; Oerter, Hans; Minikin, Andreas; Wagenbach, Dietmar (1994): Snow-accumulation rates and isotopic content (2H, 3H) of near-surface firn from the Filchner-Ronne Ice Shelf, Antarctica. Annals of Glaciology, 20, 121-128, hdl:10013/epic.11645.d001*. https://doi.org/10.1594/PANGAEA.548701

Graf, W., & Oerter, H. (2006d). Annual means of density, d18O, and accumulation rates of snow pit BER02S90_02 [Data set]. *In supplement to: Graf, Wolfgang; Moser, Heribert; Reinwarth, Oskar; Kipfstuhl, Sepp; Oerter, Hans; Minikin, Andreas; Wagenbach, Dietmar (1994): Snow-accumulation rates and isotopic content (2H, 3H) of near-surface firn from the Filchner-Ronne Ice Shelf, Antarctica. Annals of Glaciology, 20, 121-128, hdl:10013/epic.11645.d001*. https://doi.org/10.1594/PANGAEA.548701

Graf, W., & Oerter, H. (2006e). Annual means of density, d18O, and accumulation rates of snow pit FRI11S90_235 [Data set]. *In supplement to: Graf, Wolfgang; Moser, Heribert; Reinwarth, Oskar; Kipfstuhl, Sepp; Oerter, Hans; Minikin, Andreas; Wagenbach, Dietmar (1994): Snow-accumulation rates and isotopic content (2H, 3H) of near-surface firn from the Filchner-Ronne Ice Shelf, Antarctica. Annals of Glaciology, 20, 121-128, hdl:10013/epic.11645.d001*. https://doi.org/10.1594/PANGAEA.548664

Graf, W., & Oerter, H. (2006f). Annual means of density, d18O, and accumulation rates of snow pit FRI12S90_236 [Data set]. *In supplement to: Graf, Wolfgang; Moser, Heribert; Reinwarth, Oskar; Kipfstuhl, Sepp; Oerter, Hans; Minikin, Andreas; Wagenbach, Dietmar (1994): Snow-accumulation rates and isotopic content (2H, 3H) of near-surface firn from the Filchner-Ronne Ice Shelf, Antarctica. Annals of Glaciology, 20, 121-128, hdl:10013/epic.11645.d001*. https://doi.org/10.1594/PANGAEA.548665

Graf, W., & Oerter, H. (2006g). Annual means of density, d18O, and accumulation rates of snow pit FRI12S90_236 [Data set]. *In supplement to: Graf, Wolfgang; Moser, Heribert; Reinwarth, Oskar; Kipfstuhl, Sepp; Oerter, Hans; Minikin, Andreas; Wagenbach, Dietmar (1994): Snow-accumulation rates and isotopic content (2H, 3H) of near-surface firn from the Filchner-Ronne Ice Shelf, Antarctica. Annals of Glaciology, 20, 121-128, hdl:10013/epic.11645.d001*. https://doi.org/10.1594/PANGAEA.548665

Graf, W., & Oerter, H. (2006h). Annual means of density, d18O, and accumulation rates of snow pit FRI13S90_335 [Data set]. *In supplement to: Graf, Wolfgang; Moser, Heribert; Reinwarth, Oskar; Kipfstuhl, Sepp; Oerter, Hans; Minikin, Andreas; Wagenbach, Dietmar (1994): Snow-accumulation rates and isotopic content (2H, 3H) of near-surface firn from the Filchner-Ronne Ice Shelf, Antarctica. Annals of Glaciology, 20, 121-128, hdl:10013/epic.11645.d001*. https://doi.org/10.1594/PANGAEA.548666

Graf, W., & Oerter, H. (2006i). Annual means of density, d18O, and accumulation rates of snow pit FRI15S90_131 [Data set]. *In supplement to: Graf, Wolfgang; Moser, Heribert; Reinwarth, Oskar; Kipfstuhl, Sepp; Oerter, Hans; Minikin, Andreas; Wagenbach, Dietmar (1994): Snow-accumulation*

rates and isotopic content (2H, 3H) of near-surface firn from the Filchner-Ronne Ice Shelf, Antarctica. Annals of Glaciology, 20, 121-128, hdl:10013/epic.11645.d001. https://doi.org/10.1594/PANGAEA.548667

Graf, W., & Oerter, H. (2006j). Annual means of density, d18O, and accumulation rates of snow pit FRI16S90_230 [Data set]. *In supplement to: Graf, Wolfgang; Moser, Heribert; Reinwarth, Oskar; Kipfstuhl, Sepp; Oerter, Hans; Minikin, Andreas; Wagenbach, Dietmar (1994): Snow-accumulation rates and isotopic content (2H, 3H) of near-surface firn from the Filchner-Ronne Ice Shelf, Antarctica. Annals of Glaciology, 20, 121-128, hdl:10013/epic.11645.d001.* https://doi.org/10.1594/PANGAEA.548668

Graf, W., & Oerter, H. (2006k). Annual means of density, d18O, and accumulation rates of snow pit FRI17S90_231 [Data set]. *In supplement to: Graf, Wolfgang; Moser, Heribert; Reinwarth, Oskar; Kipfstuhl, Sepp; Oerter, Hans; Minikin, Andreas; Wagenbach, Dietmar (1994): Snow-accumulation rates and isotopic content (2H, 3H) of near-surface firn from the Filchner-Ronne Ice Shelf, Antarctica. Annals of Glaciology, 20, 121-128, hdl:10013/epic.11645.d001.* https://doi.org/10.1594/PANGAEA.548669

Graf, W., & Oerter, H. (2006l). Annual means of density, d18O, deuterium, and accumulation rates of firn core FRI21C90_HWF [Data set]. *In supplement to: Graf, Wolfgang; Moser, Heribert; Reinwarth, Oskar; Kipfstuhl, Sepp; Oerter, Hans; Minikin, Andreas; Wagenbach, Dietmar (1994): Snow-accumulation rates and isotopic content (2H, 3H) of near-surface firn from the Filchner-Ronne Ice Shelf, Antarctica. Annals of Glaciology, 20, 121-128, hdl:10013/epic.11645.d001.* https://doi.org/10.1594/PANGAEA.548652

Graf, W., & Oerter, H. (2006m). Annual means of density, d18O, deuterium, and accumulation rates of snow pit FRI18S90_330 [Data set]. *In supplement to: Graf, Wolfgang; Moser, Heribert; Reinwarth, Oskar; Kipfstuhl, Sepp; Oerter, Hans; Minikin, Andreas; Wagenbach, Dietmar (1994): Snow-accumulation rates and isotopic content (2H, 3H) of near-surface firn from the Filchner-Ronne Ice Shelf, Antarctica. Annals of Glaciology, 20, 121-128, hdl:10013/epic.11645.d001.* https://doi.org/10.1594/PANGAEA.548670

Graf, W., & Oerter, H. (2006n). Annual means of density, d18O, deuterium, tritium, and accumulation rates of firn core FRI10C90_136 [Data set]. *In supplement to: Graf, Wolfgang; Moser, Heribert; Reinwarth, Oskar; Kipfstuhl, Sepp; Oerter, Hans; Minikin, Andreas; Wagenbach, Dietmar (1994): Snow-accumulation rates and isotopic content (2H, 3H) of near-surface firn from the Filchner-Ronne Ice Shelf, Antarctica. Annals of Glaciology, 20, 121-128, hdl:10013/epic.11645.d001.* https://doi.org/10.1594/PANGAEA.548641

Graf, W., & Oerter, H. (2006o). Annual means of density, d18O, deuterium, tritium, and accumulation rates of firn core FRI12C90_236 [Data set]. *In supplement to: Graf, Wolfgang; Moser, Heribert; Reinwarth, Oskar; Kipfstuhl, Sepp; Oerter, Hans; Minikin, Andreas; Wagenbach, Dietmar (1994): Snow-accumulation rates and isotopic content (2H, 3H) of near-surface firn from the Filchner-Ronne Ice Shelf, Antarctica. Annals of Glaciology, 20, 121-128, hdl:10013/epic.11645.d001.* https://doi.org/10.1594/PANGAEA.548643

Graf, W., & Oerter, H. (2006p). Annual means of density, d18O, deuterium, tritium, and accumulation rates of firn core FRI14C90_336 [Data set]. *In supplement to: Graf, Wolfgang; Moser, Heribert; Reinwarth, Oskar; Kipfstuhl, Sepp; Oerter, Hans; Minikin, Andreas; Wagenbach, Dietmar (1994): Snow-accumulation rates and isotopic content (2H, 3H) of near-surface firn from the Filchner-Ronne Ice Shelf, Antarctica. Annals of Glaciology, 20, 121-128, hdl:10013/epic.11645.d001.* https://doi.org/10.1594/PANGAEA.548645

Graf, W., & Oerter, H. (2006q). Annual means of density, d18O, deuterium, tritium, and accumulation rates of firn core FRI16C90_230 [Data set]. *In supplement to: Graf, Wolfgang; Moser, Heribert; Reinwarth, Oskar; Kipfstuhl, Sepp; Oerter, Hans; Minikin, Andreas; Wagenbach, Dietmar (1994): Snow-accumulation rates and isotopic content (2H, 3H) of near-surface firn from the Filchner-Ronne Ice Shelf, Antarctica. Annals of Glaciology, 20, 121-128, hdl:10013/epic.11645.d001.* https://doi.org/10.1594/PANGAEA.548647

Graf, W., & Oerter, H. (2006r). Annual means of density, d18O, deuterium, tritium, and accumulation rates of firn core FRI18C90_330 [Data set]. *In supplement to: Graf, Wolfgang; Moser, Heribert; Reinwarth, Oskar; Kipfstuhl, Sepp; Oerter, Hans; Minikin, Andreas; Wagenbach, Dietmar (1994): Snow-accumulation rates and isotopic content (2H, 3H) of near-surface firn from the Filchner-Ronne Ice Shelf, Antarctica. Annals of Glaciology, 20, 121-128, hdl:10013/epic.11645.d001*. https://doi.org/10.1594/PANGAEA.548649

Graf, W., & Oerter, H. (2006s). Annual means of density, d18O, deuterium, tritium, and accumulation rates of firn core FRI19C90_05 [Data set]. *In supplement to: Graf, Wolfgang; Moser, Heribert; Reinwarth, Oskar; Kipfstuhl, Sepp; Oerter, Hans; Minikin, Andreas; Wagenbach, Dietmar (1994): Snow-accumulation rates and isotopic content (2H, 3H) of near-surface firn from the Filchner-Ronne Ice Shelf, Antarctica. Annals of Glaciology, 20, 121-128, hdl:10013/epic.11645.d001*. https://doi.org/10.1594/PANGAEA.548650

Graf, W., & Oerter, H. (2006t). Annual means of density, d18O, deuterium, tritium, and accumulation rates of firn core FRI20C90_06 [Data set]. *In supplement to: Graf, Wolfgang; Moser, Heribert; Reinwarth, Oskar; Kipfstuhl, Sepp; Oerter, Hans; Minikin, Andreas; Wagenbach, Dietmar (1994): Snow-accumulation rates and isotopic content (2H, 3H) of near-surface firn from the Filchner-Ronne Ice Shelf, Antarctica. Annals of Glaciology, 20, 121-128, hdl:10013/epic.11645.d001*. https://doi.org/10.1594/PANGAEA.548651

Graf, W., & Oerter, H. (2006u). Annual means of density, deuterium, and accumulation rates of firn core FRI09C90_90 [Data set]. *In supplement to: Graf, Wolfgang; Moser, Heribert; Reinwarth, Oskar; Kipfstuhl, Sepp; Oerter, Hans; Minikin, Andreas; Wagenbach, Dietmar (1994): Snow-accumulation rates and isotopic content (2H, 3H) of near-surface firn from the Filchner-Ronne Ice Shelf, Antarctica. Annals of Glaciology, 20, 121-128, hdl:10013/epic.11645.d001*. https://doi.org/10.1594/PANGAEA.548640

Graf, W., & Oerter, H. (2006v). Annual means of density, deuterium, and accumulation rates of firn core FRI11C90_235 [Data set]. *In supplement to: Graf, Wolfgang; Moser, Heribert; Reinwarth, Oskar; Kipfstuhl, Sepp; Oerter, Hans; Minikin, Andreas; Wagenbach, Dietmar (1994): Snow-accumulation rates and isotopic content (2H, 3H) of near-surface firn from the Filchner-Ronne Ice Shelf, Antarctica. Annals of Glaciology, 20, 121-128, hdl:10013/epic.11645.d001*. https://doi.org/10.1594/PANGAEA.548642

Graf, W., & Oerter, H. (2006w). Annual means of density, deuterium, and accumulation rates of firn core FRI13C90_335 [Data set]. *In supplement to: Graf, Wolfgang; Moser, Heribert; Reinwarth, Oskar; Kipfstuhl, Sepp; Oerter, Hans; Minikin, Andreas; Wagenbach, Dietmar (1994): Snow-accumulation rates and isotopic content (2H, 3H) of near-surface firn from the Filchner-Ronne Ice Shelf, Antarctica. Annals of Glaciology, 20, 121-128, hdl:10013/epic.11645.d001*. https://doi.org/10.1594/PANGAEA.548644

Graf, W., & Oerter, H. (2006x). Annual means of density, deuterium, and accumulation rates of firn core FRI15C90_131 [Data set]. *In supplement to: Graf, Wolfgang; Moser, Heribert; Reinwarth, Oskar; Kipfstuhl, Sepp; Oerter, Hans; Minikin, Andreas; Wagenbach, Dietmar (1994): Snow-accumulation rates and isotopic content (2H, 3H) of near-surface firn from the Filchner-Ronne Ice Shelf, Antarctica. Annals of Glaciology, 20, 121-128, hdl:10013/epic.11645.d001*. https://doi.org/10.1594/PANGAEA.548646

Graf, W., & Oerter, H. (2006y). Annual means of density, deuterium, and accumulation rates of firn core FRI17C90_231 [Data set]. *In supplement to: Graf, Wolfgang; Moser, Heribert; Reinwarth, Oskar; Kipfstuhl, Sepp; Oerter, Hans; Minikin, Andreas; Wagenbach, Dietmar (1994): Snow-accumulation rates and isotopic content (2H, 3H) of near-surface firn from the Filchner-Ronne Ice Shelf, Antarctica. Annals of Glaciology, 20, 121-128, hdl:10013/epic.11645.d001*. https://doi.org/10.1594/PANGAEA.548648

Graf, W., & Oerter, H. (2006z). Density and d18O of firn core FRI02C92_246 [Data set]. *In supplement to: Graf, Wolfgang; Moser, Heribert; Reinwarth, Oskar; Kipfstuhl, Sepp; Oerter, Hans; Minikin, Andreas; Wagenbach, Dietmar (1994): Snow-accumulation rates and isotopic content (2H, 3H) of*

near-surface firn from the Filchner-Ronne Ice Shelf, Antarctica. Annals of Glaciology, 20, 121-128, hdl:10013/epic.11645.d001. https://doi.org/10.1594/PANGAEA.548623

Graf, W., & Oerter, H. (2006aa). Density and d18O of snow pit FRI10S90_136 [Data set]. *In supplement to: Graf, Wolfgang; Moser, Heribert; Reinwarth, Oskar; Kipfstuhl, Sepp; Oerter, Hans; Minikin, Andreas; Wagenbach, Dietmar (1994): Snow-accumulation rates and isotopic content (2H, 3H) of near-surface firn from the Filchner-Ronne Ice Shelf, Antarctica. Annals of Glaciology, 20, 121-128, hdl:10013/epic.11645.d001*. https://doi.org/10.1594/PANGAEA.548655

Graf, W., & Oerter, H. (2006ab). Density and d18O of snow pit FRI11S90_235 [Data set]. *In supplement to: Graf, Wolfgang; Moser, Heribert; Reinwarth, Oskar; Kipfstuhl, Sepp; Oerter, Hans; Minikin, Andreas; Wagenbach, Dietmar (1994): Snow-accumulation rates and isotopic content (2H, 3H) of near-surface firn from the Filchner-Ronne Ice Shelf, Antarctica. Annals of Glaciology, 20, 121-128, hdl:10013/epic.11645.d001*. https://doi.org/10.1594/PANGAEA.548656

Graf, W., & Oerter, H. (2006ac). Density and d18O of snow pit FRI12S90_236 [Data set]. *In supplement to: Graf, Wolfgang; Moser, Heribert; Reinwarth, Oskar; Kipfstuhl, Sepp; Oerter, Hans; Minikin, Andreas; Wagenbach, Dietmar (1994): Snow-accumulation rates and isotopic content (2H, 3H) of near-surface firn from the Filchner-Ronne Ice Shelf, Antarctica. Annals of Glaciology, 20, 121-128, hdl:10013/epic.11645.d001*. https://doi.org/10.1594/PANGAEA.548657

Graf, W., & Oerter, H. (2006ad). Density and d18O of snow pit FRI13S90_335 [Data set]. *In supplement to: Graf, Wolfgang; Moser, Heribert; Reinwarth, Oskar; Kipfstuhl, Sepp; Oerter, Hans; Minikin, Andreas; Wagenbach, Dietmar (1994): Snow-accumulation rates and isotopic content (2H, 3H) of near-surface firn from the Filchner-Ronne Ice Shelf, Antarctica. Annals of Glaciology, 20, 121-128, hdl:10013/epic.11645.d001*. https://doi.org/10.1594/PANGAEA.548658

Graf, W., & Oerter, H. (2006ae). Density and d18O of snow pit FRI15S90_131 [Data set]. *In supplement to: Graf, Wolfgang; Moser, Heribert; Reinwarth, Oskar; Kipfstuhl, Sepp; Oerter, Hans; Minikin, Andreas; Wagenbach, Dietmar (1994): Snow-accumulation rates and isotopic content (2H, 3H) of near-surface firn from the Filchner-Ronne Ice Shelf, Antarctica. Annals of Glaciology, 20, 121-128, hdl:10013/epic.11645.d001*. https://doi.org/10.1594/PANGAEA.548659

Graf, W., & Oerter, H. (2006af). Density and d18O of snow pit FRI16S90_230 [Data set]. *In supplement to: Graf, Wolfgang; Moser, Heribert; Reinwarth, Oskar; Kipfstuhl, Sepp; Oerter, Hans; Minikin, Andreas; Wagenbach, Dietmar (1994): Snow-accumulation rates and isotopic content (2H, 3H) of near-surface firn from the Filchner-Ronne Ice Shelf, Antarctica. Annals of Glaciology, 20, 121-128, hdl:10013/epic.11645.d001*. https://doi.org/10.1594/PANGAEA.548660

Graf, W., & Oerter, H. (2006ag). Density and d18O of snow pit FRI17S90_231 [Data set]. *In supplement to: Graf, Wolfgang; Moser, Heribert; Reinwarth, Oskar; Kipfstuhl, Sepp; Oerter, Hans; Minikin, Andreas; Wagenbach, Dietmar (1994): Snow-accumulation rates and isotopic content (2H, 3H) of near-surface firn from the Filchner-Ronne Ice Shelf, Antarctica. Annals of Glaciology, 20, 121-128, hdl:10013/epic.11645.d001*. https://doi.org/10.1594/PANGAEA.548661

Graf, W., & Oerter, H. (2006ah). Density and deuterium of firn core FRI09C90_90 [Data set]. *In supplement to: Graf, Wolfgang; Moser, Heribert; Reinwarth, Oskar; Kipfstuhl, Sepp; Oerter, Hans; Minikin, Andreas; Wagenbach, Dietmar (1994): Snow-accumulation rates and isotopic content (2H, 3H) of near-surface firn from the Filchner-Ronne Ice Shelf, Antarctica. Annals of Glaciology, 20, 121-128, hdl:10013/epic.11645.d001*. https://doi.org/10.1594/PANGAEA.548624

Graf, W., & Oerter, H. (2006ai). Density and deuterium of firn core FRI11C90_235 [Data set]. *In supplement to: Graf, Wolfgang; Moser, Heribert; Reinwarth, Oskar; Kipfstuhl, Sepp; Oerter, Hans; Minikin, Andreas; Wagenbach, Dietmar (1994): Snow-accumulation rates and isotopic content (2H, 3H) of near-surface firn from the Filchner-Ronne Ice Shelf, Antarctica. Annals of Glaciology, 20, 121-128, hdl:10013/epic.11645.d001*. https://doi.org/10.1594/PANGAEA.548626

Graf, W., & Oerter, H. (2006aj). Density and deuterium of firn core FRI13C90_335 [Data set]. *In supplement to: Graf, Wolfgang; Moser, Heribert; Reinwarth, Oskar; Kipfstuhl, Sepp; Oerter, Hans; Minikin, Andreas; Wagenbach, Dietmar (1994): Snow-accumulation rates and isotopic content (2H,*

3H) of near-surface firn from the Filchner-Ronne Ice Shelf, Antarctica. Annals of Glaciology, 20, 121-128, hdl:10013/epic.11645.d001. https://doi.org/10.1594/PANGAEA.548628

Graf, W., & Oerter, H. (2006ak). Density and deuterium of firn core FRI15C90_131 [Data set]. *In supplement to: Graf, Wolfgang; Moser, Heribert; Reinwarth, Oskar; Kipfstuhl, Sepp; Oerter, Hans; Minikin, Andreas; Wagenbach, Dietmar (1994): Snow-accumulation rates and isotopic content (2H, 3H) of near-surface firn from the Filchner-Ronne Ice Shelf, Antarctica. Annals of Glaciology, 20, 121-128, hdl:10013/epic.11645.d001*. https://doi.org/10.1594/PANGAEA.548630

Graf, W., & Oerter, H. (2006al). Density and deuterium of firn core FRI17C90_231 [Data set]. *In supplement to: Graf, Wolfgang; Moser, Heribert; Reinwarth, Oskar; Kipfstuhl, Sepp; Oerter, Hans; Minikin, Andreas; Wagenbach, Dietmar (1994): Snow-accumulation rates and isotopic content (2H, 3H) of near-surface firn from the Filchner-Ronne Ice Shelf, Antarctica. Annals of Glaciology, 20, 121-128, hdl:10013/epic.11645.d001*. https://doi.org/10.1594/PANGAEA.548632

Graf, W., & Oerter, H. (2006am). Density, d18O, and deuterium of firn core FRI21C90_HWF [Data set]. *In supplement to: Graf, Wolfgang; Moser, Heribert; Reinwarth, Oskar; Kipfstuhl, Sepp; Oerter, Hans; Minikin, Andreas; Wagenbach, Dietmar (1994): Snow-accumulation rates and isotopic content (2H, 3H) of near-surface firn from the Filchner-Ronne Ice Shelf, Antarctica. Annals of Glaciology, 20, 121-128, hdl:10013/epic.11645.d001*. https://doi.org/10.1594/PANGAEA.548636

Graf, W., & Oerter, H. (2006an). Density, d18O and deuterium of snow pit FRI18S90_330 [Data set]. *In supplement to: Graf, Wolfgang; Moser, Heribert; Reinwarth, Oskar; Kipfstuhl, Sepp; Oerter, Hans; Minikin, Andreas; Wagenbach, Dietmar (1994): Snow-accumulation rates and isotopic content (2H, 3H) of near-surface firn from the Filchner-Ronne Ice Shelf, Antarctica. Annals of Glaciology, 20, 121-128, hdl:10013/epic.11645.d001*. https://doi.org/10.1594/PANGAEA.548662

Graf, W., & Oerter, H. (2006ao). Density, d18O, deuterium, and tritium of firn core FRI10C90_136 [Data set]. *In supplement to: Graf, Wolfgang; Moser, Heribert; Reinwarth, Oskar; Kipfstuhl, Sepp; Oerter, Hans; Minikin, Andreas; Wagenbach, Dietmar (1994): Snow-accumulation rates and isotopic content (2H, 3H) of near-surface firn from the Filchner-Ronne Ice Shelf, Antarctica. Annals of Glaciology, 20, 121-128, hdl:10013/epic.11645.d001*. https://doi.org/10.1594/PANGAEA.548625

Graf, W., & Oerter, H. (2006ap). Density, d18O, deuterium, and tritium of firn core FRI12C90_236 [Data set]. *In supplement to: Graf, Wolfgang; Moser, Heribert; Reinwarth, Oskar; Kipfstuhl, Sepp; Oerter, Hans; Minikin, Andreas; Wagenbach, Dietmar (1994): Snow-accumulation rates and isotopic content (2H, 3H) of near-surface firn from the Filchner-Ronne Ice Shelf, Antarctica. Annals of Glaciology, 20, 121-128, hdl:10013/epic.11645.d001*. https://doi.org/10.1594/PANGAEA.548627

Graf, W., & Oerter, H. (2006aq). Density, d18O, deuterium, and tritium of firn core FRI14C90_336 [Data set]. *In supplement to: Graf, Wolfgang; Moser, Heribert; Reinwarth, Oskar; Kipfstuhl, Sepp; Oerter, Hans; Minikin, Andreas; Wagenbach, Dietmar (1994): Snow-accumulation rates and isotopic content (2H, 3H) of near-surface firn from the Filchner-Ronne Ice Shelf, Antarctica. Annals of Glaciology, 20, 121-128, hdl:10013/epic.11645.d001*. https://doi.org/10.1594/PANGAEA.548629

Graf, W., & Oerter, H. (2006ar). Density, d18O, deuterium, and tritium of firn core FRI16C90_230 [Data set]. *In supplement to: Graf, Wolfgang; Moser, Heribert; Reinwarth, Oskar; Kipfstuhl, Sepp; Oerter, Hans; Minikin, Andreas; Wagenbach, Dietmar (1994): Snow-accumulation rates and isotopic content (2H, 3H) of near-surface firn from the Filchner-Ronne Ice Shelf, Antarctica. Annals of Glaciology, 20, 121-128, hdl:10013/epic.11645.d001*. https://doi.org/10.1594/PANGAEA.548631

Graf, W., & Oerter, H. (2006as). Density, d18O, deuterium, and tritium of firn core FRI18C90_330 [Data set]. *In supplement to: Graf, Wolfgang; Moser, Heribert; Reinwarth, Oskar; Kipfstuhl, Sepp; Oerter, Hans; Minikin, Andreas; Wagenbach, Dietmar (1994): Snow-accumulation rates and isotopic content (2H, 3H) of near-surface firn from the Filchner-Ronne Ice Shelf, Antarctica. Annals of Glaciology, 20, 121-128, hdl:10013/epic.11645.d001*. https://doi.org/10.1594/PANGAEA.548633

Graf, W., & Oerter, H. (2006at). Density, d18O, deuterium, and tritium of firn core FRI19C90_05 [Data set]. *In supplement to: Graf, Wolfgang; Moser, Heribert; Reinwarth, Oskar; Kipfstuhl, Sepp; Oerter, Hans; Minikin, Andreas; Wagenbach, Dietmar (1994): Snow-accumulation rates and isotopic content*

(2H, 3H) of near-surface firn from the Filchner-Ronne Ice Shelf, Antarctica. Annals of Glaciology, 20, 121-128, hdl:10013/epic.11645.d001. https://doi.org/10.1594/PANGAEA.548634

Graf, W., & Oerter, H. (2006au). High resolution density, conductivity, deuterium, and d18O of ice core FRI12C92_15 [Data set]. *In supplement to: Graf, Wolfgang; Moser, Heribert; Reinwarth, Oskar; Kipfstuhl, Sepp; Oerter, Hans; Minikin, Andreas; Wagenbach, Dietmar (1994): Snow-accumulation rates and isotopic content (2H, 3H) of near-surface firn from the Filchner-Ronne Ice Shelf, Antarctica. Annals of Glaciology, 20, 121-128, hdl:10013/epic.11645.d001*. https://doi.org/10.1594/PANGAEA.548744

Graf, W., Moser, H., Oerter, H., Reinwarth, O., & Stichler, W. (1988a). Annual means of density, d18O, and accumulation rates of ice core FRI07C84_340 [Data set]. *In supplement to: Graf, W et al. (1988): Accumulation and ice core-studies on Filchner-Ronne Ice Shelf, Antarctica. Annals of Glaciology, 11, 23-31, hdl:10013/epic.25953.d001*. https://doi.org/10.1594/PANGAEA.549170

Graf, W., Moser, H., Oerter, H., Reinwarth, O., & Stichler, W. (1988b). Annual means of density, d18O, and accumulation rates of snow pit FRI05S86_240 [Data set]. *In supplement to: Graf, W et al. (1988): Accumulation and ice core-studies on Filchner-Ronne Ice Shelf, Antarctica. Annals of Glaciology, 11, 23-31, hdl:10013/epic.25953.d001*. https://doi.org/10.1594/PANGAEA.548930

Graf, W., Moser, H., Oerter, H., Reinwarth, O., & Stichler, W. (1988c). Density and d18O of snow pit FRI01S84_141 [Data set]. *In supplement to: Graf, W et al. (1988): Accumulation and ice core-studies on Filchner-Ronne Ice Shelf, Antarctica. Annals of Glaciology, 11, 23-31, hdl:10013/epic.25953.d001*. https://doi.org/10.1594/PANGAEA.548909

Graf, W., Moser, H., Oerter, H., Reinwarth, O., & Stichler, W. (1988d). Density and d18O of snow pit FRI03S86_345 [Data set]. *In supplement to: Graf, W et al. (1988): Accumulation and ice core-studies on Filchner-Ronne Ice Shelf, Antarctica. Annals of Glaciology, 11, 23-31, hdl:10013/epic.25953.d001*. https://doi.org/10.1594/PANGAEA.548910

Graf, W., Moser, H., Oerter, H., Reinwarth, O., & Stichler, W. (1988e). Density and d18O of snow pit FRI04S84_140 [Data set]. *In supplement to: Graf, W et al. (1988): Accumulation and ice core-studies on Filchner-Ronne Ice Shelf, Antarctica. Annals of Glaciology, 11, 23-31, hdl:10013/epic.25953.d001*. https://doi.org/10.1594/PANGAEA.548911

Graf, W., Moser, H., Oerter, H., Reinwarth, O., & Stichler, W. (1988f). Density and d18O of snow pit FRI05S84_240 [Data set]. *In supplement to: Graf, W et al. (1988): Accumulation and ice core-studies on Filchner-Ronne Ice Shelf, Antarctica. Annals of Glaciology, 11, 23-31, hdl:10013/epic.25953.d001*. https://doi.org/10.1594/PANGAEA.548912

Graf, W., Moser, H., Oerter, H., Reinwarth, O., & Stichler, W. (1988g). Density and d18O of snow pit FRI06S84_241 [Data set]. *In supplement to: Graf, W et al. (1988): Accumulation and ice core-studies on Filchner-Ronne Ice Shelf, Antarctica. Annals of Glaciology, 11, 23-31, hdl:10013/epic.25953.d001*. https://doi.org/10.1594/PANGAEA.548915

Graf, W., Moser, H., Oerter, H., Reinwarth, O., & Stichler, W. (1988h). Density and d18O of snow pit FRI07S84_340 [Data set]. *In supplement to: Graf, W et al. (1988): Accumulation and ice core-studies on Filchner-Ronne Ice Shelf, Antarctica. Annals of Glaciology, 11, 23-31, hdl:10013/epic.25953.d001*. https://doi.org/10.1594/PANGAEA.548916

Graf, W., Moser, H., Oerter, H., Reinwarth, O., & Stichler, W. (1988i). Density and d18O of snow pit FRI07S86_340 [Data set]. *In supplement to: Graf, W et al. (1988): Accumulation and ice core-studies on Filchner-Ronne Ice Shelf, Antarctica. Annals of Glaciology, 11, 23-31, hdl:10013/epic.25953.d001*. https://doi.org/10.1594/PANGAEA.548917

Graf, W., Moser, H., Oerter, H., Reinwarth, O., & Stichler, W. (1988j). Density and d18O of snow pit FRI08S84_341 [Data set]. *In supplement to: Graf, W et al. (1988): Accumulation and ice core-studies on Filchner-Ronne Ice Shelf, Antarctica. Annals of Glaciology, 11, 23-31, hdl:10013/epic.25953.d001*. https://doi.org/10.1594/PANGAEA.548918

Graf, W., Moser, H., Oerter, H., Reinwarth, O., & Stichler, W. (1988k). Density and d18O of snow pit FRI08S86_341 [Data set]. *In supplement to: Graf, W et al. (1988): Accumulation and ice core-studies*

on Filchner-Ronne Ice Shelf, Antarctica. Annals of Glaciology, 11, 23-31, hdl:10013/epic.25953.d001. https://doi.org/10.1594/PANGAEA.548919
Graf, W., Moser, H., Oerter, H., Reinwarth, O., & Stichler, W. (1988l). Density and d18O of snow pit FRI13S86_335 [Data set]. *In supplement to: Graf, W et al. (1988): Accumulation and ice core-studies on Filchner-Ronne Ice Shelf, Antarctica. Annals of Glaciology, 11, 23-31, hdl:10013/epic.25953.d001*. https://doi.org/10.1594/PANGAEA.548920
Graf, W., Moser, H., Oerter, H., Reinwarth, O., & Stichler, W. (1988m). Density and d18O of snow pit FRI15S86_131 [Data set]. *In supplement to: Graf, W et al. (1988): Accumulation and ice core-studies on Filchner-Ronne Ice Shelf, Antarctica. Annals of Glaciology, 11, 23-31, hdl:10013/epic.25953.d001*. https://doi.org/10.1594/PANGAEA.548921
Graf, W., Moser, H., Oerter, H., Reinwarth, O., & Stichler, W. (1988n). Density and d18O of snow pit FRI16S86_230 [Data set]. *In supplement to: Graf, W et al. (1988): Accumulation and ice core-studies on Filchner-Ronne Ice Shelf, Antarctica. Annals of Glaciology, 11, 23-31, hdl:10013/epic.25953.d001*. https://doi.org/10.1594/PANGAEA.548922
Graf, W., Moser, H., Oerter, H., Reinwarth, O., & Stichler, W. (1988o). Density and d18O of snow pit FRI17S86_231 [Data set]. *In supplement to: Graf, W et al. (1988): Accumulation and ice core-studies on Filchner-Ronne Ice Shelf, Antarctica. Annals of Glaciology, 11, 23-31, hdl:10013/epic.25953.d001*. https://doi.org/10.1594/PANGAEA.548925
Graf, W., Moser, H., Oerter, H., Reinwarth, O., & Stichler, W. (1988p). Density and d18O of snow pit FRI18S86_330 [Data set]. *In supplement to: Graf, W et al. (1988): Accumulation and ice core-studies on Filchner-Ronne Ice Shelf, Antarctica. Annals of Glaciology, 11, 23-31, hdl:10013/epic.25953.d001*. https://doi.org/10.1594/PANGAEA.548924
Graf, W., Moser, H., Oerter, H., Reinwarth, O., & Stichler, W. (1988q). Density and d18O of snow pit FRI0686S_241 [Data set]. *In supplement to: Graf, W et al. (1988): Accumulation and ice core-studies on Filchner-Ronne Ice Shelf, Antarctica. Annals of Glaciology, 11, 23-31, hdl:10013/epic.25953.d001*. https://doi.org/10.1594/PANGAEA.548914
Graf, W., Reinwarth, O., Oerter, H., Mayer, C., & Lambrecht, A. (1999a). Annual means of density, d18O, and accumulation rates of firn core FRI23C95_16 [Data set]. *In supplement to: Graf, W et al. (1999): Surface accumulation on Foundation Ice Stream, Antarctica. Annals of Glaciology, 29, 23-28, https://doi.org/10.3189/172756499781820987*. https://doi.org/10.1594/PANGAEA.548504
Graf, W., Reinwarth, O., Oerter, H., Mayer, C., & Lambrecht, A. (1999b). Annual means of density, d18O, and accumulation rates of firn core FRI23C95_16 [Data set]. *In supplement to: Graf, W et al. (1999): Surface accumulation on Foundation Ice Stream, Antarctica. Annals of Glaciology, 29, 23-28, https://doi.org/10.3189/172756499781820987*. https://doi.org/10.1594/PANGAEA.548504
Graf, W., Reinwarth, O., Oerter, H., Mayer, C., & Lambrecht, A. (1999c). Annual means of density, d18O, and accumulation rates of firn core FRI25C95_14 [Data set]. *In supplement to: Graf, W et al. (1999): Surface accumulation on Foundation Ice Stream, Antarctica. Annals of Glaciology, 29, 23-28, https://doi.org/10.3189/172756499781820987*. https://doi.org/10.1594/PANGAEA.548506
Graf, W., Reinwarth, O., Oerter, H., Mayer, C., & Lambrecht, A. (1999d). Annual means of density, d18O, and accumulation rates of firn core FRI26C95_13 [Data set]. *In supplement to: Graf, W et al. (1999): Surface accumulation on Foundation Ice Stream, Antarctica. Annals of Glaciology, 29, 23-28, https://doi.org/10.3189/172756499781820987*. https://doi.org/10.1594/PANGAEA.548507
Graf, W., Reinwarth, O., Oerter, H., Mayer, C., & Lambrecht, A. (1999e). Annual means of density, d18O, and accumulation rates of firn core FRI27C95_12 [Data set]. *In supplement to: Graf, W et al. (1999): Surface accumulation on Foundation Ice Stream, Antarctica. Annals of Glaciology, 29, 23-28, https://doi.org/10.3189/172756499781820987*. https://doi.org/10.1594/PANGAEA.548508
Graf, W., Reinwarth, O., Oerter, H., Mayer, C., & Lambrecht, A. (1999f). Annual means of density, d18O, and accumulation rates of firn core FRI28C95_11 [Data set]. *In supplement to: Graf, W et al. (1999): Surface accumulation on Foundation Ice Stream, Antarctica. Annals of Glaciology, 29, 23-28, https://doi.org/10.3189/172756499781820987*. https://doi.org/10.1594/PANGAEA.548509

Graf, W., Reinwarth, O., Oerter, H., Mayer, C., & Lambrecht, A. (1999g). Annual means of density, d18O, and accumulation rates of firn core FRI29C95_10 [Data set]. *In supplement to: Graf, W et al. (1999): Surface accumulation on Foundation Ice Stream, Antarctica. Annals of Glaciology, 29, 23-28, https://doi.org/10.3189/172756499781820987*. https://doi.org/10.1594/PANGAEA.548510

Graf, W., Reinwarth, O., Oerter, H., Mayer, C., & Lambrecht, A. (1999h). Annual means of density, d18O, and accumulation rates of firn core FRI29C95_10 [Data set]. *In supplement to: Graf, W et al. (1999): Surface accumulation on Foundation Ice Stream, Antarctica. Annals of Glaciology, 29, 23-28, https://doi.org/10.3189/172756499781820987*. https://doi.org/10.1594/PANGAEA.548510

Graf, W., Reinwarth, O., Oerter, H., Mayer, C., & Lambrecht, A. (1999i). Annual means of density, d18O, and accumulation rates of firn core FRI33C95_06 [Data set]. *In supplement to: Graf, W et al. (1999): Surface accumulation on Foundation Ice Stream, Antarctica. Annals of Glaciology, 29, 23-28, https://doi.org/10.3189/172756499781820987*. https://doi.org/10.1594/PANGAEA.548512

Graf, W., Reinwarth, O., Oerter, H., Mayer, C., & Lambrecht, A. (1999j). Annual means of density, d18O, deuterium, and accumulation rates of firn core FRI34C95_03 [Data set]. *In supplement to: Graf, W et al. (1999): Surface accumulation on Foundation Ice Stream, Antarctica. Annals of Glaciology, 29, 23-28, https://doi.org/10.3189/172756499781820987*. https://doi.org/10.1594/PANGAEA.548513

Graf, W., Reinwarth, O., Oerter, H., Mayer, C., & Lambrecht, A. (1999k). Annual means of density, d18O, deuterium, tritium, and accumulation rates of firn core FRI32C95_07 [Data set]. *In supplement to: Graf, W et al. (1999): Surface accumulation on Foundation Ice Stream, Antarctica. Annals of Glaciology, 29, 23-28, https://doi.org/10.3189/172756499781820987*. https://doi.org/10.1594/PANGAEA.548511

Graf, W., Reinwarth, O., Oerter, H., Mayer, C., & Lambrecht, A. (1999l). Annual means of density, d18O, deuterium, tritium, and accumulation rates of firn core FRI35C95_01 [Data set]. *In supplement to: Graf, W et al. (1999): Surface accumulation on Foundation Ice Stream, Antarctica. Annals of Glaciology, 29, 23-28, https://doi.org/10.3189/172756499781820987*. https://doi.org/10.1594/PANGAEA.548514

Graf, W., Reinwarth, O., Oerter, H., Mayer, C., & Lambrecht, A. (1999m). Annual means of density, d18O, deuterium, tritium, and accumulation rates of firn core FRI38C95_04 [Data set]. *In supplement to: Graf, W et al. (1999): Surface accumulation on Foundation Ice Stream, Antarctica. Annals of Glaciology, 29, 23-28, https://doi.org/10.3189/172756499781820987*. https://doi.org/10.1594/PANGAEA.548515

Graf, W., Reinwarth, O., Oerter, H., Mayer, C., & Lambrecht, A. (1999n). Density and d18O of firn core FRI24C95_15 [Data set]. *In supplement to: Graf, W et al. (1999): Surface accumulation on Foundation Ice Stream, Antarctica. Annals of Glaciology, 29, 23-28, https://doi.org/10.3189/172756499781820987*. https://doi.org/10.1594/PANGAEA.548448

Graf, W., Reinwarth, O., Oerter, H., Mayer, C., & Lambrecht, A. (1999o). Density and d18O of firn core FRI25C95_14 [Data set]. *In supplement to: Graf, W et al. (1999): Surface accumulation on Foundation Ice Stream, Antarctica. Annals of Glaciology, 29, 23-28, https://doi.org/10.3189/172756499781820987*. https://doi.org/10.1594/PANGAEA.548449

Graf, W., Reinwarth, O., Oerter, H., Mayer, C., & Lambrecht, A. (1999p). Density and d18O of firn core FRI27C95_12 [Data set]. *In supplement to: Graf, W et al. (1999): Surface accumulation on Foundation Ice Stream, Antarctica. Annals of Glaciology, 29, 23-28, https://doi.org/10.3189/172756499781820987*. https://doi.org/10.1594/PANGAEA.548451

Graf, W., Reinwarth, O., Oerter, H., Mayer, C., & Lambrecht, A. (1999q). Density and d18O of firn core FRI28C95_11 [Data set]. *In supplement to: Graf, W et al. (1999): Surface accumulation on Foundation Ice Stream, Antarctica. Annals of Glaciology, 29, 23-28, https://doi.org/10.3189/172756499781820987*. https://doi.org/10.1594/PANGAEA.548452

Graf, W., Reinwarth, O., Oerter, H., Mayer, C., & Lambrecht, A. (1999r). Density and d18O of firn core FRI30C95_09 [Data set]. *In supplement to: Graf, W et al. (1999): Surface accumulation on*

Foundation Ice Stream, Antarctica. Annals of Glaciology, 29, 23-28, https://doi.org/10.3189/172756499781820987. https://doi.org/10.1594/PANGAEA.548454
Graf, W., Reinwarth, O., Oerter, H., Mayer, C., & Lambrecht, A. (1999s). Density and d18O of firn core FRI31C95_08 [Data set]. *In supplement to: Graf, W et al. (1999): Surface accumulation on Foundation Ice Stream, Antarctica. Annals of Glaciology, 29, 23-28, https://doi.org/10.3189/172756499781820987*. https://doi.org/10.1594/PANGAEA.548455
Graf, W., Reinwarth, O., Oerter, H., Mayer, C., & Lambrecht, A. (1999t). Density and d18O of firn core FRI33C95_06 [Data set]. *In supplement to: Graf, W et al. (1999): Surface accumulation on Foundation Ice Stream, Antarctica. Annals of Glaciology, 29, 23-28, https://doi.org/10.3189/172756499781820987*. https://doi.org/10.1594/PANGAEA.548457
Graf, W., Reinwarth, O., Oerter, H., Mayer, C., & Lambrecht, A. (1999u). Density, d18O, and deuterium of firn core FRI36C95_02 [Data set]. *In supplement to: Graf, W et al. (1999): Surface accumulation on Foundation Ice Stream, Antarctica. Annals of Glaciology, 29, 23-28, https://doi.org/10.3189/172756499781820987*. https://doi.org/10.1594/PANGAEA.548460
Graf, W., Reinwarth, O., Oerter, H., Mayer, C., & Lambrecht, A. (1999v). Density, d18O, and deuterium of firn core FRI37C95_05 [Data set]. *In supplement to: Graf, W et al. (1999): Surface accumulation on Foundation Ice Stream, Antarctica. Annals of Glaciology, 29, 23-28, https://doi.org/10.3189/172756499781820987*. https://doi.org/10.1594/PANGAEA.548461
Graf, W., Reinwarth, O., Oerter, H., Mayer, C., & Lambrecht, A. (1999w). Density, d18O, deuterium, and tritium of firn core FRI32C95_07 [Data set]. *In supplement to: Graf, W et al. (1999): Surface accumulation on Foundation Ice Stream, Antarctica. Annals of Glaciology, 29, 23-28, https://doi.org/10.3189/172756499781820987*. https://doi.org/10.1594/PANGAEA.548456
Graf, W., Reinwarth, O., Oerter, H., Mayer, C., & Lambrecht, A. (1999x). Density, d18O, deuterium, and tritium of firn core FRI35C95_01 [Data set]. *In supplement to: Graf, W et al. (1999): Surface accumulation on Foundation Ice Stream, Antarctica. Annals of Glaciology, 29, 23-28, https://doi.org/10.3189/172756499781820987*. https://doi.org/10.1594/PANGAEA.548459
Graf, W., Reinwarth, O., Oerter, H., Mayer, C., & Lambrecht, A. (1999y). Density, d18O, deuterium, and tritium of firn core FRI38C95_04 [Data set]. *In supplement to: Graf, W et al. (1999): Surface accumulation on Foundation Ice Stream, Antarctica. Annals of Glaciology, 29, 23-28, https://doi.org/10.3189/172756499781820987*. https://doi.org/10.1594/PANGAEA.548462
Graf, W., Oerter, H., Reinwarth, O., Stichler, W., Wilhelms, F., Miller, H., & Mulvaney, R. (2002a). Density and stable oxygen isotopes of firn core DML02S98_13 [Data set]. *In supplement to: Graf, W et al. (2002): Stable-isotope records from Dronning Maud Land, Antarctica. Annals of Glaciology, 35, 195-201, https://doi.org/10.3189/172756402781816492*. https://doi.org/10.1594/PANGAEA.104876
Graf, W., Oerter, H., Reinwarth, O., Stichler, W., Wilhelms, F., Miller, H., & Mulvaney, R. (2002b). Density and stable oxygen isotopes of firn core DML05C98_32 (B32) [Data set]. *In supplement to: Graf, W et al. (2002): Stable-isotope records from Dronning Maud Land, Antarctica. Annals of Glaciology, 35, 195-201, https://doi.org/10.3189/172756402781816492*. https://doi.org/10.1594/PANGAEA.104862
Graf, W., Oerter, H., Reinwarth, O., Stichler, W., Wilhelms, F., Miller, H., & Mulvaney, R. (2002c). Density and stable oxygen isotopes of firn core DML11C98_03 [Data set]. *In supplement to: Graf, W et al. (2002): Stable-isotope records from Dronning Maud Land, Antarctica. Annals of Glaciology, 35, 195-201, https://doi.org/10.3189/172756402781816492*. https://doi.org/10.1594/PANGAEA.104864
Graf, W., Oerter, H., Reinwarth, O., Stichler, W., Wilhelms, F., Miller, H., & Mulvaney, R. (2002d). Density and stable oxygen isotopes of firn core DML12C98_17 [Data set]. *In supplement to: Graf, W et al. (2002): Stable-isotope records from Dronning Maud Land, Antarctica. Annals of Glaciology, 35, 195-201, https://doi.org/10.3189/172756402781816492*. https://doi.org/10.1594/PANGAEA.104865

Graf, W., Oerter, H., Reinwarth, O., Stichler, W., Wilhelms, F., Miller, H., & Mulvaney, R. (2002e). Density and stable oxygen isotopes of firn core DML13C98_16 [Data set]. *In supplement to: Graf, W et al. (2002): Stable-isotope records from Dronning Maud Land, Antarctica. Annals of Glaciology, 35, 195-201, https://doi.org/10.3189/172756402781816492*. https://doi.org/10.1594/PANGAEA.104866

Graf, W., Oerter, H., Reinwarth, O., Stichler, W., Wilhelms, F., Miller, H., & Mulvaney, R. (2002f). Density and stable oxygen isotopes of firn core DML14C98_15 [Data set]. *In supplement to: Graf, W et al. (2002): Stable-isotope records from Dronning Maud Land, Antarctica. Annals of Glaciology, 35, 195-201, https://doi.org/10.3189/172756402781816492*. https://doi.org/10.1594/PANGAEA.104867

Graf, W., Oerter, H., Reinwarth, O., Stichler, W., Wilhelms, F., Miller, H., & Mulvaney, R. (2002g). Density and stable oxygen isotopes of firn core DML15C98_14 [Data set]. *In supplement to: Graf, W et al. (2002): Stable-isotope records from Dronning Maud Land, Antarctica. Annals of Glaciology, 35, 195-201, https://doi.org/10.3189/172756402781816492*. https://doi.org/10.1594/PANGAEA.104868

Graf, W., Oerter, H., Reinwarth, O., Stichler, W., Wilhelms, F., Miller, H., & Mulvaney, R. (2002h). Density and stable oxygen isotopes of firn core DML17C98_33 (B33) [Data set]. *In supplement to: Graf, W et al. (2002): Stable-isotope records from Dronning Maud Land, Antarctica. Annals of Glaciology, 35, 195-201, https://doi.org/10.3189/172756402781816492*. https://doi.org/10.1594/PANGAEA.104869

Graf, W., Oerter, H., Reinwarth, O., Stichler, W., Wilhelms, F., Miller, H., & Mulvaney, R. (2002i). Density and stable oxygen isotopes of firn core DML18C98_04 [Data set]. *In supplement to: Graf, W et al. (2002): Stable-isotope records from Dronning Maud Land, Antarctica. Annals of Glaciology, 35, 195-201, https://doi.org/10.3189/172756402781816492*. https://doi.org/10.1594/PANGAEA.104870

Graf, W., Oerter, H., Reinwarth, O., Stichler, W., Wilhelms, F., Miller, H., & Mulvaney, R. (2002j). Density and stable oxygen isotopes of firn core DML20C98_08 [Data set]. *In supplement to: Graf, W et al. (2002): Stable-isotope records from Dronning Maud Land, Antarctica. Annals of Glaciology, 35, 195-201, https://doi.org/10.3189/172756402781816492*. https://doi.org/10.1594/PANGAEA.104872

Graf, W., Oerter, H., Reinwarth, O., Stichler, W., Wilhelms, F., Miller, H., & Mulvaney, R. (2002k). Density and stable oxygen isotopes of firn core DML22C98_11 [Data set]. *In supplement to: Graf, W et al. (2002): Stable-isotope records from Dronning Maud Land, Antarctica. Annals of Glaciology, 35, 195-201, https://doi.org/10.3189/172756402781816492*. https://doi.org/10.1594/PANGAEA.104874

Graf, W., Oerter, H., Reinwarth, O., Stichler, W., Wilhelms, F., Miller, H., & Mulvaney, R. (2002l). Density and stable oxygen isotopes of firn core DML23C98_12 [Data set]. *In supplement to: Graf, W et al. (2002): Stable-isotope records from Dronning Maud Land, Antarctica. Annals of Glaciology, 35, 195-201, https://doi.org/10.3189/172756402781816492*. https://doi.org/10.1594/PANGAEA.104875

Graf, W., Oerter, H., Reinwarth, O., Stichler, W., Wilhelms, F., Miller, H., & Mulvaney, R. (2002m). Physical properties of firn core DML25C00_01 [Data set]. *In supplement to: Graf, W et al. (2002): Stable-isotope records from Dronning Maud Land, Antarctica. Annals of Glaciology, 35, 195-201, https://doi.org/10.3189/172756402781816492*. https://doi.org/10.1594/PANGAEA.58443

Graf, W., Oerter, H., Reinwarth, O., Stichler, W., Wilhelms, F., Miller, H., & Mulvaney, R. (2002n). Physical properties of firn core DML27C00_04 [Data set]. *In supplement to: Graf, W et al. (2002): Stable-isotope records from Dronning Maud Land, Antarctica. Annals of Glaciology, 35, 195-201, https://doi.org/10.3189/172756402781816492*. https://doi.org/10.1594/PANGAEA.58445

Graf, W., Oerter, H., Reinwarth, O., Stichler, W., Wilhelms, F., Miller, H., & Mulvaney, R. (2002o). Physical properties of firn core NM03C95_06 [Data set]. *In supplement to: Graf, W et al. (2002):*

Stable-isotope records from Dronning Maud Land, Antarctica. Annals of Glaciology, 35, 195-201, https://doi.org/10.3189/172756402781816492. https://doi.org/10.1594/PANGAEA.58791
Haas, C., Beckers, J., King, J., Silis, A., Stroeve, J., Wilkinson, J., et al. (2017). Ice and Snow Thickness Variability and Change in the High Arctic Ocean Observed by In Situ Measurements. *Geophysical Research Letters*, *44*(20), 10,462-10,469. https://doi.org/10.1002/2017GL075434
Hall, D. K., Comiso, J. C., DiGirolamo, N. E., Shuman, C. A., Box, J. E., & Koenig, L. S. (2013). Variability in the surface temperature and melt extent of the Greenland ice sheet from MODIS. *Geophysical Research Letters*, *40*(10), 2114–2120. https://doi.org/10.1002/grl.50240
Hanna, E., Huybrechts, P., Cappelen, J., Steffen, K., Bales, R. C., Burgess, E., et al. (2011). Greenland Ice Sheet surface mass balance 1870 to 2010 based on Twentieth Century Reanalysis, and links with global climate forcing. *Journal of Geophysical Research: Atmospheres*, *116*(D24). https://doi.org/10.1029/2011JD016387
Hanna, E., Navarro, F. J., Pattyn, F., Domingues, C. M., Fettweis, X., Ivins, E. R., et al. (2013). Ice-sheet mass balance and climate change. *Nature*, *498*(7452), 51–59. https://doi.org/10.1038/nature12238
Harper, J., Humphrey, N., Pfeffer, W. T., Brown, J., & Fettweis, X. (2012). Greenland ice-sheet contribution to sea-level rise buffered by meltwater storage in firn. *Nature*, *491*(7423), 240–243. https://doi.org/10.1038/nature11566
Hastings, M., & Dibb, J. E. (2017). Personal Communication.
Hawley, R. L., Courville, Z. R., Kehrl, L. M., Lutz, E. R., Osterberg, E. C., Overly, T. B., & Wong, G. J. (2014). Recent accumulation variability in northwest Greenland from ground-penetrating radar and shallow cores along the Greenland Inland Traverse. *Journal of Glaciology*, *60*(220), 375–382. https://doi.org/10.3189/2014JoG13J141
Helm, V., Humbert, A., & Miller, H. (2014). Elevation and elevation change of Greenland and Antarctica derived from CryoSat-2. *The Cryosphere*, *8*(4), 1539–1559. https://doi.org/10.5194/tc-8-1539-2014
Helm, Veit, Humbert, A., & Miller, H. (2014). Elevation Model of Greenland derived from CryoSat-2 in the period 2011 to 2013, links to DEM and uncertainty map as GeoTIFF [Data set]. *In supplement to: Helm, V et al. (2014): Elevation and elevation change of Greenland and Antarctica derived from CryoSat-2. The Cryosphere, 8(4), 1539-1559, https://doi.org/10.5194/tc-8-1539-2014*. https://doi.org/10.1594/PANGAEA.831393
Hermann, M., Box, J. E., Fausto, R. S., Colgan, W. T., Langen, P. L., Mottram, R., et al. (2018). Application of PROMICE Q-Transect in Situ Accumulation and Ablation Measurements (2000–2017) to Constrain Mass Balance at the Southern Tip of the Greenland Ice Sheet. *Journal of Geophysical Research: Earth Surface*, *123*(6), 1235–1256. https://doi.org/10.1029/2017JF004408
Herron, M. M., & Langway, C. C. (1980). Firn Densification: An Empirical Model. *Journal of Glaciology*, *25*(93), 373–385. https://doi.org/10.3189/S0022143000015239
Hinkel, J., Lincke, D., Vafeidis, A. T., Perrette, M., Nicholls, R. J., Tol, R. S. J., et al. (2014). Coastal flood damage and adaptation costs under 21st century sea-level rise. *Proceedings of the National Academy of Sciences*, *111*(9), 3292–3297. https://doi.org/10.1073/pnas.1222469111
Hofer, S., Tedstone, A. J., Fettweis, X., & Bamber, J. L. (2017). Decreasing cloud cover drives the recent mass loss on the Greenland Ice Sheet. *Science Advances*, *3*(6), e1700584. https://doi.org/10.1126/sciadv.1700584
Hörhold, M. W., Kipfstuhl, S., Wilhelms, F., Freitag, J., & Frenzel, A. (2011). The densification of layered polar firn. *Journal of Geophysical Research: Earth Surface*, *116*(F1). https://doi.org/10.1029/2009JF001630
Howat, I. M., Porter, C., Smith, B. E., Noh, M.-J., & Morin, P. (2019). The Reference Elevation Model of Antarctica. *The Cryosphere*, *13*(2), 665–674. https://doi.org/10.5194/tc-13-665-2019
Hubbard, B., Tison, J.-L., Philippe, M., Heene, B., Pattyn, F., Malone, T., & Freitag, J. (2013). Ice shelf density reconstructed from optical televiewer borehole logging. *Geophysical Research Letters*, *40*(22), 5882–5887. https://doi.org/10.1002/2013GL058023

Humbert, A., Gross, D., Müller, R., Braun, M., van de Wal, R. S. W., van den Broeke, M. R., et al. (2010). Deformation and failure of the ice bridge on the Wilkins Ice Shelf, Antarctica. *Annals of Glaciology*, *51*(55), 49–55. https://doi.org/10.3189/172756410791392709
Humbert, Angelika, & Braun, M. (2008). The Wilkins Ice Shelf, Antarctica: break-up along failure zones. *Journal of Glaciology*, *54*(188), 943–944. https://doi.org/10.3189/002214308787780012
Hurdle, J. (2020). As Sea Levels Rise, Will Drinking Water Supplies Be at Risk? Retrieved from https://e360.yale.edu/features/as-sea-levels-rise-will-drinking-water-supplies-be-at-risk
IMBIE team. (2018). Mass balance of the Antarctic Ice Sheet from 1992 to 2017. *Nature*, *558*(7709), 219–222. https://doi.org/10.1038/s41586-018-0179-y
Jeon, T., Seo, K.-W., Youm, K., Chen, J., & Wilson, C. R. (2018). Global sea level change signatures observed by GRACE satellite gravimetry. *Scientific Reports*, *8*(1). https://doi.org/10.1038/s41598-018-31972-8
Jones, N. L. (1999). SEEP2D Primer. Enviornmental Modelling Research Laboratory, Brigham Young University.
King, J., Howell, S., Derksen, C., Rutter, N., Toose, P., Beckers, J. F., et al. (2015). Evaluation of Operation IceBridge quick-look snow depth estimates on sea ice. *Geophysical Research Letters*, *42*(21), 9302–9310. https://doi.org/10.1002/2015GL066389
Kingslake, J., Ely, J. C., Das, I., & Bell, R. E. (2017). Widespread movement of meltwater onto and across Antarctic ice shelves. *Nature*, *544*(7650), 349–352. https://doi.org/10.1038/nature22049
Kjeldsen, K. K., Korsgaard, N. J., Bjørk, A. A., Khan, S. A., Box, J. E., Funder, S., et al. (2015). Spatial and temporal distribution of mass loss from the Greenland Ice Sheet since AD 1900. *Nature*, *528*(7582), 396–400. https://doi.org/10.1038/nature16183
Koenig, L., & Brucker, L. (2011). Satellite-Era Accumulation Traverse 2011 (SEAT11) snowpit density data.
Koenig, L., Box, J., & Kurtz, N. (2013). Improving Surface Mass Balance Over Ice Sheets and Snow Depth on Sea Ice. *Eos, Transactions American Geophysical Union*, *94*(10), 100–100. https://doi.org/10.1002/2013EO100006
Koenig, L. S., Miège, C., Forster, R. R., & Brucker, L. (2014). Initial in situ measurements of perennial meltwater storage in the Greenland firn aquifer. *Geophysical Research Letters*, *41*(1), 81–85. https://doi.org/10.1002/2013GL058083
Koenig, L. S., Ivanoff, A., Alexander, P. M., MacGregor, J. A., Fettweis, X., Panzer, B., et al. (2016). Annual Greenland accumulation rates (2009–2012) from airborne snow radar. *The Cryosphere*, *10*(4), 1739–1752. https://doi.org/10.5194/tc-10-1739-2016
Kovacs, A., Gow, A. J., & Morey, R. M. (1995). The in-situ dielectric constant of polar firn revisited. *Cold Regions Science and Technology*, *23*(3), 245–256. https://doi.org/10.1016/0165-232X(94)00016-Q
Kreutz, K. (2011). Microparticle, Conductivity, and Density Measurements from the WAIS Divide Deep Ice Core, Antarctica [Data set]. U.S. Antarctic Program Data Center (USAP-DC), via National Snow and Ice Data Center (NSIDC). https://doi.org/10.7265/N5K07264
Kuipers Munneke, P., Ligtenberg, S. R. M., Noël, B. P. Y., Howat, I. M., Box, J. E., Mosley-Thompson, E., et al. (2015). Elevation change of the Greenland Ice Sheet due to surface mass balance and firn processes, 1960–2014. *The Cryosphere*, *9*(6), 2009–2025. https://doi.org/10.5194/tc-9-2009-2015
Kulp, S. A., & Strauss, B. H. (2019). New elevation data triple estimates of global vulnerability to sea-level rise and coastal flooding. *Nature Communications*, *10*(1), 4844. https://doi.org/10.1038/s41467-019-12808-z
Kurtz, N. (2012). IceBridge Sea Ice Freeboard, Snow Depth, and Thickness, Version 1. NASA National Snow and Ice Data Center Distributed Active Archive Center. https://doi.org/10.5067/7XJ9HRV50O57
Kwok, R., Kurtz, N. T., Brucker, L., Ivanoff, A., Newman, T., Farrell, S. L., et al. (2017). Intercomparison of snow depth retrievals over Arctic sea ice from radar data acquired by Operation IceBridge. *The Cryosphere*, *11*(6), 2571–2593. https://doi.org/10.5194/tc-11-2571-2017

Laepple, T., Hörhold, M., Münch, T., Freitag, J., Wegner, A., & Kipfstuhl, S. (2016). Layering of surface snow and firn at Kohnen Station, Antarctica: Noise or seasonal signal? *Journal of Geophysical Research: Earth Surface*, *121*(10), 1849–1860. https://doi.org/10.1002/2016JF003919

Lenaerts, J. T. M., van den Broeke, M. R., van Angelen, J. H., van Meijgaard, E., & Déry, S. J. (2012). Drifting snow climate of the Greenland ice sheet: a study with a regional climate model. *The Cryosphere*, *6*(4), 891–899. https://doi.org/10.5194/tc-6-891-2012

Lenaerts, J. T. M., Lhermitte, S., Drews, R., Ligtenberg, S. R. M., Berger, S., Helm, V., et al. (2017). Meltwater produced by wind–albedo interaction stored in an East Antarctic ice shelf. *Nature Climate Change*, *7*(1), 58–62. https://doi.org/10.1038/nclimate3180

Lenaerts, Jan T. M., Ligtenberg, S. R. M., Medley, B., Berg, W. J. V. de, Konrad, H., Nicolas, J. P., et al. (2018). Climate and surface mass balance of coastal West Antarctica resolved by regional climate modelling. *Annals of Glaciology*, *59*(76pt1), 29–41. https://doi.org/10.1017/aog.2017.42

Lenaerts, Jan T. M., Medley, B., Broeke, M. R. van den, & Wouters, B. (2019). Observing and Modeling Ice Sheet Surface Mass Balance. *Reviews of Geophysics*, *57*(2), 376–420. https://doi.org/10.1029/2018RG000622

Lewis, M. J., Tison, J. L., Weissling, B., Delille, B., Ackley, S. F., Brabant, F., & Xie, H. (2011). Sea ice and snow cover characteristics during the winter–spring transition in the Bellingshausen Sea: An overview of SIMBA 2007. *Deep Sea Research Part II: Topical Studies in Oceanography*, *58*(9), 1019–1038. https://doi.org/10.1016/j.dsr2.2010.10.027

Ligtenberg, S. R. M., Helsen, M. M., & van den Broeke, M. R. (2011). An improved semi-empirical model for the densification of Antarctic firn. *The Cryosphere*, *5*(4), 809–819. https://doi.org/10.5194/tc-5-809-2011

Ligtenberg, Stefan R. M., Kuipers Munneke, P., Noël, B. P. Y., & Broeke, M. R. van den. (2018). Brief communication: Improved simulation of the present-day Greenland firn layer (1960–2016). *The Cryosphere*, *12*(5), 1643–1649. https://doi.org/10.5194/tc-12-1643-2018

Liston, G. E., Haehnel, R. B., Sturm, M., Hiemstra, C. A., Berezovskaya, S., & Tabler, R. D. (2007). Simulating complex snow distributions in windy environments using SnowTran-3D. *Journal of Glaciology*, *53*(181), 241–256. https://doi.org/10.3189/172756507782202865

Looyenga, H. (1965). Dielectric constants of homogeneous mixture. *Molecular Physics*, *9*(6), 501–511. https://doi.org/10.1080/00268976500100671

Lucas-Picher, P., Wulff-Nielsen, M., Christensen, J. H., Aðalgeirsdóttir, G., Mottram, R., & Simonsen, S. B. (2012). Very high resolution regional climate model simulations over Greenland: Identifying added value. *Journal of Geophysical Research: Atmospheres*, *117*(D2). https://doi.org/10.1029/2011JD016267

MacFerrin, M., Machguth, H., van As, D., Charalampidis, C., Stevens, M., Vandecrux, B., et al. ((in review)). Rapid expansion of Greenland's low-permeability ice slabs in a warming climate. *Nature*.

MacFerrin, M., Stevens, M., Abdalati, W., & Waddington, E. ((In Prep)). The Firn Compaction Verification and Reconnaissance (FirnCover) dataset.

Machguth, H., MacFerrin, M., As, D. van, Box, J. E., Charalampidis, C., Colgan, W., et al. (2016). Greenland meltwater storage in firn limited by near-surface ice formation. *Nature Climate Change*, *6*(4), 390–393. https://doi.org/10.1038/nclimate2899

Machguth, H., Thomsen, H. H., Weidick, A., Ahlstrøm, A. P., Abermann, J., Andersen, M. L., et al. (2016). Greenland surface mass-balance observations from the ice-sheet ablation area and local glaciers. *Journal of Glaciology*, *62*(235), 861–887. https://doi.org/10.1017/jog.2016.75

Matsuoka, K., Skoglund, A., & Roth, G. (2018). Quantarctica [Data set]. Norwegian Polar Institute. https://doi.org/10.21334/npolar.2018.8516e961

Mayewski, P., & Dixon, D. A. (2013). US International Trans-Antarctic Scientific Expedition (US ITASE) Glaciochemical Data. Version 2. [US_ITASE_Core Info-SWE-Density_2013.xlsx]. Boulder, Colorado USA: National Snow and Ice Data Center.

Mayewski, P., & Whitlow, S. (2009a). Regional Survey of Greenland, 1988 - Snow Pit Data, Version 1.0 [Data set]. UCAR/NCAR - Earth Observing Laboratory. https://doi.org/10.5065/D6154F6J

Mayewski, P., & Whitlow, S. (2009b). Snow Pit and Ice Core Data from Southern Greenland, 1984, Version 1.0 [Data set]. UCAR/NCAR - Earth Observing Laboratory. https://doi.org/10.5065/D6S180MH
Mayewski, P., & Whitlow, S. (2009c). Snow Pit Data from Greenland Summit, 1987, Version 1.0 [Data set]. UCAR/NCAR - Earth Observing Laboratory. https://doi.org/10.5065/D63X84RQ
Mayewski, P., & Whitlow, S. (2009d). Snow Pit Data from Greenland Summit, 1989 to 1993, Version 1.0 [Data set]. UCAR/NCAR - Earth Observing Laboratory. https://doi.org/10.5065/D6NP22KX
McGrath, D., Colgan, W., Bayou, N., Muto, A., & Steffen, K. (2013). Recent warming at Summit, Greenland: Global context and implications. *Geophysical Research Letters*, *40*(10), 2091–2096. https://doi.org/10.1002/grl.50456
Medley, B., Joughin, I., Das, S. B., Steig, E. J., Conway, H., Gogineni, S., et al. (2013). Airborne-radar and ice-core observations of annual snow accumulation over Thwaites Glacier, West Antarctica confirm the spatiotemporal variability of global and regional atmospheric models: SNOW ACCUMULATION OVER THWAITES GLACIER. *Geophysical Research Letters*, *40*(14), 3649–3654. https://doi.org/10.1002/grl.50706
Miège, C., Forster, R. R., Box, J. E., Burgess, E. W., McConnell, J. R., Pasteris, D. R., & Spikes, V. B. (2013). Southeast Greenland high accumulation rates derived from firn cores and ground-penetrating radar. *Annals of Glaciology*, *54*(63), 322–332. https://doi.org/10.3189/2013AoG63A358
Miège, C., Forster, R. R., Brucker, L., Koenig, L. S., Solomon, D. K., Paden, J. D., et al. (2016). Spatial extent and temporal variability of Greenland firn aquifers detected by ground and airborne radars. *Journal of Geophysical Research: Earth Surface*, *121*(12), 2381–2398. https://doi.org/10.1002/2016JF003869
Miles, K. E., Willis, I. C., Benedek, C. L., Williamson, A. G., & Tedesco, M. (2017). Toward Monitoring Surface and Subsurface Lakes on the Greenland Ice Sheet Using Sentinel-1 SAR and Landsat-8 OLI Imagery. *Frontiers in Earth Science*, *5*. https://doi.org/10.3389/feart.2017.00058
Miller, H., & Schwager, M. (2000a). Density of ice core ngt37C95.2 from the North Greenland Traverse [Data set]. https://doi.org/10.1594/PANGAEA.57798
Miller, H., & Schwager, M. (2000b). Density of ice core ngt42C95.2 from the North Greenland Traverse [Data set]. https://doi.org/10.1594/PANGAEA.57655
Miller, O., Solomon, D. K., Miège, C., Koenig, L., Forster, R., Schmerr, N., et al. (2018). Direct Evidence of Meltwater Flow Within a Firn Aquifer in Southeast Greenland. *Geophysical Research Letters*, *45*(1), 207–215. https://doi.org/10.1002/2017GL075707
Miller, O., Solomon, D. K., Miège, C., Koenig, L., Forster, R., Schmerr, N., et al. (2020). Hydrology of a Perennial Firn Aquifer in Southeast Greenland: An Overview Driven by Field Data. *Water Resources Research*, *56*(8). https://doi.org/10.1029/2019WR026348
Miller, O. L., Solomon, D. K., Miège, C., Koenig, L. S., Forster, R. R., Montgomery, L. N., et al. (2017). Hydraulic Conductivity of a Firn Aquifer in Southeast Greenland. *Frontiers in Earth Science*, *5*. https://doi.org/10.3389/feart.2017.00038
Mock, S. J. (1967a). Accumulation patterns on the Greenland ice sheet. Hanover, N.H. : U.S. Army Materiel Command, Cold Regions Research & Engineering Laboratory.
Mock, S. J. (1967b). Calculated Patterns of Accumulation on the Greenland Ice Sheet. *Journal of Glaciology*, *6*(48), 795–803. https://doi.org/10.3189/S0022143000020104
Montgomery, L., Koenig, L., & Alexander, P. (2018). The SUMup dataset: compiled measurements of surface mass balance components over ice sheets and sea ice with analysis over Greenland. *Earth System Science Data*, *10*(4), 1959–1985. https://doi.org/10.5194/essd-10-1959-2018
Montgomery, L., Koenig, L., Lenaerts, J. T. M., & Kuipers Munneke, P. (2020a). Accumulation rates (2009–2017) in Southeast Greenland derived from airborne snow radar and comparison with regional climate models. *Annals of Glaciology*, 1–9. https://doi.org/10.1017/aog.2020.8
Montgomery, L., Miège, C., Miller, J., Scambos, T. A., Wallin, B., Miller, O., et al. (2020b). Hydrologic properties of a highly permeable firn aquifer in the Wilkins Ice Shelf, Antarctica. *Geophysical Research Letters*. https://doi.org/10.1029/2020GL089552

Morris, E. M. (2008). A theoretical analysis of the neutron scattering method of measuring snow and ice density. *Journal of Geophysical Research: Earth Surface*, *113*(F3). https://doi.org/10.1029/2007JF000962
Morris, E. M., & Wingham, D. J. (2014). Densification of polar snow: Measurements, modeling, and implications for altimetry. *Journal of Geophysical Research: Earth Surface*, *119*(2), 349–365. https://doi.org/10.1002/2013JF002898
Mosley-Thompson, E., McConnell, J. R., Bales, R. C., Li, Z., Lin, P.-N., Steffen, K., et al. (2001). Local to regional-scale variability of annual net accumulation on the Greenland ice sheet from PARCA cores. *Journal of Geophysical Research: Atmospheres*, *106*(D24), 33839–33851. https://doi.org/10.1029/2001JD900067
Mouginot, J., Rignot, E., Bjørk, A. A., Broeke, M. van den, Millan, R., Morlighem, M., et al. (2019). Forty-six years of Greenland Ice Sheet mass balance from 1972 to 2018. *Proceedings of the National Academy of Sciences*, *116*(19), 9239–9244. https://doi.org/10.1073/pnas.1904242116
Munneke, P. K., M. Ligtenberg, S. R., van den Broeke, M. R., van Angelen, J. H., & Forster, R. R. (2014). Explaining the presence of perennial liquid water bodies in the firn of the Greenland Ice Sheet: KUIPERS MUNNEKE ET AL. *Geophysical Research Letters*, *41*(2), 476–483. https://doi.org/10.1002/2013GL058389
Nghiem, S. V., Hall, D. K., Mote, T. L., Tedesco, M., Albert, M. R., Keegan, K., et al. (2012). The extreme melt across the Greenland ice sheet in 2012. *Geophysical Research Letters*, *39*(20). https://doi.org/10.1029/2012GL053611
Noël, B. (2016). A daily, 1 km resolution data set of downscaled Greenland ice sheet surface mass balance (1958–2015). *The Cryosphere*, 17.
Noël, B., Berg, W. J. van de, Wessem, J. M. van, Meijgaard, E. van, As, D. van, Lenaerts, J. T. M., et al. (2018). Modelling the climate and surface mass balance of polar ice sheets using RACMO2 – Part 1: Greenland (1958–2016). *The Cryosphere*, *12*(3), 811–831. https://doi.org/10.5194/tc-12-811-2018
Oerter, H. (2002). Density of firn core DML28C01_00 [Data set]. *Alfred Wegener Institute, Helmholtz Center for Polar and Marine Research, Bremerhaven*. https://doi.org/10.1594/PANGAEA.69513
Oerter, H. (2008a). Annual means of d18O and accumulation rates of snow pit DML76S05_11 [Data set]. https://doi.org/10.1594/PANGAEA.708113
Oerter, H. (2008b). Annual means of d18O and accumulation rates of snow pit DML77S05_12 [Data set]. https://doi.org/10.1594/PANGAEA.708114
Oerter, H. (2008c). Annual means of d18O and accumulation rates of snow pit DML78S05_13 [Data set]. https://doi.org/10.1594/PANGAEA.708115
Oerter, H. (2008d). Annual means of d18O and accumulation rates of snow pit DML79S05_14 [Data set]. https://doi.org/10.1594/PANGAEA.708116
Oerter, H. (2008e). Annual means of d18O and accumulation rates of snow pit DML80S05_15 [Data set]. https://doi.org/10.1594/PANGAEA.708117
Oerter, H. (2008f). Annual means of d18O and accumulation rates of snow pit DML81S05_16 [Data set]. https://doi.org/10.1594/PANGAEA.708118
Oerter, H. (2008g). Annual means of d18O and accumulation rates of snow pit DML82S05_17 [Data set]. https://doi.org/10.1594/PANGAEA.708119
Oerter, H. (2008h). Annual means of d18O and accumulation rates of snow pit DML83S05_18 [Data set]. https://doi.org/10.1594/PANGAEA.708120
Oerter, H. (2008i). Annual means of d18O and accumulation rates of snow pit DML84S05_19 [Data set]. https://doi.org/10.1594/PANGAEA.708121
Oerter, H. (2008j). Annual means of d18O and accumulation rates of snow pit DML85S05_20 [Data set]. https://doi.org/10.1594/PANGAEA.708122
Oerter, H. (2008k). Annual means of d18O and accumulation rates of snow pit DML86S05_21 [Data set]. https://doi.org/10.1594/PANGAEA.708123
Oerter, H. (2008l). Annual means of d18O and accumulation rates of snow pit DML87S05_22 [Data set]. https://doi.org/10.1594/PANGAEA.708124

Oerter, H. (2008m). Annual means of d18O and accumulation rates of snow pit DML88S05_23 [Data set]. https://doi.org/10.1594/PANGAEA.708125
Oerter, H. (2008n). Annual means of d18O and accumulation rates of snow pit DML89S05_24 [Data set]. https://doi.org/10.1594/PANGAEA.708126
Oerter, H. (2008o). Annual means of d18O and accumulation rates of snow pit DML90S05_25 [Data set]. https://doi.org/10.1594/PANGAEA.708127
Oerter, H. (2008p). Density and d18O in 10 cm resolution of snow pit DML76S05_11 [Data set]. https://doi.org/10.1594/PANGAEA.708097
Oerter, H. (2008q). Density and d18O in 10 cm resolution of snow pit DML77S05_12 [Data set]. https://doi.org/10.1594/PANGAEA.708098
Oerter, H. (2008r). Density and d18O in 10 cm resolution of snow pit DML78S05_13 [Data set]. https://doi.org/10.1594/PANGAEA.708099
Oerter, H. (2008s). Density and d18O in 10 cm resolution of snow pit DML79S05_14 [Data set]. https://doi.org/10.1594/PANGAEA.708100
Oerter, H. (2008t). Density and d18O in 10 cm resolution of snow pit DML80S05_15 [Data set]. https://doi.org/10.1594/PANGAEA.708101
Oerter, H. (2008u). Density and d18O in 10 cm resolution of snow pit DML81S05_16 [Data set]. https://doi.org/10.1594/PANGAEA.708102
Oerter, H. (2008v). Density and d18O in 10 cm resolution of snow pit DML82S05_17 [Data set]. https://doi.org/10.1594/PANGAEA.708103
Oerter, H. (2008w). Density and d18O in 10 cm resolution of snow pit DML83S05_18 [Data set]. https://doi.org/10.1594/PANGAEA.708104
Oerter, H. (2008x). Density and d18O in 10 cm resolution of snow pit DML84S05_19 [Data set]. https://doi.org/10.1594/PANGAEA.708105
Oerter, H. (2008y). Density and d18O in 10 cm resolution of snow pit DML85S05_20 [Data set]. https://doi.org/10.1594/PANGAEA.708106
Oerter, H. (2008z). Density and d18O in 10 cm resolution of snow pit DML86S05_21 [Data set]. https://doi.org/10.1594/PANGAEA.708107
Oerter, H. (2008aa). Density and d18O in 10 cm resolution of snow pit DML87S05_22 [Data set]. https://doi.org/10.1594/PANGAEA.708108
Oerter, H. (2008ab). Density and d18O in 10 cm resolution of snow pit DML88S05_23 [Data set]. https://doi.org/10.1594/PANGAEA.708109
Oerter, H. (2008ac). Density and d18O in 10 cm resolution of snow pit DML89S05_24 [Data set]. https://doi.org/10.1594/PANGAEA.708110
Oerter, H. (2008ad). Density and d18O in 10 cm resolution of snow pit DML90S05_25 [Data set]. https://doi.org/10.1594/PANGAEA.708111
Oerter, H. (2008ae). High resolution density and d18O of snow pit DML87S05_22 [Data set]. https://doi.org/10.1594/PANGAEA.708093
Oerter, H., Graf, W., Wilhelms, F., Minikin, A., & Miller, H. (1999a). Physical properties of firn core DML01C97_00 [Data set]. *In supplement to: Oerter, H et al. (1999): Accumulation studies on Amundsenisen, Dronning Maud Land, by means of tritium, DEP and stable isotope measurements: first results from the 1995/96 and 1996/97 field seasons. Annals of Glaciology, 29, 1-9, https://doi.org/10.3189/172756499781820914*. https://doi.org/10.1594/PANGAEA.58434
Oerter, H., Graf, W., Wilhelms, F., Minikin, A., & Miller, H. (1999b). Physical properties of firn core DML03C97_00 [Data set]. *In supplement to: Oerter, H et al. (1999): Accumulation studies on Amundsenisen, Dronning Maud Land, by means of tritium, DEP and stable isotope measurements: first results from the 1995/96 and 1996/97 field seasons. Annals of Glaciology, 29, 1-9, https://doi.org/10.3189/172756499781820914*. https://doi.org/10.1594/PANGAEA.58794
Oerter, H., Graf, W., Wilhelms, F., Minikin, A., & Miller, H. (1999c). Physical properties of firn core DML04C97_00 [Data set]. *In supplement to: Oerter, H et al. (1999): Accumulation studies on Amundsenisen, Dronning Maud Land, by means of tritium, DEP and stable isotope measurements:*

first results from the 1995/96 and 1996/97 field seasons. Annals of Glaciology, 29, 1-9, https://doi.org/10.3189/172756499781820914. https://doi.org/10.1594/PANGAEA.58436
Oerter, H., Graf, W., Wilhelms, F., Minikin, A., & Miller, H. (1999d). Physical properties of firn core DML05C97_00 [Data set]. *In supplement to: Oerter, H et al. (1999): Accumulation studies on Amundsenisen, Dronning Maud Land, by means of tritium, DEP and stable isotope measurements: first results from the 1995/96 and 1996/97 field seasons. Annals of Glaciology, 29, 1-9, https://doi.org/10.3189/172756499781820914*. https://doi.org/10.1594/PANGAEA.58795
Oerter, H., Graf, W., Wilhelms, F., Minikin, A., & Miller, H. (1999e). Physical properties of firn core DML06C97_00 [Data set]. *In supplement to: Oerter, H et al. (1999): Accumulation studies on Amundsenisen, Dronning Maud Land, by means of tritium, DEP and stable isotope measurements: first results from the 1995/96 and 1996/97 field seasons. Annals of Glaciology, 29, 1-9, https://doi.org/10.3189/172756499781820914*. https://doi.org/10.1594/PANGAEA.58796
Oerter, H., Graf, W., Wilhelms, F., Minikin, A., & Miller, H. (1999f). Physical properties of firn core DML07C97_00 [Data set]. *In supplement to: Oerter, H et al. (1999): Accumulation studies on Amundsenisen, Dronning Maud Land, by means of tritium, DEP and stable isotope measurements: first results from the 1995/96 and 1996/97 field seasons. Annals of Glaciology, 29, 1-9, https://doi.org/10.3189/172756499781820914*. https://doi.org/10.1594/PANGAEA.58792
Oerter, H., Graf, W., Wilhelms, F., Minikin, A., & Miller, H. (1999g). Physical properties of firn core DML08C97_00 [Data set]. *In supplement to: Oerter, H et al. (1999): Accumulation studies on Amundsenisen, Dronning Maud Land, by means of tritium, DEP and stable isotope measurements: first results from the 1995/96 and 1996/97 field seasons. Annals of Glaciology, 29, 1-9, https://doi.org/10.3189/172756499781820914*. https://doi.org/10.1594/PANGAEA.58440
Oerter, H., Graf, W., Wilhelms, F., Minikin, A., & Miller, H. (1999h). Physical properties of firn core DML09C97_00 [Data set]. *In supplement to: Oerter, H et al. (1999): Accumulation studies on Amundsenisen, Dronning Maud Land, by means of tritium, DEP and stable isotope measurements: first results from the 1995/96 and 1996/97 field seasons. Annals of Glaciology, 29, 1-9, https://doi.org/10.3189/172756499781820914*. https://doi.org/10.1594/PANGAEA.58793
Oerter, H., Wilhelms, F., Jung-Rothenhäusler, F., Göktas, F., Miller, H., Graf, W., & Sommer, S. (2000a). Physical properties of firn core DML03C98_09 [Data set]. *In supplement to: Oerter, H et al. (2000): Accumulation rates in Dronning Maud Land, Antarctica, as revealed by dielectric-profiling measurements of shallow firn cores. Annals of Glaciology, 30, 27-34, https://doi.org/10.3189/172756400781820705*. https://doi.org/10.1594/PANGAEA.58410
Oerter, H., Wilhelms, F., Jung-Rothenhäusler, F., Göktas, F., Miller, H., Graf, W., & Sommer, S. (2000b). Physical properties of firn core DML05C98_06 [Data set]. *In supplement to: Oerter, H et al. (2000): Accumulation rates in Dronning Maud Land, Antarctica, as revealed by dielectric-profiling measurements of shallow firn cores. Annals of Glaciology, 30, 27-34, https://doi.org/10.3189/172756400781820705*. https://doi.org/10.1594/PANGAEA.58407
Oerter, H., Wilhelms, F., Jung-Rothenhäusler, F., Göktas, F., Miller, H., Graf, W., & Sommer, S. (2000c). Physical properties of firn core DML05C98_07 [Data set]. *In supplement to: Oerter, H et al. (2000): Accumulation rates in Dronning Maud Land, Antarctica, as revealed by dielectric-profiling measurements of shallow firn cores. Annals of Glaciology, 30, 27-34, https://doi.org/10.3189/172756400781820705*. https://doi.org/10.1594/PANGAEA.58806
Oerter, H., Wilhelms, F., Jung-Rothenhäusler, F., Göktas, F., Miller, H., Graf, W., & Sommer, S. (2000d). Physical properties of firn core DML12C98_17 [Data set]. *In supplement to: Oerter, H et al. (2000): Accumulation rates in Dronning Maud Land, Antarctica, as revealed by dielectric-profiling measurements of shallow firn cores. Annals of Glaciology, 30, 27-34, https://doi.org/10.3189/172756400781820705*. https://doi.org/10.1594/PANGAEA.58418
Oerter, H., Wilhelms, F., Jung-Rothenhäusler, F., Göktas, F., Miller, H., Graf, W., & Sommer, S. (2000e). Physical properties of firn core DML16C98_13 [Data set]. *In supplement to: Oerter, H et al. (2000): Accumulation rates in Dronning Maud Land, Antarctica, as revealed by dielectric-profiling*

measurements of shallow firn cores. Annals of Glaciology, 30, 27-34, https://doi.org/10.3189/172756400781820705. https://doi.org/10.1594/PANGAEA.58414
Oerter, H., Wilhelms, F., Jung-Rothenhäusler, F., Göktas, F., Miller, H., Graf, W., & Sommer, S. (2000f). Physical properties of firn core DML19C98_05 [Data set]. *In supplement to: Oerter, H et al. (2000): Accumulation rates in Dronning Maud Land, Antarctica, as revealed by dielectric-profiling measurements of shallow firn cores. Annals of Glaciology, 30, 27-34, https://doi.org/10.3189/172756400781820705*. https://doi.org/10.1594/PANGAEA.58406
Oerter, H., Wilhelms, F., Jung-Rothenhäusler, F., Göktas, F., Miller, H., Graf, W., & Sommer, S. (2000g). Physical properties of firn core DML21C98_10 [Data set]. *In supplement to: Oerter, H et al. (2000): Accumulation rates in Dronning Maud Land, Antarctica, as revealed by dielectric-profiling measurements of shallow firn cores. Annals of Glaciology, 30, 27-34, https://doi.org/10.3189/172756400781820705*. https://doi.org/10.1594/PANGAEA.58807
Oerter, H., Wilhelms, F., Jung-Rothenhäusler, F., Göktas, F., Miller, H., Graf, W., & Sommer, S. (2000h). Physical properties of firn core DML24C98_18 [Data set]. *In supplement to: Oerter, H et al. (2000): Accumulation rates in Dronning Maud Land, Antarctica, as revealed by dielectric-profiling measurements of shallow firn cores. Annals of Glaciology, 30, 27-34, https://doi.org/10.3189/172756400781820705*. https://doi.org/10.1594/PANGAEA.58419
Oerter, H., Wilhelms, F., Jung-Rothenhäusler, F., Göktas, F., Miller, H., Graf, W., & Sommer, S. (2000i). Physical properties of firn core DML60C98_02 [Data set]. *In supplement to: Oerter, H et al. (2000): Accumulation rates in Dronning Maud Land, Antarctica, as revealed by dielectric-profiling measurements of shallow firn cores. Annals of Glaciology, 30, 27-34, https://doi.org/10.3189/172756400781820705*. https://doi.org/10.1594/PANGAEA.58797
Oerter, H., Wilhelms, F., Jung-Rothenhäusler, F., Göktas, F., Miller, H., Graf, W., & Sommer, S. (2000j). Physical properties of firn core NM03C98_01 [Data set]. *In supplement to: Oerter, H et al. (2000): Accumulation rates in Dronning Maud Land, Antarctica, as revealed by dielectric-profiling measurements of shallow firn cores. Annals of Glaciology, 30, 27-34, https://doi.org/10.3189/172756400781820705*. https://doi.org/10.1594/PANGAEA.58799
Ohmura, A. (1991). ETH Greenland Expedition I, progress report no. 1, April 1989 to February, 1991. Tech. Report, Department of Geography, ETH Zürich, 108 pp.
Ohmura, A. (1992). ETH Greenland Expedition II, progress Rep. 2, April 1991 to October, 1992. Tech. Report, Department of Geography, ETH Zürich, 94 pp.
Ohmura, A., & Reeh, N. (1991). New precipitation and accumulation maps for Greenland. *Journal of Glaciology*, *37*(125), 140–148. https://doi.org/10.3189/S0022143000042891
Oppenheimer, M., Glavovic, B. C., Hinkel, J., van de Wal, R., Magnan, A. K., Abd-Elgawad, A., et al. (2019). Sea Level Rise and Implications for Low-Lying Islands, Coasts and Communities. In: IPCC Special Report on the Ocean and Cryosphere in a Changing Climate [H.-O. Pörtner, D.C. Roberts, V. Masson-Delmotte, P. Zhai, M. Tignor, E. Poloczanska, K. Mintenbeck, A. Alegría, M. Nicolai, A. Okem, J. Petzold, B. Rama, N.M. Weyer (eds.)]. In press.
Overly, T. B., Hawley, R. L., Helm, V., Morris, E. M., & Chaudhary, R. N. (2016). Greenland annual accumulation along the EGIG line, 1959–2004, from ASIRAS airborne radar and neutron-probe density measurements. *The Cryosphere*, *10*(4), 1679–1694. https://doi.org/10.5194/tc-10-1679-2016
Paden, J., Leuschen, C., Rodriguez-Morales, F., & Hale, R. (2014). IceBridge Snow Radar L1B Geolocated Radar Echo Strength Profiles, Version 2. https://doi.org/10.5067/faztwp500v70
Panzer, B., Gomez-Garcia, D., Leuschen, C., Paden, J., Rodriguez-Morales, F., Patel, A., et al. (2013). An ultra-wideband, microwave radar for measuring snow thickness on sea ice and mapping near-surface internal layers in polar firn. *Journal of Glaciology*, *59*(214), 244–254. https://doi.org/10.3189/2013JoG12J128
Pattyn, F., Ritz, C., Hanna, E., Asay-Davis, X., DeConto, R., Durand, G., et al. (2018). The Greenland and Antarctic ice sheets under 1.5 °C global warming. *Nature Climate Change*, *8*(12), 1053–1061. https://doi.org/10.1038/s41558-018-0305-8

Philippe, M., Tison, J.-L., Fjøsne, K., Hubbard, B., Kjær, H. A., Lenaerts, J. T. M., et al. (2016). Annual layer thicknesses and age-depth (oldest estimate) of Derwael Ice Rise (IC12), Dronning Maud Land, East Antarctica [Data set]. *Supplement to: Philippe, M et al. (2016): Ice core evidence for a 20th century increase in surface mass balance in coastal Dronning Maud Land, East Antarctica. The Cryosphere, 10(5), 2501-2516, https://doi.org/10.5194/tc-10-2501-2016*. https://doi.org/10.1594/PANGAEA.857574

Phillips, H. A. (1998). Surface meltstreams on the Amery Ice Shelf, East Antarctica. *Annals of Glaciology*, *27*, 177–181. https://doi.org/10.3189/1998AoG27-1-177-181

Pitcher, L. H., & Smith, L. C. (2019). Supraglacial Streams and Rivers. *Annual Review of Earth and Planetary Sciences*, *47*(1), 421–452. https://doi.org/10.1146/annurev-earth-053018-060212

Pitrak, M., Mares, S., & Kobr, M. (2007). A Simple Borehole Dilution Technique in Measuring Horizontal Ground Water Flow. *Ground Water*, *45*(1), 89–92. https://doi.org/10.1111/j.1745-6584.2006.00258.x

Poinar, K., Joughin, I., Lilien, D., Brucker, L., Kehrl, L., & Nowicki, S. (2017). Drainage of Southeast Greenland Firn Aquifer Water through Crevasses to the Bed. *Frontiers in Earth Science*, *5*. https://doi.org/10.3389/feart.2017.00005

Pollard, D., DeConto, R. M., & Alley, R. B. (2015). Potential Antarctic Ice Sheet retreat driven by hydrofracturing and ice cliff failure. *Earth and Planetary Science Letters*, *412*, 112–121. https://doi.org/10.1016/j.epsl.2014.12.035

Pritchard, H. D., Ligtenberg, S. R. M., Fricker, H. A., Vaughan, D. G., van den Broeke, M. R., & Padman, L. (2012). Antarctic ice-sheet loss driven by basal melting of ice shelves. *Nature*, *484*(7395), 502–505. https://doi.org/10.1038/nature10968

Rahnemoonfar, M., Varshney, D., Yari, M., & Paden, J. (2020). Deep Ice Layer Tracking and Thickness Estimation using Fully Convolutional Networks. *ArXiv:2009.00191 [Cs, Eess]*. Retrieved from http://arxiv.org/abs/2009.00191

Ramillien, G., Cazenave, A., & Brunau, O. (2004). Global time variations of hydrological signals from GRACE satellite gravimetry. *Geophysical Journal International*, *158*(3), 813–826. https://doi.org/10.1111/j.1365-246X.2004.02328.x

Reeh, N., Fisher, D. A., Koerner, R. M., & Clausen, H. B. (2005). An empirical firn-densification model comprising ice lenses. *Annals of Glaciology*, *42*, 101–106. https://doi.org/10.3189/172756405781812871

Renaud, A. (1959). Etude physiques et chimiques sur la glace de l'indlandsis du Groenland. Medd. Groenland, 2(177), pp. 100-107.

Richter-Menge, J., Overland, J. E., & Mathis, J. T. (2016). Arctic Report Card: Update for 2016 – LSU Law Center: Climate Change Law and Policy Project.

Rignot, E., Jacobs, S., Mouginot, J., & Scheuchl, B. (2013). Ice-Shelf Melting Around Antarctica. *Science*, *341*(6143), 266–270. https://doi.org/10.1126/science.1235798

Rignot, Eric, Mouginot, J., Scheuchl, B., Broeke, M. van den, Wessem, M. J. van, & Morlighem, M. (2019). Four decades of Antarctic Ice Sheet mass balance from 1979–2017. *Proceedings of the National Academy of Sciences*, *116*(4), 1095–1103. https://doi.org/10.1073/pnas.1812883116

Ryan, J. C., Smith, L. C., Wu, M., Cooley, S. W., Miège, C., Montgomery, L. N., et al. (2020). Evaluation of CloudSat's Cloud-Profiling Radar for Mapping Snowfall Rates Across the Greenland Ice Sheet. *Journal of Geophysical Research: Atmospheres*, *125*(4), e2019JD031411. https://doi.org/10.1029/2019JD031411

Scambos, T. A. (2004). Glacier acceleration and thinning after ice shelf collapse in the Larsen B embayment, Antarctica. *Geophysical Research Letters*, *31*(18). https://doi.org/10.1029/2004GL020670

Scambos, Ted, Hulbe, C., & Fahnestock, M. (2003). Climate-Induced Ice Shelf Disintegration in the Antarctic Peninsula. In E. Domack, A. Levente, A. Burnet, R. Bindschadler, P. Convey, & M. Kirby (Eds.), *Antarctic Research Series* (pp. 79–92). Washington, D. C.: American Geophysical Union. https://doi.org/10.1029/AR079p0079

Scambos, Ted A., Hulbe, C., Fahnestock, M., & Bohlander, J. (2000). The link between climate warming and break-up of ice shelves in the Antarctic Peninsula. *Journal of Glaciology*, *46*(154), 516–530. https://doi.org/10.3189/172756500781833043

Scambos, Theodore, Fricker, H., Liu, C.-C., Bohlander, J., Fastook, J., Sargent, A., et al. (2009). Ice shelf disintegration by plate bending and hydro-fracture: Satellite observations and model results of the 2008 Wilkins ice shelf break-ups. *Earth and Planetary Science Letters - EARTH PLANET SCI LETT*, *280*, 51–60. https://doi.org/10.1016/j.epsl.2008.12.027

Schaller, C. F., Freitag, J., Kipfstuhl, S., Laepple, T., Steen-Larsen, H. C., & Eisen, O. (2016). A representative density profile of the North Greenland snowpack. *The Cryosphere*, *10*(5), 1991–2002. https://doi.org/10.5194/tc-10-1991-2016

Schaller, C. F., Kipfstuhl, S., Steen-Larsen, H.-C., Freitag, J., & Eisen, O. (2017). Spatial variability of density stratigraphy and melt features for two polar snowpacks in Greenland and East Antarctica [Data set]. https://doi.org/10.1594/PANGAEA.884003

Schlosser, E., & Oerter, H. (2002a). Annual mean values of d18O of firn core NM02C89_01 [Data set]. *In supplement to: Schlosser, E; Oerter, H (2002): Shallow firn cones from Neumayer, Ekströmisen, Antartica: a comparison of accumulation rates and stable-isotope ratios. Annals of Glaciology, 35, 91-96, https://doi.org/10.3189/172756402781816915*. https://doi.org/10.1594/PANGAEA.690383

Schlosser, E., & Oerter, H. (2002b). Annual mean values of d180 and accumulation rate of ice core NM03C98_01 [Data set]. *In supplement to: Schlosser, E; Oerter, H (2002): Shallow firn cones from Neumayer, Ekströmisen, Antartica: a comparison of accumulation rates and stable-isotope ratios. Annals of Glaciology, 35, 91-96, https://doi.org/10.3189/172756402781816915*. https://doi.org/10.1594/PANGAEA.690397

Schlosser, E., & Oerter, H. (2002c). Density and d18O of firn core NM02C89_01 [Data set]. *In supplement to: Schlosser, E; Oerter, H (2002): Shallow firn cones from Neumayer, Ekströmisen, Antartica: a comparison of accumulation rates and stable-isotope ratios. Annals of Glaciology, 35, 91-96, https://doi.org/10.3189/172756402781816915*. https://doi.org/10.1594/PANGAEA.690382

Schmidt, L. S., Langen, P. L., Aðalgeirsdóttir, G., Pálsson, F., Guðmundsson, S., & Gunnarsson, A. (2018). Sensitivity of Glacier Runoff to Winter Snow Thickness Investigated for Vatnajökull Ice Cap, Iceland, Using Numerical Models and Observations. *Atmosphere*, *9*(11), 450. https://doi.org/10.3390/atmos9110450

Schröder, L., Horwath, M., Dietrich, R., Helm, V., van den Broeke, M. R., & Ligtenberg, S. R. M. (2019). Four decades of Antarctic surface elevation changes from multi-mission satellite altimetry. *The Cryosphere*, *13*(2), 427–449. https://doi.org/10.5194/tc-13-427-2019

Seroussi, H., Nowicki, S., Payne, A. J., Goelzer, H., Lipscomb, W. H., Abe-Ouchi, A., et al. (2020). ISMIP6 Antarctica: a multi-model ensemble of the Antarctic ice sheet evolution over the 21st century. *The Cryosphere*, *14*(9), 3033–3070. https://doi.org/10.5194/tc-14-3033-2020

Serreze, M. C., & Francis, J. A. (2006). The Arctic on the fast track of change. *Weather*, *61*(3), 65–69. https://doi.org/10.1256/wea.197.05

Shepherd, A., Ivins, E. R., A, G., Barletta, V. R., Bentley, M. J., Bettadpur, S., et al. (2012). A Reconciled Estimate of Ice-Sheet Mass Balance. *Science*, *338*(6111), 1183–1189. https://doi.org/10.1126/science.1228102

Shepherd, A., Ivins, E., Rignot, E., Smith, B., van den Broeke, M., Velicogna, I., et al. (2019). Mass balance of the Greenland Ice Sheet from 1992 to 2018. *Nature*. https://doi.org/10.1038/s41586-019-1855-2

Siegert, M., Atkinson, A., Banwell, A., Brandon, M., Convey, P., Davies, B., et al. (2019). The Antarctic Peninsula Under a 1.5°C Global Warming Scenario. *Frontiers in Environmental Science*, *7*. https://doi.org/10.3389/fenvs.2019.00102

Siegert, M. J. (2017). Why Should We Worry About Sea Level Change? *Frontiers for Young Minds*, *5*. https://doi.org/10.3389/frym.2017.00041

Siegert, M. J., Ross, N., & Le Brocq, A. M. (2016). Recent advances in understanding Antarctic subglacial lakes and hydrology. *Philosophical Transactions of the Royal Society A: Mathematical, Physical and Engineering Sciences*, *374*(2059), 20140306. https://doi.org/10.1098/rsta.2014.0306

Smith, B., Fricker, H. A., Gardner, A. S., Medley, B., Nilsson, J., Paolo, F. S., et al. (2020). Pervasive ice sheet mass loss reflects competing ocean and atmosphere processes. *Science*, eaaz5845. https://doi.org/10.1126/science.aaz5845

Smith, L. C., Chu, V. W., Yang, K., Gleason, C. J., Pitcher, L. H., Rennermalm, A. K., et al. (2015). Efficient meltwater drainage through supraglacial streams and rivers on the southwest Greenland ice sheet. *Proceedings of the National Academy of Sciences*, *112*(4), 1001–1006. https://doi.org/10.1073/pnas.1413024112

Steger, C. R., Reijmer, C. H., van den Broeke, M. R., Wever, N., Forster, R. R., Koenig, L. S., et al. (2017). Firn Meltwater Retention on the Greenland Ice Sheet: A Model Comparison. *Frontiers in Earth Science*, *5*. https://doi.org/10.3389/feart.2017.00003

Studinger, M. 2014, updated 2020. IceBridge ATM L2 Icessn Elevation, Slope, and Roughness, Version 2. [Subset Used: 2014]. Boulder, Colorado USA. NASA National Snow and Ice Data Center Distributed Active Archive Center. doi: https://doi.org/10.5067/CPRXXK3F39RV. [Date Accessed: 2018]. (n.d.).

Sturm, M., Holmgren, J., & Perovich, D. K. (2002). Winter snow cover on the sea ice of the Arctic Ocean at the Surface Heat Budget of the Arctic Ocean (SHEBA): Temporal evolution and spatial variability. *Journal of Geophysical Research: Oceans*, *107*(C10), SHE 23-1-SHE 23-17. https://doi.org/10.1029/2000JC000400

Sundal, A. V., Shepherd, A., Nienow, P., Hanna, E., Palmer, S., & Huybrechts, P. (2009). Evolution of supra-glacial lakes across the Greenland Ice Sheet. *Remote Sensing of Environment*, *113*(10), 2164–2171. https://doi.org/10.1016/j.rse.2009.05.018

Takahashi, S., & Kameda, T. (2007). Snow density for measuring surface mass balance using the stake method. *Journal of Glaciology*, *53*(183), 677–680. https://doi.org/10.3189/002214307784409360

The IMBIE Team. (2020). Mass balance of the Greenland Ice Sheet from 1992 to 2018. *Nature*, *579*(7798), 233–239. https://doi.org/10.1038/s41586-019-1855-2

Thomas, E. R., van Wessem, J. M., Roberts, J., Isaksson, E., Schlosser, E., Fudge, T. J., et al. (2017). Regional Antarctic snow accumulation over the past 1000 years. *Clim. Past*, *13*(11), 1491–1513. https://doi.org/10.5194/cp-13-1491-2017

Turner, K., Harris, C., Lindsay, J. M., Mahoney, A. R., Schaeffer, R., & Witte, C. (2018). unpublished field observations, Ikaaġvik Sikukun project.

Turner, K., Ayre, M., Baadshaug, O., Clark, A., Alexeev, V., Doulgeris, A. P., et al. (2018). Unpublished field observations, INTPART Arctic Field Summer Schools: Norway-Canada-USA collaboration (NFR project 261786/H30) supported by NSF and Ukpeaġvik Iñupiat Corporation.

V. Spikes, G. H. (2005). US International Trans-Antarctic Scientific Expedition (US ITASE): GPR Profiles and Accumulation Mapping [Data set]. U.S. Antarctic Program Data Center (USAP-DC), via National Snow and Ice Data Center (NSIDC). https://doi.org/10.7265/N5GH9FV6

Vandecrux, B., Fausto, R. S., Langen, P. L., Van As, D., MacFerrin, M., Colgan, W. T., et al. (2018). Drivers of Firn Density on the Greenland Ice Sheet Revealed by Weather Station Observations and Modelling. *Journal of Geophysical Research: Earth Surface*. https://doi.org/10.1029/2017JF004597

Vandecrux, Baptiste, MacFerrin, M., Machguth, H., Colgan, W. T., van As, D., Heilig, A., et al. (2019). Firn data compilation reveals widespread decrease of firn air content in western Greenland. *The Cryosphere*, *13*(3), 845–859. https://doi.org/10.5194/tc-13-845-2019

Vaughan, David G., & Russell, J. (1997). Compilation of surface mass balance measurements in Antarctica. Internal Rep., 56 pp., ES4/8/1/1997/1, Br. Antarct. Surv., Cambridge, UK.

Vaughan, David G., Marshall, G. J., Connolley, W. M., Parkinson, C., Mulvaney, R., Hodgson, D. A., et al. (2003). Recent Rapid Regional Climate Warming on the Antarctic Peninsula. *Climatic Change*, *60*(3), 243–274. https://doi.org/10.1023/A:1026021217991

Vaughan, D.G., Mantripp, D. R., Sievers, J., & Doake, C. S. M. (1993). A synthesis of remote sensing data on Wilkins Ice Shelf, Antarctica. *Annals of Glaciology*, *17*, 211–218. https://doi.org/10.3189/S0260305500012866

Velicogna, I., Sutterley, T. C., & Broeke, M. R. van den. (2014). Regional acceleration in ice mass loss from Greenland and Antarctica using GRACE time-variable gravity data. *Geophysical Research Letters*, *41*(22), 8130–8137. https://doi.org/10.1002/2014GL061052

Verfaillie, D., Fily, M., Le Meur, E., Magand, O., Jourdain, B., Arnaud, L., & Favier, V. (2012). Snow accumulation variability derived from radar and firn core data along a 600 km transect in Adelie Land, East Antarctic plateau. *The Cryosphere*, *6*(6), 1345–1358. https://doi.org/10.5194/tc-6-1345-2012

Verjans, V., Leeson, A. A., Stevens, C. M., MacFerrin, M., Noël, B., & van den Broeke, M. R. (2019). Development of physically based liquid water schemes for Greenland firn-densification models. *The Cryosphere*, *13*(7), 1819–1842. https://doi.org/10.5194/tc-13-1819-2019

Wagenbach, D., Graf, W., Minikin, A., Trefzer, U., Kipfstuhl, S., Oerter, H., & Blindow, N. (1994a). Annual means of density, d18O, deuterium, tritium, and accumulation rates of firn core BER01C90_01 [Data set]. *In supplement to: Wagenbach, D et al. (1994): Reconnaissance of chemical and isotopic firn properties on top of Berkner Island, Antarctica. Annals of Glaciology, 20, 307-312, hdl:10013/epic.15271.d001*. https://doi.org/10.1594/PANGAEA.548637

Wagenbach, D., Graf, W., Minikin, A., Trefzer, U., Kipfstuhl, S., Oerter, H., & Blindow, N. (1994b). Density and d18O of snow pit BER01S90_01 [Data set]. *In supplement to: Wagenbach, D et al. (1994): Reconnaissance of chemical and isotopic firn properties on top of Berkner Island, Antarctica. Annals of Glaciology, 20, 307-312, hdl:10013/epic.15271.d001*. https://doi.org/10.1594/PANGAEA.548653

Wagenbach, D., Graf, W., Minikin, A., Trefzer, U., Kipfstuhl, S., Oerter, H., & Blindow, N. (1994c). Density and d18O of snow pit BER02S90_02 [Data set]. *In supplement to: Wagenbach, D et al. (1994): Reconnaissance of chemical and isotopic firn properties on top of Berkner Island, Antarctica. Annals of Glaciology, 20, 307-312, hdl:10013/epic.15271.d001*. https://doi.org/10.1594/PANGAEA.548654

Wagenbach, D., Graf, W., Minikin, A., Trefzer, U., Kipfstuhl, S., Oerter, H., & Blindow, N. (1994d). Density, d18O, deuterium, and tritium of firn core BER02C90_02 [Data set]. *In supplement to: Wagenbach, D et al. (1994): Reconnaissance of chemical and isotopic firn properties on top of Berkner Island, Antarctica. Annals of Glaciology, 20, 307-312, hdl:10013/epic.15271.d001*. https://doi.org/10.1594/PANGAEA.548622

Wang, Y., Ding, M., van Wessem, J. M., Schlosser, E., Altnau, S., van den Broeke, M. R., et al. (2016). A Comparison of Antarctic Ice Sheet Surface Mass Balance from Atmospheric Climate Models and In Situ Observations. *Journal of Climate*, *29*(14), 5317–5337. https://doi.org/10.1175/JCLI-D-15-0642.1

Warren, S. G., Rigor, I. G., Untersteiner, N., Radionov, V. F., Bryazgin, N. N., Aleksandrov, Y. I., & Colony, R. (1999). Snow Depth on Arctic Sea Ice. *Journal of Climate*, *12*(6), 1814–1829. https://doi.org/10.1175/1520-0442(1999)012<1814:SDOASI>2.0.CO;2

Webster, M. A., Rigor, I. G., Nghiem, S. V., Kurtz, N. T., Farrell, S. L., Perovich, D. K., & Sturm, M. (2014). Interdecadal changes in snow depth on Arctic sea ice. *Journal of Geophysical Research: Oceans*, *119*(8), 5395–5406. https://doi.org/10.1002/2014JC009985

van Wessem, J. M., Ligtenberg, S. R. M., Reijmer, C. H., van de Berg, W. J., van den Broeke, M. R., Barrand, N. E., et al. (2016). The modelled surface mass balance of the Antarctic Peninsula at 5.5 km horizontal resolution. *The Cryosphere*, *10*(1), 271–285. https://doi.org/10.5194/tc-10-271-2016

van Wessem, J. Melchior, Steger, C. R., Wever, N., & van den Broeke, M. R. (2020). *Modelling perennial firn aquifers in the Antarctic Peninsula (1979–2016)* (preprint). Snow/Snow Physics. https://doi.org/10.5194/tc-2020-148

Wever, N., Fierz, C., Mitterer, C., Hirashima, H., & Lehning, M. (2014). Solving Richards Equation for snow improves snowpack meltwater runoff estimations in detailed multi-layer snowpack model. *The Cryosphere*, *8*(1), 257–274. https://doi.org/10.5194/tc-8-257-2014

Wilhelms, F. (1996). eitfähigkeits- und Dichtemessung an Eisbohrkernen / Measuring the Conductivity and Density of Ice Cores (diplom). Universität Bonn.
Wilhelms, F. (2005). Explaining the dielectric properties of firn as a density-and-conductivity mixed permittivity (DECOMP). *Geophysical Research Letters*, *32*(16). https://doi.org/10.1029/2005GL022808
Wilhelms, Frank. (2000a). Density of ice core ngt03C93.2 from the North Greenland Traverse [Data set]. https://doi.org/10.1594/PANGAEA.56560
Wilhelms, Frank. (2000b). Density of ice core ngt06C93.2 from the North Greenland Traverse [Data set]. https://doi.org/10.1594/PANGAEA.57153
Wilhelms, Frank. (2000c). Density of ice core ngt14C93.2 from the North Greenland Traverse [Data set]. https://doi.org/10.1594/PANGAEA.56615
Wilhelms, Frank. (2000d). Density of ice core ngt27C94.2 from the North Greenland Traverse [Data set]. https://doi.org/10.1594/PANGAEA.57296
Zwally, H. J., & Jun, L. (2002). Seasonal and interannual variations of firn densification and ice-sheet surface elevation at the Greenland summit. *Journal of Glaciology*, *48*(161), 199–207. https://doi.org/10.3189/172756502781831403